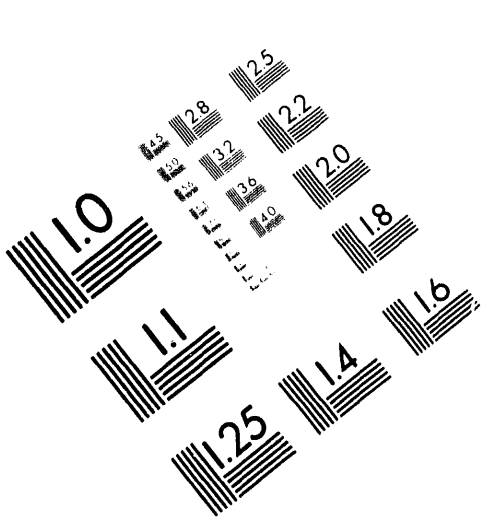

Association for Information and Image Management

1100 Wayne Avenue, Suite 1100
Silver Spring, Maryland 20910

301/587-8202

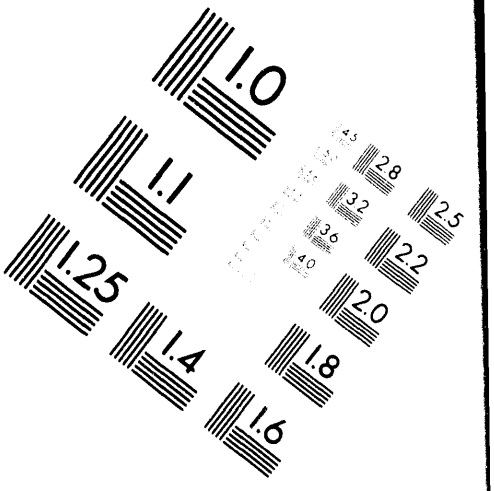

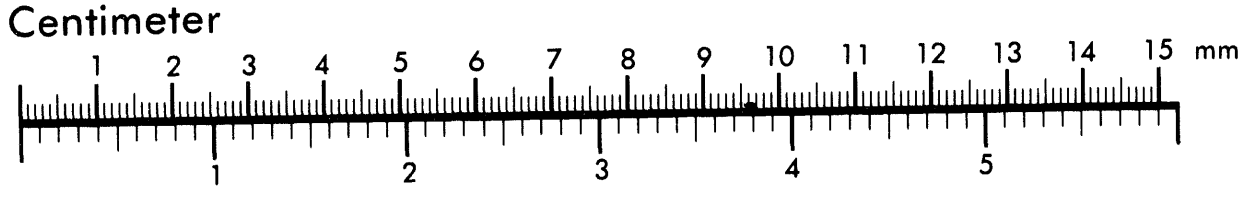

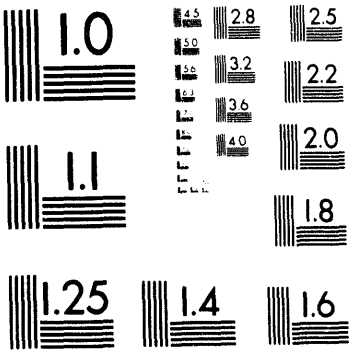

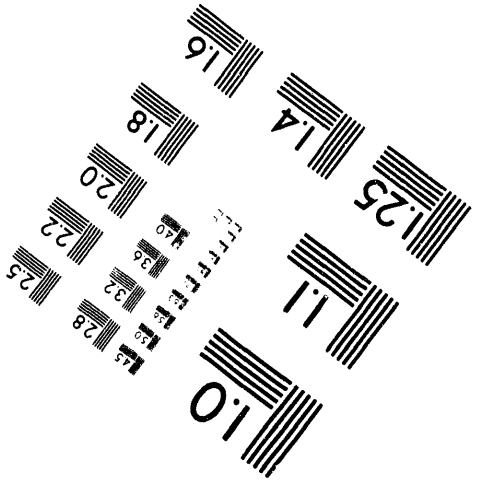

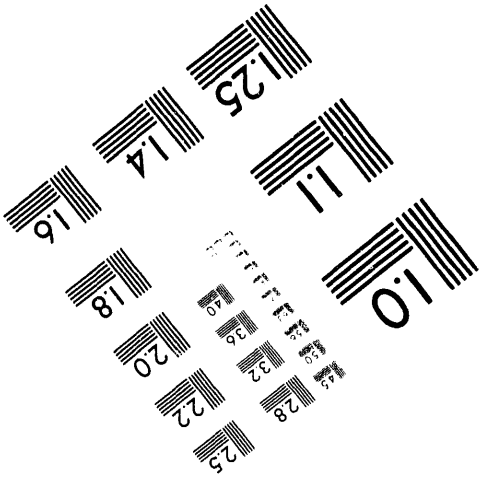

1 of 2

DOE/ER/40397--T1

CALT-63-669

CALIFORNIA INSTITUTE OF TECHNOLOGY
Pasadena, CA 91125

Norman Bridge Laboratory of Physics 161-33
Phone (818) 395-4281, **Telex** 675425, **FAX** (818) 568-8263

PROGRESS REPORT

CONTRACT DE-FG03-88ER40397

PROPERTIES OF NUCLEI AND ELEMENTARY PARTICLES

AT LOW AND INTERMEDIATE ENERGIES

Between July 1992 and August 1993

CALT-63-669

CONTRACT DE-FG03-88ER40397

PROPERTIES OF NUCLEI AND ELEMENTARY PARTICLES AT LOW AND INTERMEDIATE ENERGIES

California Institute of Technology, Pasadena, CA 91125

FELIX BOEHM, Principal Investigator

PROGRESS REPORT

Between July 1992 and August 1993

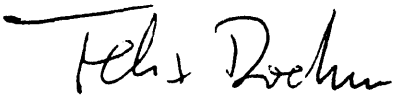

Felix Boehm

PROGRESS REPORT 1993

Brief Summary of Progress

1. Double Beta Decay of ^{136}Xe with the Caltech High Pressure Time Projection Chamber.

F. Boehm, H. Henrikson, and K. Lou (Caltech)
J. Busto, V. Jorgens, M. Treichel, J.C. Vuilleumier, J.-L. Vuilleumier (Neuchatel),
K. Gabathuler (PSI)

The high pressure enriched ^{136}Xe time projection chamber built at Caltech and installed in the Gotthard tunnel laboratory in Switzerland, has been operating since early 1991. To date, about 6830 h of data have been accumulated and analyzed. An extensive publication describing the results has been written and submitted to Phys. Rev. D (see CALT 63-651 in Progress Report Section). Results have also been presented at several APS meetings and at Neutrino-92 in Granada. At the present time we have the most sensitive data for double beta decay in ^{136}Xe setting limits for the neutrinoless double beta decay half life of $T_{1/2} > 3.4\times10^{23}y$ (90% CL). The resulting neutrino mass limit is about 2.8eV and the limit for the majoron coupling is 2.4 $\times10^{-4}$. These results have comparable sensitivity to those from recent ^{76}Ge decay experiments and are currently in the forefront of low energy neutrino physics. Ours is the only TPC experiment with high sensitivity allowing exploration of the neutrinoless mode.

During 1991 and most of 1992, the TPC has worked well, with only occasional down-time, mostly from a re-occurring problem with the anode plane (small shifts in the gain map as well as discharges). Recently, this problem with the anode has exasperated. This, together with a new problem stemming from a slow deformation of the xy-plane has prevented us from running the TPC over extended periods. For that reason, the TPC has been shut down in April 93 for major repair. A new anode and a

new xy-plane have been designed and will be built in Neuchatel and at PSI with the help of subcontractors. Both should be ready for installation by late Fall 93.

With the TPC back on the air in late 1993, we anticipate to study the 2-neutrino mode (using a reduced gas pressure of 2.5 atm in order to enlarge the low energy trajectories) as well as the majoron mode. For the former, both enriched and depleted xenon will be used to facilitate background subtraction. We anticipate to also attack the problem of the dark matter. Data taking will continue through 1994 with the new anode and xy plane, profiting from the steadily improving background conditions (decreasing cosmogenic ^{68}Ge - ^{68}Ga background with half-life of 275d). In an attempt to reduce radon-induced low energy background we have now drawn up plans and ordered equipment for a refrigeration unit to be installed in the Xe gas recirculation line. Freezing out the radon should reduce the Th-chain background so that we should be able to identify the 2-neutrino mode (for which we presently have only an upper limit). To further help the background situation, a muon veto has recently been installed.

2. A 12 Ton Low Energy Neutrino Detector for Neutrino Oscillation Studies at the San Onofre Reactor Station

Mark Chen, C. Delany, H. Henrikson, R. Hertenberger, N. Mascarenhas,
V. Novikov, F. Boehm and P. Vogel (Caltech)

As outlined in last year's Proposal and presented in detail in the accompanying Report entitled "The Caltech Neutrino Experiment at San Onofre" we are designing a 12 ton liquid scintillation detector for studying neutrino oscillations via the reaction $\bar{\nu}_e p \rightarrow e^+ n$. Our goal with this detector is to reach a sensitivity for the mass parameter Δm^2 of 10^{-3} eV^2 for mixing angles $\sin^2 2\Theta$ of ≥ 0.1. The interest in studying the range of the mass parameter Δm^2 between 2×10^{-2} (the limit from the Gosgen experiment) and 10^{-3} has been triggered by recent results from the solar neutrino detectors (Homestake, Kamiokande, Gallex) and from the anomalous atmospheric neutrino ratio (see Appendix for a detailed discussion).

Our 12 ton liquid scintillator will be installed at 0.65km from the San Onofre reactors in a underground vault at a shallow depth of 25mwe. Both, the reaction positrons with energies between 1 to 10MeV and the reaction neutrons will be detected. A valid signal consists of a prompt coincidence between the positron and two 511 keV annihilation gamma rays, followed by a delayed signal from a neutron capture gamma ray. This scheme minimizes the fast neutron background as explained in the Appendix.

Our detector comprises 32 segmented acrylic cells, each with dimensions of 9m x 0.5 m x 0.12m. We have developed a mineral oil based liquid scintillator with high light yield (60 % of anthracene) and large attenuation length (10 m at 435 nm). The scintillator cocktail can be prepared in-house at a significant saving. As an alternative to the proton rich scintillator, we are also developing a Gd-loaded scintillator. Here we are helped by earlier work in this lab using the commercial NE344a scintillator as well as by our own chemical developments. The principal advantage of Gd-loaded scintillator is it's lower background owing in part to the shorter time window (100μs compared to 500μs) and to the higher energy threshold (above 4MeV).

We have conducted extensive studies, both by experiments and by modeling, of the parameters of the proposed 12 ton San Onofre Neutrino Detector relating to the detector response, rate, efficiency, and background. The studies also include work on two 2.5m prototype scintillator cells. A detailed account of all these investigations is contained in the accompanying San Onofre Report.

Among the issues still under investigation are the neutron production yield and neutron multiplicity from cosmic ray muons at 25mwe. While the muon-capture neutron rates are fairly well documented in literature, there is a considerable spread in reported data on muon-spallation rates For that reason we are now planning a dedicated experiment on muon-nucleus interaction involving emission of neutrons to be described below.

Experimental studies of the backgrounds have been carried out at Stanford (see Appendix to San Onofre Report) and also in the reactor's tendon gallery. For this purpose, a 140 liter 12 cell detector (re-using the Gosgen cells) has been fully instrumented in the 4-fold coincidence mode and installed in the tendon gallery 25m from the core of the San-Onofre Unit 2. Besides studying backgrounds, the detector allows

us to observe neutrino events (about 10/d). The detector is currently operating and data taking is in progress. The reactor-off cycle to begin June 5, 1993, will provide complementary background information. At the end of the current test run, the tendon gallery detector will be enlarged by the addition of 6 more cells (for a neutrino event rate of about 20/d).

Inasmuch as the neutrino flux and spectrum are well known (to about 3%) at all times, determined by reactor power and core history, and supplemented by experimental studies and theoretical calculations of fission electron spectra (see Kwon et al. and references quoted), our experiment does not require a monitor detector, as it relies on the absolute detector calibration. Nevertheless we retain the option to use the tendon gallery detector as a monitor. As in the case of our previous reactor experiment at Goesgen, reactor-off cycles will play en important role in determining the backgrounds (for details see attached San Onofre Report).

3. New Limits on the 17 keV Neutrino

M. Chen, D. A. Imel, T. J. Radcliffe, H. Henrikson, and F. Boehm

Although several previous experiments, including one in 1984, using the Caltech double focusing spectrometer, have clearly rejected the presence of the 17 keV neutrino announced by Simpson and Hime and others, we have been moved by strong pressure from the "believers" to undertake a new measurements of the beta decay of ^{35}S. Special attention was paid to the constancy of the magnetic field which was measured with the help of a flux-gate magnetometer to 30ppm. Based on the new data obtained in 1992 and 1993 we again reject, at the 6 σ level, a neutrino in the energy range between 12 and 22 keV admixed at 0.85% to the ordinary light neutrino.

With the help of an auxiliary experiment we have demonstrated that our spectrometer is sensitive to a "kink" in the spectrum such as that expected from an admixed heavy neutrino. For this test an absorber foil was placed over part of the source giving rise to a fractional retarded spectrum.

The work is described in Phys. Rev. Lett., and also the Proceedings of Neutrino-92 (Granada). It constitutes part of the thesis of M. Chen.

4. Time Reversal and Parity Tests for Hindered Nuclear Gamma Transitions

B. Cook, H. Henrikson, V. Novikov, and F. Boehm (Caltech)

Between 1991 and part of 1993 our Caltech ^{3}He-^{4}He dilution refrigerator (built in 1970) has undergone extensive rebuilding as mentioned in last year's Report. Among the recent renewal tasks was the manufacturing of a new continuous heat exchanger, as well as the replacement of several vacuum lines. Recent runs with a ^{60}Co source implanted in Fe have demonstrated that the fridge operates again and reaches temperatures around 20 mK.

A ^{182}Ta source has been prepared by irradiation of 1mg Ta metal chips at the Missouri Research Reactor. Sources have been prepared by diffusing, in a hydrogen oven, the Ta chloride into thin Fe foil disks to be affixed to the cool finger of the fridge. The gamma rays from ^{182}Ta have been studied with a Ge detector in preparation for a extended cold run with the source.

The work during 1993 was mostly technical and preparatory. There were no scientific papers or reports.

5. Theory of Nuclear Structure and its Application

P. Vogel and E. Ormand

5.1 Introduction

The theory contingent consisted of P. Vogel (Senior Research Associate) and E. Ormand (DuBridge Fellow). Close collaboration with Prof. S. Pittel and Dr. J. Engel (Bartol Research Institute, University of Delaware) has continued. Also, some of the work involved collaboration with the personnel of the Kellogg Laboratory, Caltech (P. Vogel worked with B. Q. Chen, E. Kolbe,and K. Langanke while E. Ormand worked with C. W. Johnson, S. E. Koonin, and G. H. Lang). In addition, E. Ormand continued his previous collaboration with R. A. Broglia and his collaborators in Milano, Italy. Below we describe the individual projects and highlight the significant

accomplishments. (Sections 5.2-5.7 concern primarily the work of P. Vogel and sections 5.8-5.11 the work of E. Ormand).

5.2 Double beta decay

The nuclear matrix elements of double beta decay are fairly well understood, thanks in part to the theoretical efforts of our group [1]. Last year we developed a method to treat 2ν double beta decay populating the excited 0^+ states [2]. Experiments aimed at seeing that decay in ^{96}Zr and ^{150}Nd, in addition to the known ^{100}Mo decay analyzed in [2], are under way at Gran Sasso, and will require theoretical analysis. Also, new approaches to the theory are constantly being proposed. Recently, we have shown [3] that one of them, the so called Operator Expansion Method, does not work. In the same paper [3] we show how to treat the energy denominators properly, and reiterate that the decay of ^{48}Ca is an important test of our understanding of the mechanism of the 2ν decay. The status of the problem was briefly summarized in the talk [4].

In recognition that the study of double beta decay, in particular of the 2ν mode, has reached an important milestone, we have been invited (P. Vogel and M. Moe of UC Irvine) to write a review on the subject for the Annual Review of Nuclear and Particle Science. The work on the paper is in the initial stages.

5.3 Atmospheric neutrinos

The disagreement between the measured and expected ν_μ/ν_e ratio reported by the Kamiokande and IMB groups is one of the outstanding problems of present day neutrino physics. We have reevaluated the underlying (ν,^{16}O) cross sections for the quasi-elastic charged current reaction in the hope of eliminating one of the larger uncertainties in the interpretation of these experiments. In our work [5] we include the Coulomb interaction of outgoing protons and charged leptons, a realistic finite-volume mean field, and the residual nucleon-nucleon interaction. None of these effects are accurately represented in the Monte Carlo simulations used to predict event rates due to μ and e neutrinos from cosmic-ray collisions in the atmosphere. We nevertheless conclude that the neglected physics cannot account for the anomalous μ/e ratio. The absolute rates do change, however, by 10-15%, and that could be important for

the proper interpretation of the experimental results.

5.4 Solar neutrinos

Now, as the information on the flux of solar neutrinos is rapidly expanding, a quantitative analysis of the individual components of the solar ν spectrum is in order; determination of the ^{7}Be neutrino flux is particularly important. We have shown previously [7] that ^{127}I is a potentially powerful detector, sensitive to the ^{7}Be neutrinos. A calibration of the detecting reaction is under way at LAMPF with the beam dump (i.e. muon decay at rest) ν_e spectrum; preliminary results suggest that the cross section for iodine is indeed significantly larger than for the existing detector based on ^{37}Cl. Another calibration experiment, the (p,n) reaction on ^{127}I, has been scheduled at the Indiana University Cyclotron Lab. A large ^{127}I detector has been proposed; it will be also useful as a unique supernova ν_e detector.

We began the work on expanding our previous calculations to cover the higher energies (and hence forbidden transitions) relevant to that measurement. This project is being pursued in collaboration with J. Engel and S. Pittel of the Bartol Institute.

5.5 Search for dark matter

Another application of nuclear structure involves evaluation of the cross section of the various dark matter candidate particles on nuclei. A detailed study of ^{93}Nb has been published [8], and a review summarizing the nuclear structure issues [9] has been written. The results were also reported in the invited talk [10] at the Neutrino-92 conference in Granada. Further work on the subject, in particular on the interaction of neutralinos - the stable supersymmetric neutral fermions - with nuclei, will involve the problems of scaling, i.e. how the cross section or, respectively, the expected signal depends on the corresponding parameters, and what effects the recent developments in the study of the nucleon spin structure have on these quantities.

5.6 Nuclear shell model

As an alternative to the exact shell model, one can use a truncation scheme based on the concept of approximate symmetry of the nuclear hamiltonian, followed by an exact diagonalization. One of possible symmetries is the Wigner spin-isospin SU(4). We evaluated [11] the "goodness" of SU(4) symmetry, by expanding the nuclear wave functions obtained by the shell model diagonalization in terms of the eigenstates of SU(4). We carried out this program for the full *s*,*d* shell and for some nuclei of the *f*,*p* shell. We found that the SU(4) in real nuclei is quite badly broken and thus we have, hopefully, solved one of the classical problems of nuclear theory.

5.7 Nuclear parity nonconservation

Recently a revival of interest in the parity nonconservation in nuclei was stimulated by the experiments at LAMPF on scattering of polarized epithermal neutrons on heavy nuclei. The surprising finding that the mean asymmetry is nonvanishing and large remains unexplained. We have shown [12] that a particularly straightforward analysis in terms of the optical model potential predicts much smaller effects than the experiment indicates. Subsequently, a number of other studies reached a similar conclusion. Hence, it is possible that an as yet unknown enhancement mechanism is at work, or that the fundamental parity violating nucleon interaction is in fact poorly understood.

5.8 Atomic parity nonconservation

The interpretation of future precise experiments on atomic parity violation in terms of parameters of the Standard Model could be hampered by uncertainties in the atomic and nuclear structure. While the former can be overcome by measurement in a series of isotopes, the nuclear structure requires knowledge of the neutron density. We used [13] the nuclear Hartry-Fock method to calculate the neutron and proton densities, and predicted the weak charges for the series of cesium isotopes (^{125}Cs - ^{139}Cs) that have been proposed for the atomic parity nonconservation study. The uncertainties in the atomic parity nonconservation asymmetries associated with the uncertainties in the neutron density distribution have been estimated and found to be smaller than the anticipated experimental errors (at least for the near future).

5.9 Monte Carlo Methods for the Nuclear Shell Model

A novel method for treating the interaction shell model has been developed. The approach allows calculations much larger than those heretofore possible. The method is based on the path integral formulation of the shell model and uses Monte Carlo techniques for the integral evaluation. This is a large multiyear project, involving several physicists, and potentially many applications. The preliminary results, published in [14] are very encouraging. A large paper, summarizing the formalism, has been submitted for publication [15]. A number of other applications will be reported in subsequent papers. Work on this project was the primary effort of E. Ormand.

5.10 Spectral Properties of Shell-Model Hamiltonians

It is of interest to study the fluctuation properties of the eigenvalues of quantal systems, in particular to understand to which extent they exhibit chaotic behavior. As part of such a study in Ref. [16] the spectral properties of realistic nuclear Hamiltonians for light nuclei were investigated. The relatively weak isospin-nonconserving forces provide a useful example of the effect of symmetry breaking on the generic behavior of nuclear levels.

5.11 Giant Resonances in Hot Nuclei

In the continuing effort to study nuclear structure at finite temperatures the influence of time-dependent thermal fluctuations of the nuclear surface on the properties of the giant dipole resonance was investigated in Ref. [17]. Effects of different time scales for fluctuations in the deformation and orientation degrees of freedom are observed.

In a related work [18] a model accounting for the time dependence of shape fluctuations in metal microclusters and their effect on the damping width of plasmon resonance is discussed. An estimate of the relaxation time of the quadrupole shape is given.

5.12 The Solar Neutrino Cross Section for ^{23}Na

In support of the design of a possible solar neutrino detector based on a large array of NaBr detectors, the solar neutrino cross sections on ^{23}Na has been calculated [19]. The shell model calculation treats all exited states of the final nucleus ^{23}Mg exactly. The solar neutrino absorption rate of 3.5 ± 1.3 SNU is obtained.

References to Section 5

[1] P. Vogel and M.R. Zirnbauer, Phys. Rev. Lett. **57**, 3148 (1986); J. Engel, P. Vogel, and M.R. Zirnbauer, Phys. Rev. **C37**, 731 (1988).

[2] A. Griffiths and P. Vogel, Phys. Rev. **C46}**, 181 (1992).

[3] J. Engel, W. C. Haxton, and P. Vogel, Phys. Rev. , **C46}**, R2153 (1992).

[4] P. Vogel, invited talk at the *XVI-th Nuclear Physics Symposium*, Oaxtepec, Mexico, January 1992; to be published in Revista Mexicana de Fisica.

[5] J. Engel, E. Kolbe, K. Langanke, and P. Vogel, Phys. Rev. D, submitted for publication.

[6] P. Vogel, invited talk at the *5th Int. Workshop on Neutrino Telescopes* , Venice, Italy, March 1993.

[7] J. Engel, S. Pittel, and P. Vogel, Phys. Rev. Lett. **67**, 426 (1991).

[8] J. Engel, S. Pittel, E. Ormand, and P. Vogel, Phys. Lett. **B275**, 119 (1992).

[9] J. Engel, S. Pittel, and P. Vogel, Int. J. of Mod. Phys. E - Reports on Nuclear Physics, **1**, 1 (1992).

[10] P. Vogel, invited talk at the *Neutrino 92* Conference, Granada, Spain, June 1992; Nucl. Phys. B (Proc. Suppl.) **31**, 149 (1993).

[11] P. Vogel and W. E. Ormand, Phys. Rev. **C 47**, 623 (1993).

[12] S. E. Koonin, C. W. Johnson, and P. Vogel, Phys. Rev. Lett., **69**, 1163 (1992).

[13] B. Q. Chen and P. Vogel, Phys. Rev. C - submitted for publication.

[14] C. W. Johnson, S. E. Koonin, G. H. Lang, and W. E. Ormand, Phys. Rev. Lett. **69**, 3157 (1992).

[15] G. H. Lang, C. W. Johnson, S. E. Koonin, and W. E. Ormand, submitted for publication.

[16] W. E. Ormand and R. A. Broglia, Phys. Rev. **C 46**, 1710 (1992).

[17] W. E. Ormand et al., Phys. Rev. Lett. **69**, 2905 (1992).

Reprints + Preprints removed

APPENDIX 1

APPENDIX 1

Anticipated Results from the San Onofre Neutrino Oscillation Experiment

M. Chen

(December 1992)

A study of the sensitivity of the San Onofre Experiment to the neutrinc oscillation parameters Δm^2 - $\sin^2 2\theta$ was made. Two separate results will be discussed. The first is a calculation of the total number of neutrino counts we except to detect in a scenario without oscillations. This calculation determines our statistical sensitivity as a function of the signal-to-background ratio in our detector. Different distances were studied to determine the regions in parameter space that can be excluded at each. The second result assumes neutrino oscillations between ν_e and ν_μ, as given by a solution to the atmospheric neutrino problem [1]. This "Monte Carlo" study simulated the resultant positron spectrum in our detector, given these parameters, to determine our sensitivity.

The following assumptions went into the calculations. The positron spectrum from the Gösgen experiment [2] was used. Sixteen energy bins were chosen for the positron energies, spaced 0.305 MeV apart. The oscillation disappearance probability, as a function of energy, was averaged flatly over each of the sixteen bins. A signal rate of 7 per day at 1 km [3] was used and the data set considered consisted of 400 days of full reactor power and 90 days of half power (i.e. one reactor shutdown for refuelling), used for background subtraction.

With these assumptions, one can calculate the anticipated statistical quality of our data. Let's take the integrated counts over the entire positron spectrum to set the excluded region in parameter space. By using only the integrated counts, we lose some spectral information that could possibly extend our excluded region. Nevertheless, the energy dependence of the oscillation probability was correctly treated bin-by-bin and the total counts were summed over the sixteen bins. Figures 1 to 3 illustrate the regions in parameter space we could exclude given various signal-to-background ratios, at various distances from the reactor core. Figures 1, 2 and 3 show the anticipated exclusion at 1 km, 650 m, and 500 m respectively. The four curves on each figure correspond to background rates of 0, 4, 7 and 14 counts per day (signal of 7 per day at 1 km, 17 per day at 650 m and 28 per

day at 500 m). The curves drawn are exclusions at the 90% confidence level, with only the statistical errors included. Note that the detector energy resolution was not included directly; rather, the finite bin width was responsible for dampening the oscillations. Also, the finite size of the detector and core was neglected.

The excluded region after 400 days of signal at 1 km is disappointing. Let us perform a quick check on the statistics of this result. For a signal-to-background of 1 : 1, we would accumulate 5600 ± 75 counts in 400 days at full power and 945 ± 31 counts during the 90 days of refuelling (half signal). Normalizing to time gives: 14 ± 0.187 per day (signal plus background) and 10.5 ± 0.342 per day (half signal plus background). We subtract off the background (error added in quadrature) giving: 3.5 ± 0.389 per day (half the signal rate). Doubling this restores the full signal rate of 7 ± 0.78 per day. Thus, the uncertainty in the rate is $\approx 11\%$ and this is not sufficient to exclude $\sin^2 2\theta = 0.1$. On the other hand, with 28 counts per day at 500 m, we can 'tolerate' an uncertainty in the count rate of 2.8 per day and still probe down to $\sin^2 2\theta = 0.1$ mixing.

The second part of this study presumes that neutrino oscillations are present as indicated by the atmospheric neutrino puzzle. The values chosen for consideration are: $\Delta m^2 = 10^{-2}$ and $\sin^2 2\theta = 0.4$ (arbitrarily chosen). Positron spectra are presented, using these parameters, with error bars determined after background subtraction. For this study, the background (rate of 7 per day) was presumed to be linear with energy with a small negative slope of about 2% per MeV (essentially flat). The same data taking period as described in the first result above was considered. Figure 4 is the "Monte Carlo" data from the experiment at 1 km distance; Figure 5 is for 650 m and Figure 6 for 500 m. The solid curves in the figures are the spectra without oscillations. The dashed curves represent the expected spectra for the chosen oscillation parameters.

Two things should be mentioned about the above results. The choice of $\Delta m^2 = 10^{-2}$ was the optimal choice at 500 m and precisely the worse choice for an experiment at 1 km (see Figures 1 and 3). One can see in those figures that a 'dip' exists in the exclusions. This dip is real yet is also simultaneously an artifact of the binning and the integration method. The true excluded region, derived from a best fit to the positron spectrum (varying oscillation parameters), would probably have a less pronounced dip. Regardless, the value of $\Delta m^2 = 10^{-2}$ occurs right at the dip in the sensitivity of a 1 km experiment. The second point concerning these results

is that these weren't true Monte Carlo calculations. The response of the detector at different energies was not included. This was really just a few random numbers thrown in the hypothetical spectra (signal and background).

In order to determine the signal-to-background ratio required in a reactor based oscillation experiment, one should consider the amount of time the signal will be acquired and the amount of background that will be taken. During collection of "background", one might still be acquiring signal at a reduced rate. For the San Onofre experiment, we anticipate that one reactor will be shutdown for three months for refuelling. During this three month period of time, we can accumulate background, but we also collect the signal at half strength. Given this less than optimal situation, we can compute the necessary signal rate to obtain an exclusion out to $\sin^2 2\theta = 0.1$, given a certain background rate, for various periods of data taking. Such a calculation can be expressed as a "rate-parabola" (Figure 7). The y-axis on such a plot is the background rate (counts per day). Drawing a line across the plot at a y-value corresponding to the anticipated background rate, one intersects the rate-parabola. The x-value at the intersection is the minimum required signal rate in order to achieve a statistical uncertainty of 5% in the integrated neutrino flux (afer background subtraction). Figure 7 displays several rate-parabolas for various data-taking periods. Included is a rate-parabola for an ideal scenario wherein the background data contains no signal whatsoever (all reactors shutdown for background collection). From the first plot in Figure 7 we see that for the canonical 400 days of data at full power and 90 days of background at half power, and for a background rate of 7 counts per day, one requires a signal rate of 21 per day in order to be able to effectively exclude oscillations down to $\sin^2 2\theta = 0.1$ after this amount of data.

References

[1] K.S. Hirata et al., **Phys. Lett. B 280** (1992) 146.

[2] G. Zacek et al., **Phys. Rev. D 34** (1986) 2621.

[3] F. Boehm, *Reactor Based Neutrino-Oscillation Experiments*, in *APS Division of Particles and Fields Fermilab Meeting* (1992).

Changes from previous document

An error in the previous exclusions was corrected (now better by 40%). Sixteen energy bins were used compared to the previous eight. Curves for zero background have been added to the exclusion plots for reference.

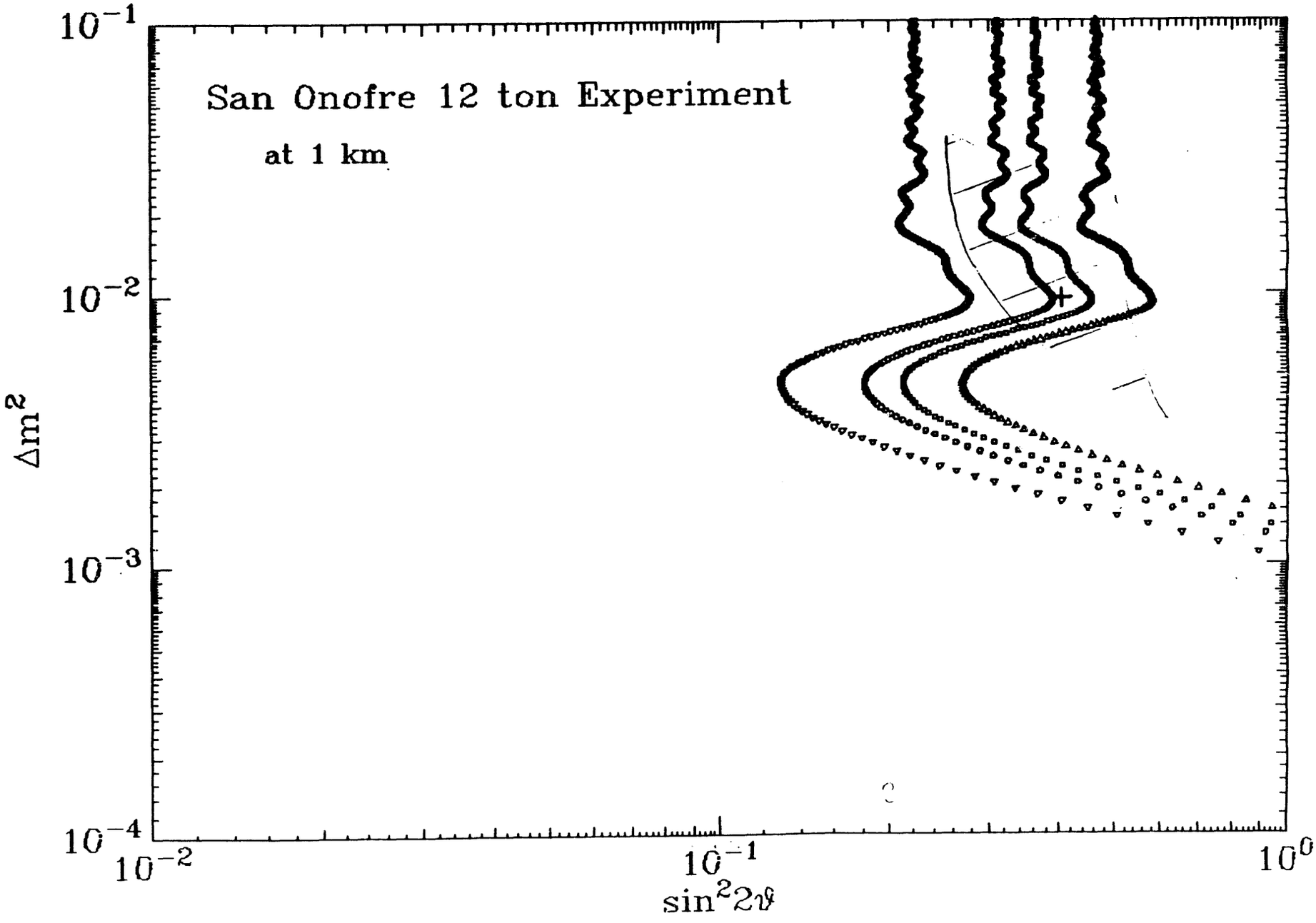
San Onofre 12 ton Experiment
at 1 km
10^{-1}
10^{-2}
10^{-3}
10^{-4}
Δm^2
10^{-2}
10^{-1}
10^{0}
$\sin^2 2\vartheta$

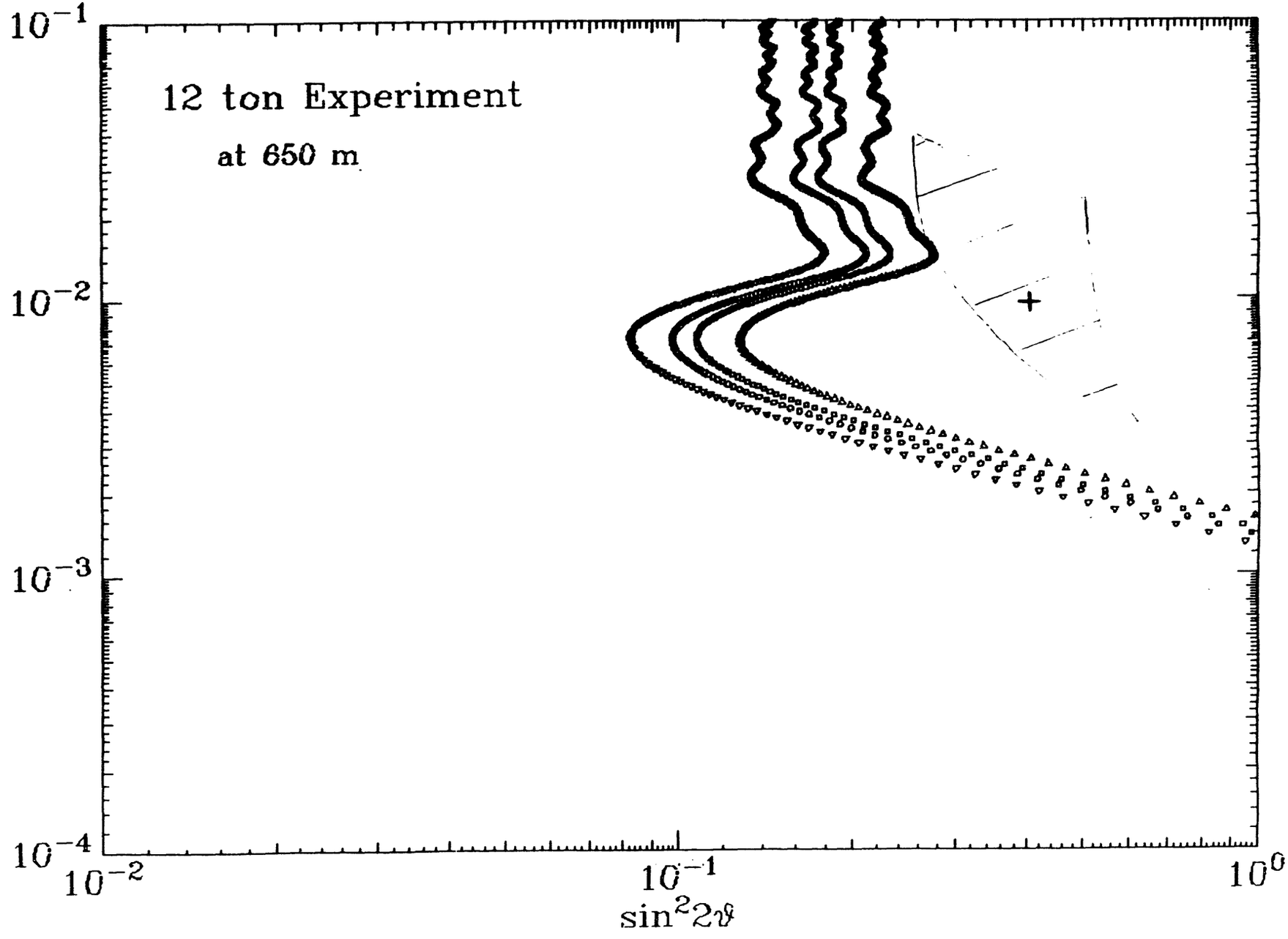
12 ton Experiment
at 650 m
10^{-1}
10^{-2}
10^{-3}
10^{-4}
Δm^2
10^{-2}
10^{-1}
10^{0}
$\sin^2 2\vartheta$

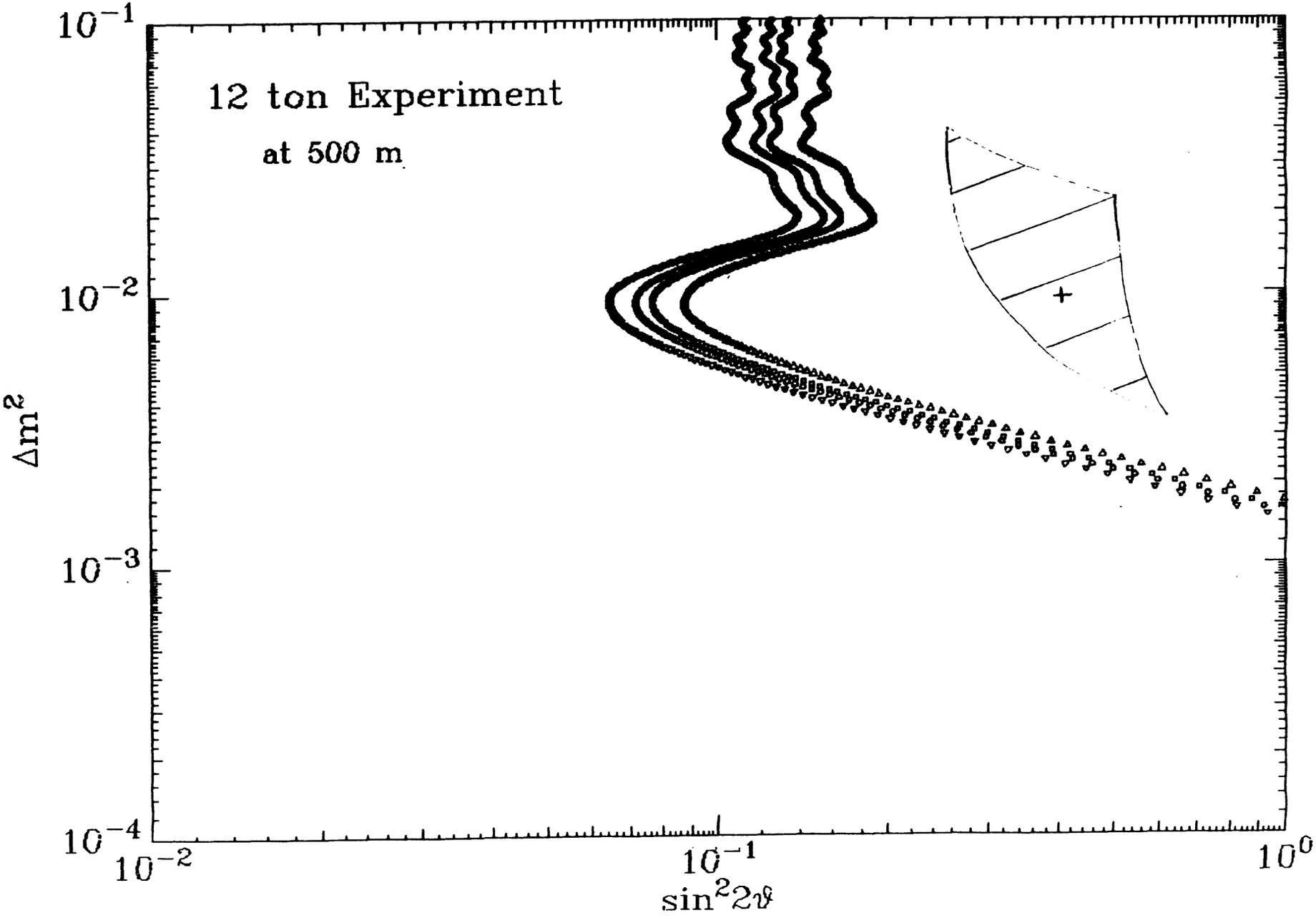
12 ton Experiment
at 500 m
10^{-1}
10^{-2}
10^{-3}
10^{-4}
Δm^2
10^{-2}
10^{-1}
10^{0}
$\sin^2 2\vartheta$

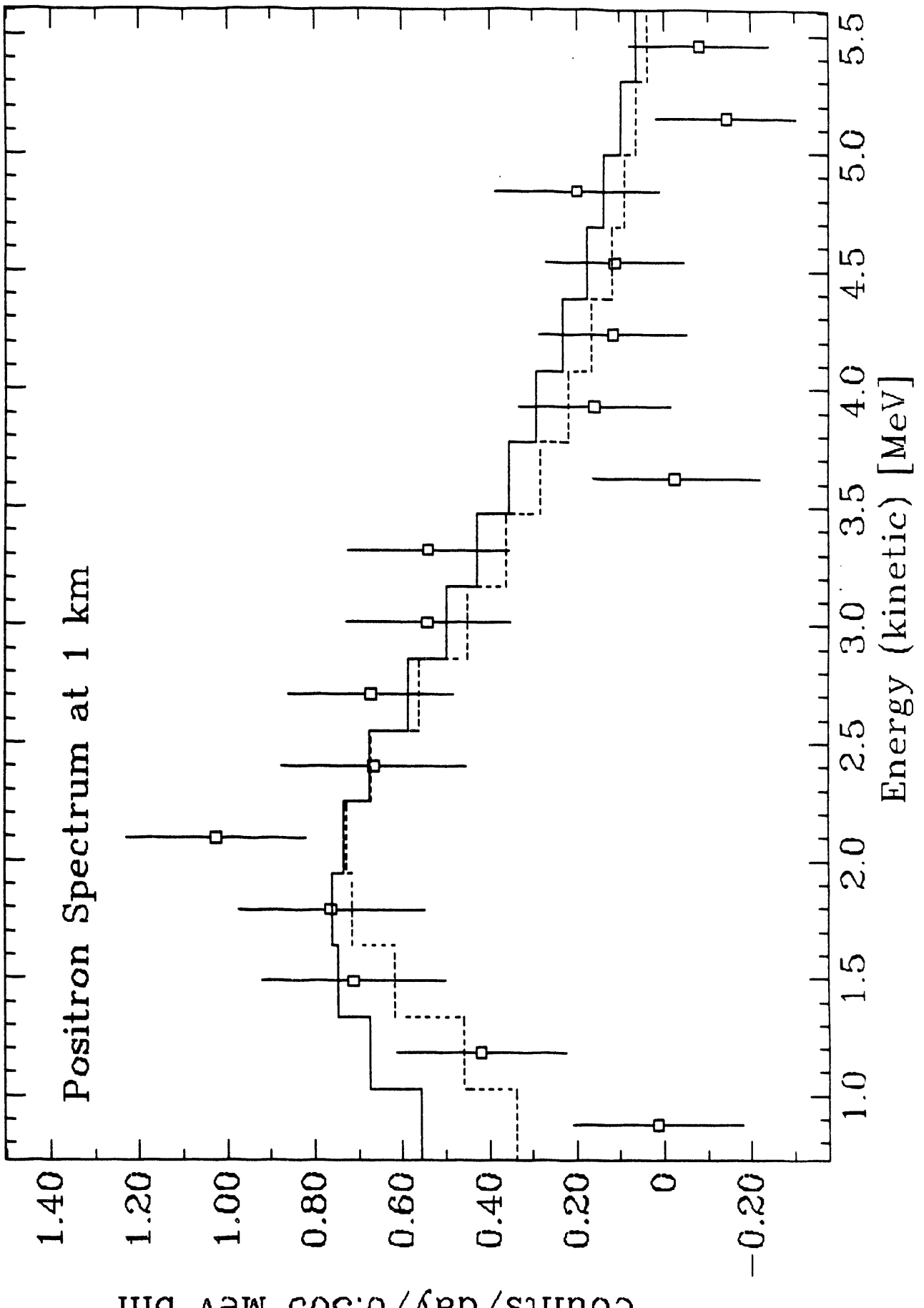
Positron Spectrum at 1 km
Counts/day/0.305 MeV bin
Energy (kinetic) [MeV]
1.40
1.20
1.00
0.80
0.60
0.40
0.20
0
−0.20
1.0
1.5
2.0
2.5
3.0
3.5
4.0
4.5
5.0
5.5

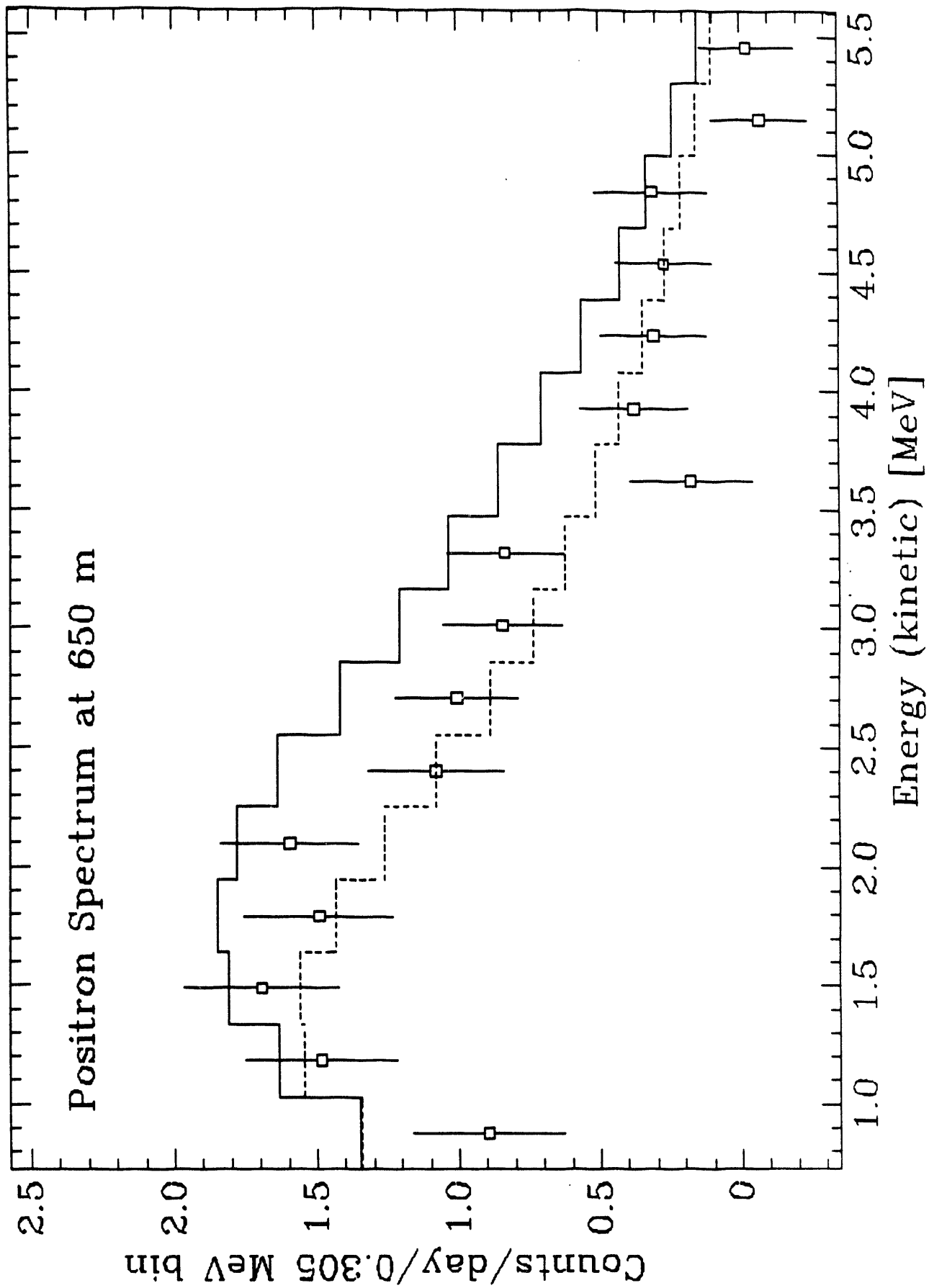
Positron Spectrum at 650 m
Counts/day/0.305 MeV bin
Energy (kinetic) [MeV]
0
0.5
1.0
1.5
2.0
2.5
1.0
1.5
2.0
2.5
3.0
3.5
4.0
4.5
5.0
5.5

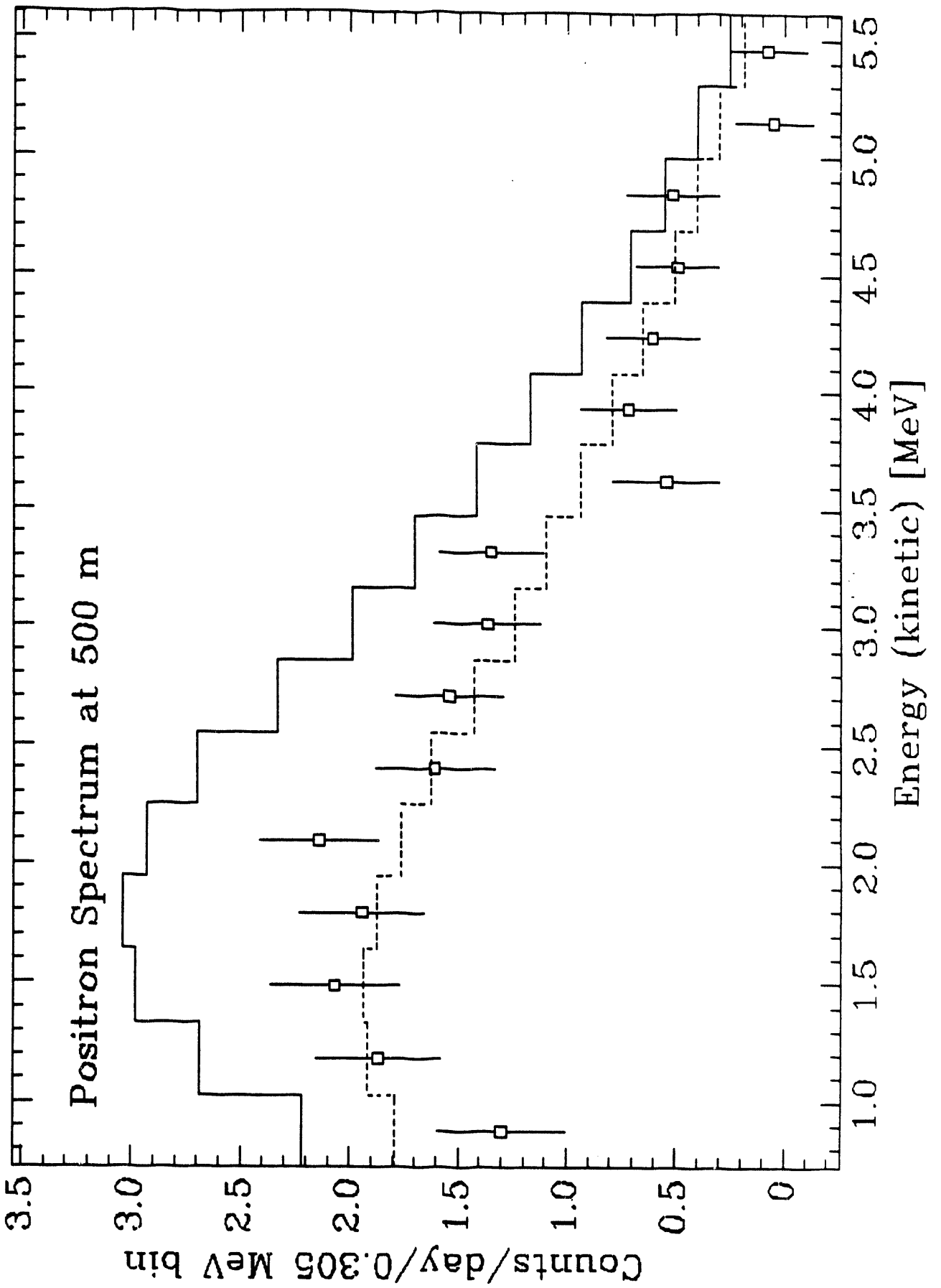
Positron Spectrum at 500 m
Counts/day/0.305 MeV bin
Energy (kinetic) [MeV]
0
0.5
1.0
1.5
2.0
2.5
3.0
3.5
1.0
1.5
2.0
2.5
3.0
3.5
4.0
4.5
5.0
5.5

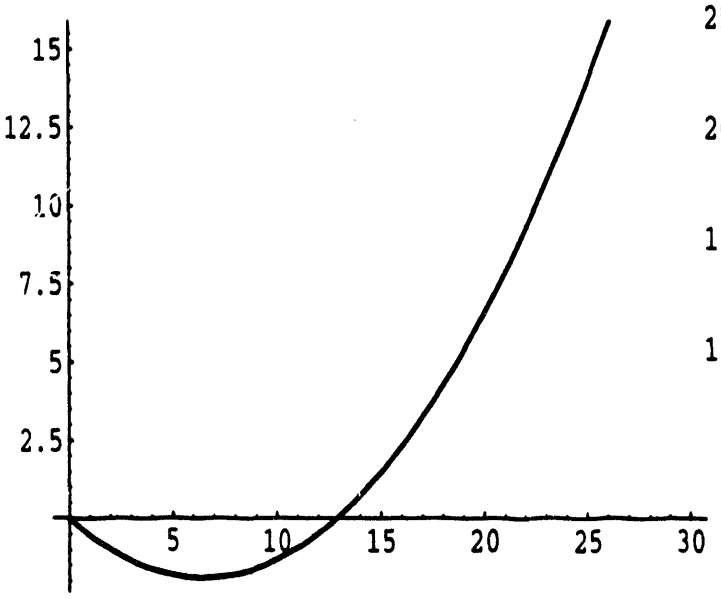

Signal: 400 days Background: 90 days

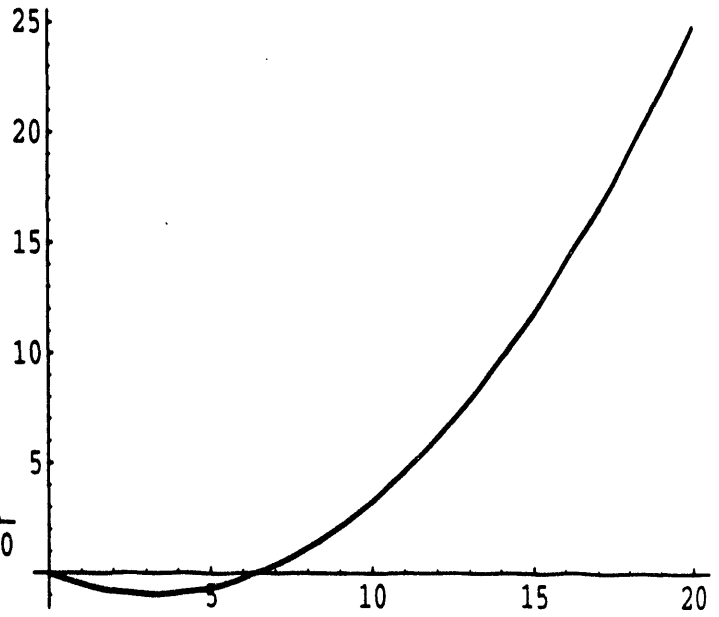

Signal: 800 days Background: 180 days

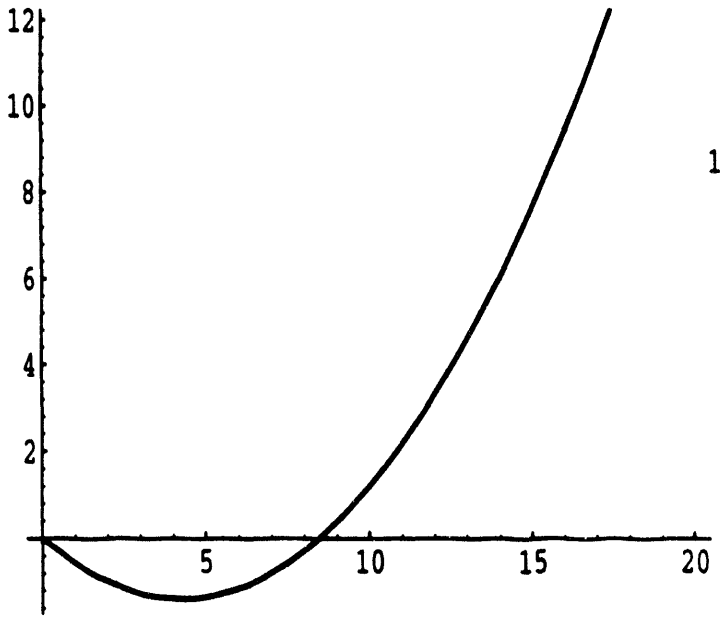

Signal: 400 days Background: 180 days

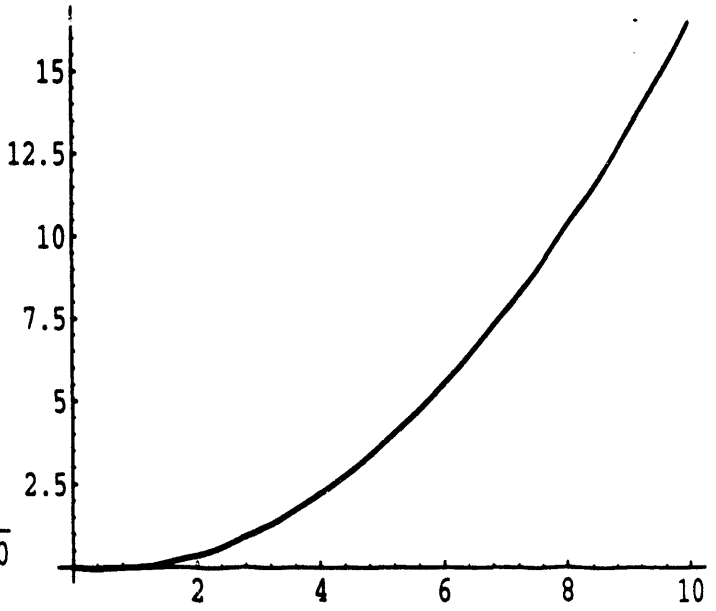

Signal: 400 days Background: 90 days

Ideal Scenario - both reactors shutdown

Figure 7 - Rate-parabolas

APPENDIX 2

APPENDIX 2

Part 1

Studies with a 2.5 Meter Long Prototype Cell

Swagato Banerjee, Chad Delany and Nicholas Mascarenhas

Introduction

Tests were initiated to study the performance of the Amperex 5 inch XP 4512 B photomultiplier tubes and the transmission length of the liquid scintillator. A realistic set-up was constructed consisting of an acrylic cell filled with liquid scintillator. We investigated the following properties:

1)Construction of the cell
2)Light Collection and Attenuation Length in a 0.5 m tall cell
3)Light Collection and Attenuation Length in a 0.25 m tall cell
4)Slewing characteristics of the PMT
5)Timing response and position reconstruction
6)Scintillator stability

1) Construction of the cell

A prototype cell was constructed using Rohm and Haas 1/4 inch thick clear UVT acrylic. We purchased a stock 8 ft long commercial grade acrylic sheet. The cell was heat deformed into shape with the help of two electrical heating strips. The protective film on both sides of the sheet was stripped along the region of the intended bend. The heating strips brought the acrylic up to its softening point and the sheet was deformed to a U shape. Appropriate spacers and clamps ensured that the U had the correct dimension (13 cm width) all along the length of the cell. After completing the bend the heaters were switched off and the acrylic allowed to reach room temperature. We inspected the sheet for crazing or signs of stress but found none. End plates were prepared out of 3/8 inch thick clear acrylic and cemented on to the U piece with Weld On acrylic cement. A lid was fabricated from aluminum. We used an inert rubber gasket to seal the lid to the cell. The lid was held in place by removable weights, this arrangement made the inside of the cell accessable from the top whenever necessary. The completed cell was 2.5 m long , 0.5 m high and 0.13 m wide. This technique could be repeated for a 9m long acrylic sheets to fabricate the cells for the San-Onofre experiment.

One or two 5-inch PMT's were installed at each end of the cell. The entire cell assembly was made light tight using Marvel Guard opaque paper. The cell was filled with a mineral oil based scintillator, 85% mineral oil, 15% pseudocumene, 3g/l PPO and 30 mg/l Bis-MSB. A green LED was used to calibrate the system. The PMTs were gain matched by adjusting the high voltage. A Na^{22} calibration source could be placed at any selected distance along the length of the cell. A third plastic scintillation counter was attached to the source and used to detect 511 keV gamma (in cascade with the 1.27 MeV

gamma ray) to make a fast 3 fold coincidence with the two PMTs on the cell. The coincidence requirement helped reject the background.

2. Light Collection and Attenuation Length in a 0.5 m tall cell

We measured the light collected as a function of the distance of the source from one end of the cell. The absolute light yield was calibrated in units of the number of photoelectrons released per unit of energy , using a green light emitting diode. Our pulse height analyser is calibrated to approximately 0.126 photoelectrons/channel (see figure 1). For a given set-up we measured the channel corresponding to the position of the Compton edge (1.06MeV), for a 1.27 MeV gamma-ray from a Na-22 calibration source.
The position of the Compton edge was plotted for each of the following cases:

i. One photomultiplier tube at one end of the cell.

ii. Two photomultiplier tubes at one end.

iii. One photomultiplier tube at each end of the cell.

i. One photomultiplier tube at one end of the cell.

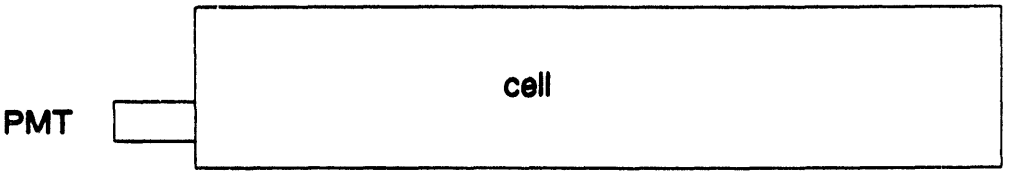

The data is well represented by a double exponential function (see figure 2) :

$Y = A\, e^{-aX} + B\, e^{-bX}$, with a $(chi)^2 = 0.429$. The fit parameters are:

A = (394 +/- 23) channels,
B = (346 +/- 19) channels,

$a = (0.023 +/- 0.002)\ (cm)^{-1}$, or 1/a = 0.43 m+/- 0.04 m

$b = (0.0016 +/- 0.0002)\ (cm)^{-1}$, or 1/a = 6.25 m +/-0.78 m ...(1).

The two exponentials are necessary to fit the large drop in light near the PMT and flatter variation away from it. The transport of light in the tank has been modelled and agrees well with the measurement. The reason for the 2 characteristic attenuation lengths seen is as follows. The attenuation length of the scintillator is a strong function of wavelength. For shorter wavelengths the attenuation length is smaller. In general there is more light produced at short

wavelengths (400nm-430nm) than at longer wavelengths > 430 nm. Near the PMT (or an end) the abundant short wavelength light makes it to the PMT and the effective attenuation length measured is characteristic of this light $\lambda \sim 1$ m. Away from the end the collected light is depleted of the short wavelength component and one measures a characteristic λ of about 6 m. It is far region which is of importance for the San-Onofre experiment, because this is our fiducial volume.

ii. Two photomultiplier tubes at one end of the cell.

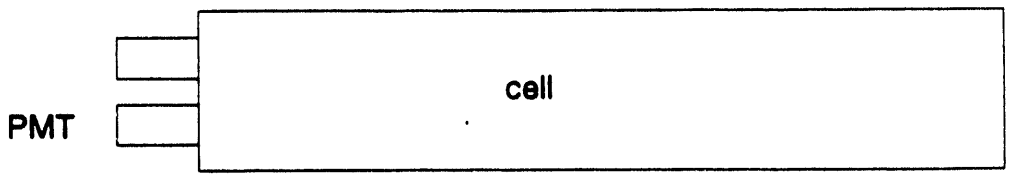

The same experiment is now repeated with two PMTs on one side of the cell (see figure 2). In this case one expects the overall curve to be twice in amplitude as in i. With similar attenuation lengths. The fit yields $(chi)^2 = 0.716$. The fit parameters are:

A = (623 +/- 21) channels,
B = (605 +/- 17) channels,
$a = (0.0148 +/- .0008)\ (cm)^{-1}$, or 1/a = 0.67 m +/- 0.04
$b = (0.0014 +/- .0001)\ (cm)^{-1}$, or 1/a = 7.14 m +/- 0.51 ... (2).

iii. One photomultiplier tube at each end of the cell.

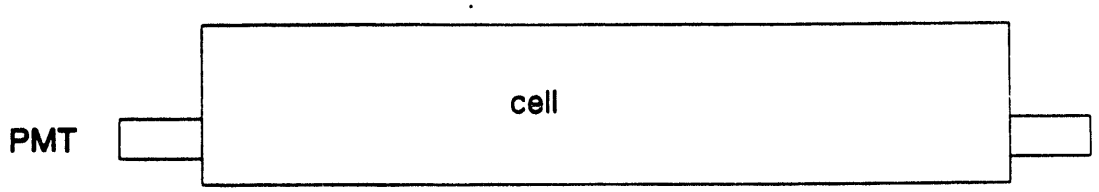

We summed the signal from each end of the cell. (see figure 3) The fit is again a double exponential fit, but of the form :
$Y = A\ e^{-aX} + B\ e^{+bX}$, as opposed to having two decaying exponentials in i and ii. A $(chi)^2$ of 1.726 was obtained. The fit parameters are:

A = (656 +/- 21) channels,

B = (217+/- 17) channels

a = (0.008 +/- 0.0006) $(cm)^{-1}$, 1/a = 1.25 m +/- 0.1 m

b = (0.005 +/- 0.0003) $(cm)^{-1}$, 1/a = 2.00 m +/-0.12m

Summary

Case (i) -

The attenuation lengths near the end is 0.43 m and away from the end is 6.25 m

Predicted light output at the end of a 8 m long cell: (96 +/- 16) channels or 12 photoelectrons/MeV.

Case (ii) -

The attenuation length is 0.67 m near the end and away from the end is 7.14 m.

The predicted light output at the end of a 8 m long cell is (197 +/- 17) channels or 24.8 photoelectrons/MeV (with this scintillator). In the 9m long experimental cell, 0.8m near each end is a buffer region. It is in this region where the largest variation in light output is

Case(iii) -

The variation in light collected from the middle to each end is about 24%.

3. Light Collection and Attenuation Length in a 0.25 m tall cell

We repeated the study in section 1 with only 25cm of scintillator in the cell. Here one can have just one PMT per side. This LED calibration for this set-up gives approximately 0.076 photoelectrons/ channel. The Compton edge (1.06 MeV) of a Na^{22} source at the center of the cell is at (646 +/- 30) channels. This gives 49 photoelectrons/MeV detected at the PMT.

(The cell was refilled to a height of 50 cm with scintillator and the Na^{22} Compton edge was then at (430 +/- 12) channels. In comparison this gives 32 photoelectrons/MeV detected.)

i. One photomultiplier tube at one end of the cell.

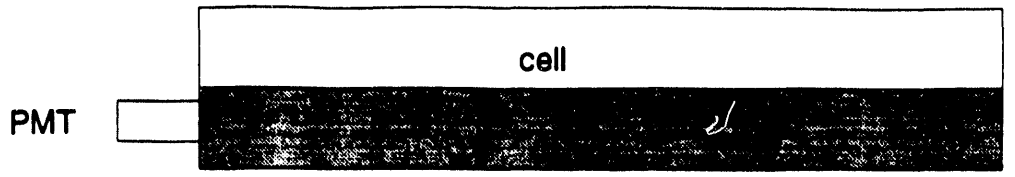

The results of an experiment with one photomultiplier tube at one end of the cell are shown in figure 5. A double exponential fit of the form :

$Y = A\,e^{-aX} + B\,e^{-bX}$ gave a $(chi)^2$ of 0.936. The fit parameters are:

A = (337 +/- 26) channels,

B = (322 +/- 25) channels,

a = (0.0048 +/- 0.0008) $(cm)^{-1}$, 1/a = 2.08 m +/-0.09m

b = (0.0024 +/- 0.0004) $(cm)^{-1}$. 1/a = 4.16 m +/-0.52m.... (3).

ii. One photomultiplier tube at each end of the cell.

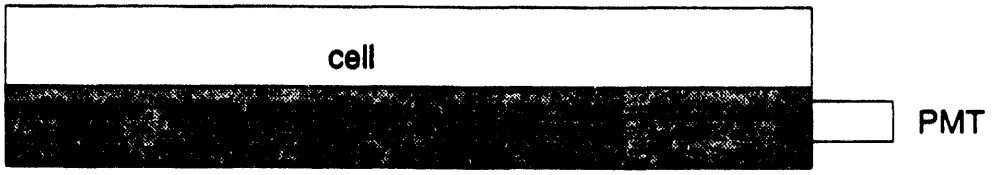

The results of the experiment with the other photomultiplier tube at the other end of the cell are shown in figure 6. This fit is also a double exponential fit of the above form with $(chi)^2 = 1.2648$. The fit parameters are:

A = (310 +/- 23) channels,

B = (314 +/- 21) channels,

a = (0.0039 +/- 0.0007) $(cm)^{-1}$, 1/a = 2.56 m +/-0.35m

b = (0.0017 +/- 0.0004) $(cm)^{-1}$. 1/a = 5.88 m +/-0.69m... (4).

Conclusion

1.) In the 0.25 m tall cell one sees as much light with one PMT per side as with a 0.5m cell with 2 PMTs per side.

Case (i) - one photomultiplier tube (right end of the cell) :
attenuation lengths : 2.08 m and 4.16 m;

Case (ii) - the other photomultiplier tube (left end of the cell):
attenuation lengths : 2.56 m and 5.88 m;

2.) For 50 cm of liquid in the cell each PMT collects 1.5 photoelectrons at a 50 keV threshold. 4 PMT's on the cell will collect 6 photoelectrons with all signals summed up.

For 25 cm of liquid in the cell each PMT collects 2.4 photoelectrons at a 50 keV threshold. 2 PMT's on the cell will collect 4.8 photoelectrons with the signals summed up.

4. Slewing characteristics of the PMT

Purpose

We measured the timing *vs.* pulse height slewing of the Phiiips XP 4512 B photomultiplier tubes in the 0.5m tall cell.

Experiment

The experimental set-up (see schematic below) was such that the two photomultiplier tubes at the two opposite ends of the 2.5 m cell detect the light from a 1.17 MeV or 1.33 MeV gamma ray (via Compton Scattering). The two photomultiplier tube signals were each fed to a 30 mV discriminator and then to a coincidence module. Another (plastic) scintillator PMT 3 was placed at the source so as to detect the other (1.33 MeV or 1.17 MeV) gamma ray from the Co^{60} source. Thus, all the three photomultiplier tubes were in coincidence.

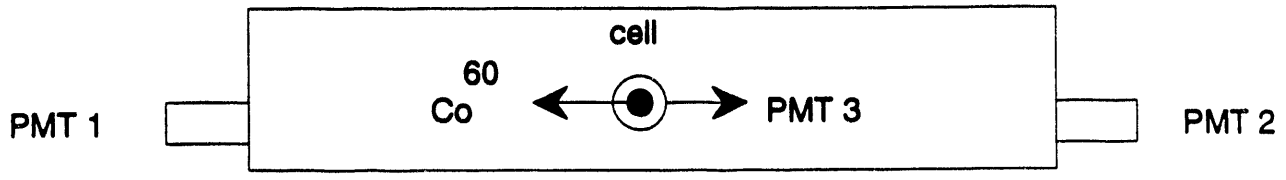

The photomultiplier tube marked PMT 2 in the schematic was programmed to detect the events occurring between 300 to 350 channels, i.e. a fixed energy window at an energy of 567keV. The photomultiplier tube marked PMT 1 in the schematic above was set-up to measure energies from zero to 700 keV in windows of 20 channels (~35 keV). PMT 3 completed the coincidence between all three PMTs and the coincidence started a TDC. The discriminator signal from PMT 1 stopped the TDC. It is this time difference (start - PMT 1)

which should show a slewing dependance of timing *vs.* pulse height.

Due to Compton scattering the detected photons have a spectrum of energies in the above-mentioned range, the lower ones having a steeper angle of collisions with electrons during the Compton scattering. Multiple scattering also results and another effect to take into consideration are the multiple reflections of the photons before and after Compton scattering prior to being detected by the photomultiplier tubes. The effect of slewing is the time response of the photomultiplier tube as a function of the amount of light the photomultiplier tube is exposed to.

Results

The time difference versus the energy of the signal detected by PMT1 is shown in figure 7. Our experiment shows a very small variation of 0.6ns in the time response of photomultiplier tube over an energy variation of about 0.5 MeV. This corresponds to a position uncertainty of 4.45 cm, which is quite small compared to 2.5 m long cell.

5. Timing Response and position reconstruction

Purpose

We measured the uncertainty timing of the Phillips XP 4512 photomultiplier tube as a function of the position of the gamma ray in the 0.5m cell. This study was performed for different energies.

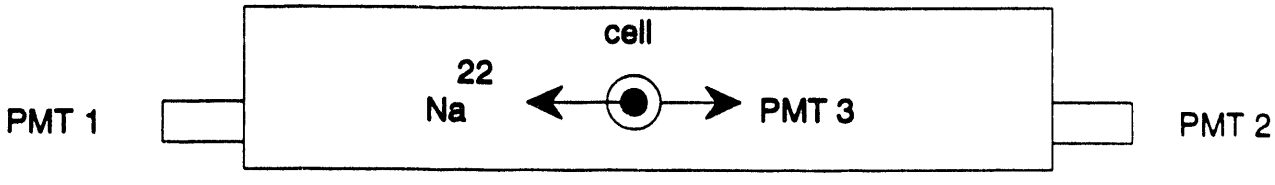

Calibration

Using a Na^{22} -source we calibrated the energy scale and matched the gains of the PMT. A calibrated delay box was then used to calibrate the TDC to 5.6 channels/ns.

Timing study for fixed energy

The Na^{22} source emits two coincident 0.511 MeV and 1.27MeV gamma rays. We trigger the detector when one gamma ray enters the cell and

the other enters a scintillation counter (PMT 3) placed near the source outside the cell. The signal from the photomultiplier tubes on the two ends of the tank (PMT1 and PMT2) is summed and the time difference between PMT1 and PMT2 is histogrammed for bins of energy 50 channels (~58 keV) wide. From the full width at half maximum of the distributions in each histogram, the uncertainty in timing response, i.e. sigma (t) of the photomultiplier was calculated.

We studied the timing response in two energy windows : one at 1.06MeV and the other at 200keV (where one had good statistics). This was repeated for different distances from the end of the cell. Then we studied the uncertainty in timing as a function of distance from one end of the cell.
Figure 8 shows the mean time difference as a function of distance for 200 keV. Figure 9 shows the uncertainty in the time difference (sigma tdiff) as a function of distance for 200 keV. These quantities were measured at 1.06 MeV and are shown in Figure 10 and Figure 11.

Conclusion

It is found that the uncertainty in timing is small (less than 1.6 ns) at 200 keV at all positions in the tank. This uncertainty is better than 1 ns at 1.06 MeV. One can convert the timing error to a position error which is summarized in the table below.

	Mean	Range
a. Uncertainty in timing response:		
(i) at constant energy (200 keV)	0.96 ns	1.18 ns.
(ii) at constant energy (1.06 MeV)	0.7 ns	0.56 ns
b. Uncertainty in position measurement:		
(i) at constant energy (200 keV)	8.36 cm.	10.27 cm.
(ii) at constant energy (1.06 MeV)	6.07 cm.	4.86 cm.

6. Scintillator stability

During the course of the studies described learned about the stability of this scintillator mix. The tank was filled to 50 cm of liquid and run for about a couple of months. Then the scintillator was drained out to have a 25 cm tall liquid. Again studies were repeated for a month. Finally the tank was refilled to 50 cm. Over the course of these changes no systematic shift was seen in light output (error about 20 %). The attenuation length measurements were repeated for each set-up after a week and the attenuation length was stable. More importantly the acrylic tank showed no signs of crazing. No leak developed in any of the cemented joints. After a year the tank remains filled with scintillator and the liquid appears very clear. From these observations it can be concluded this mix of scintillator is not aggressive to the acrylic and is quite stable.

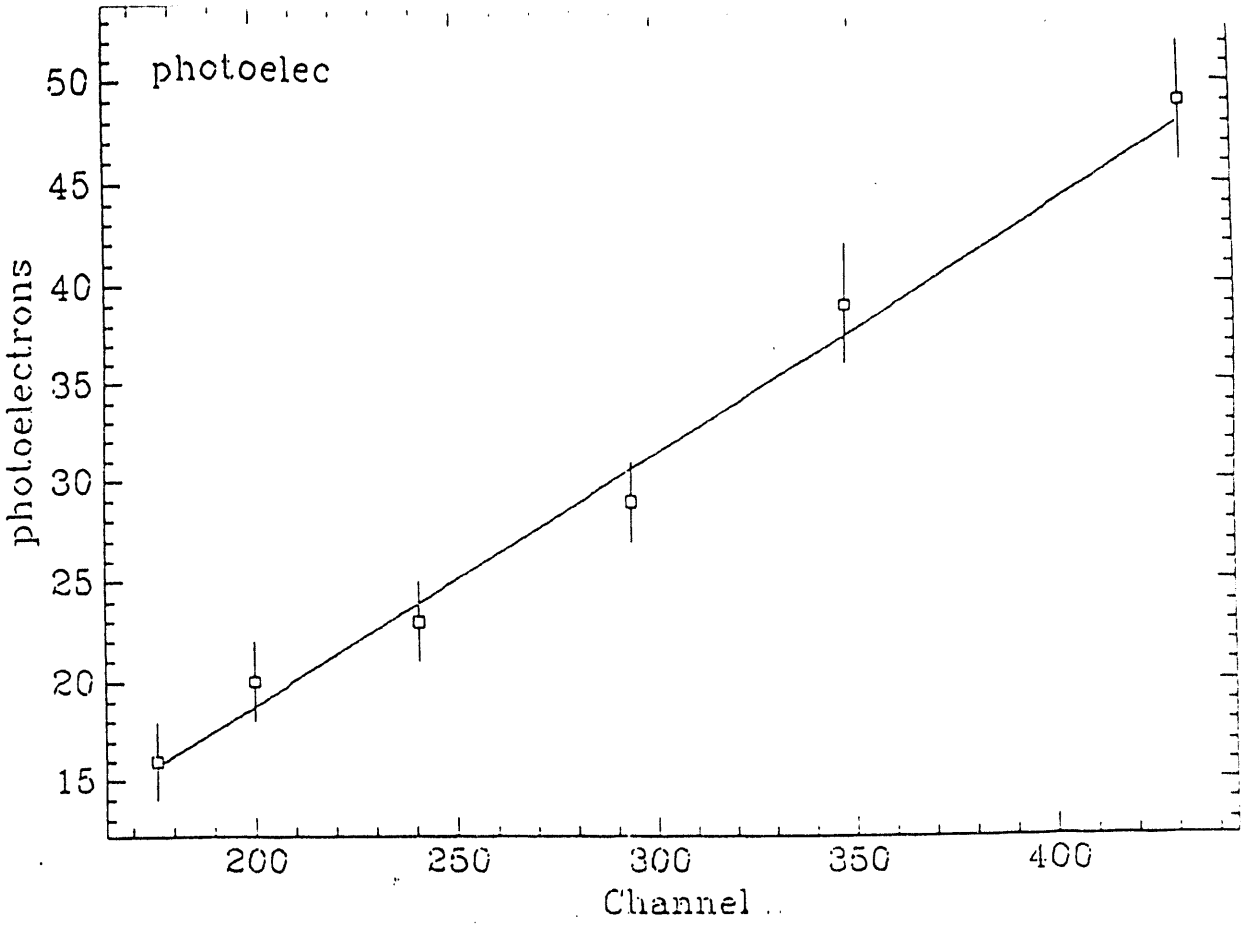

Figure 1

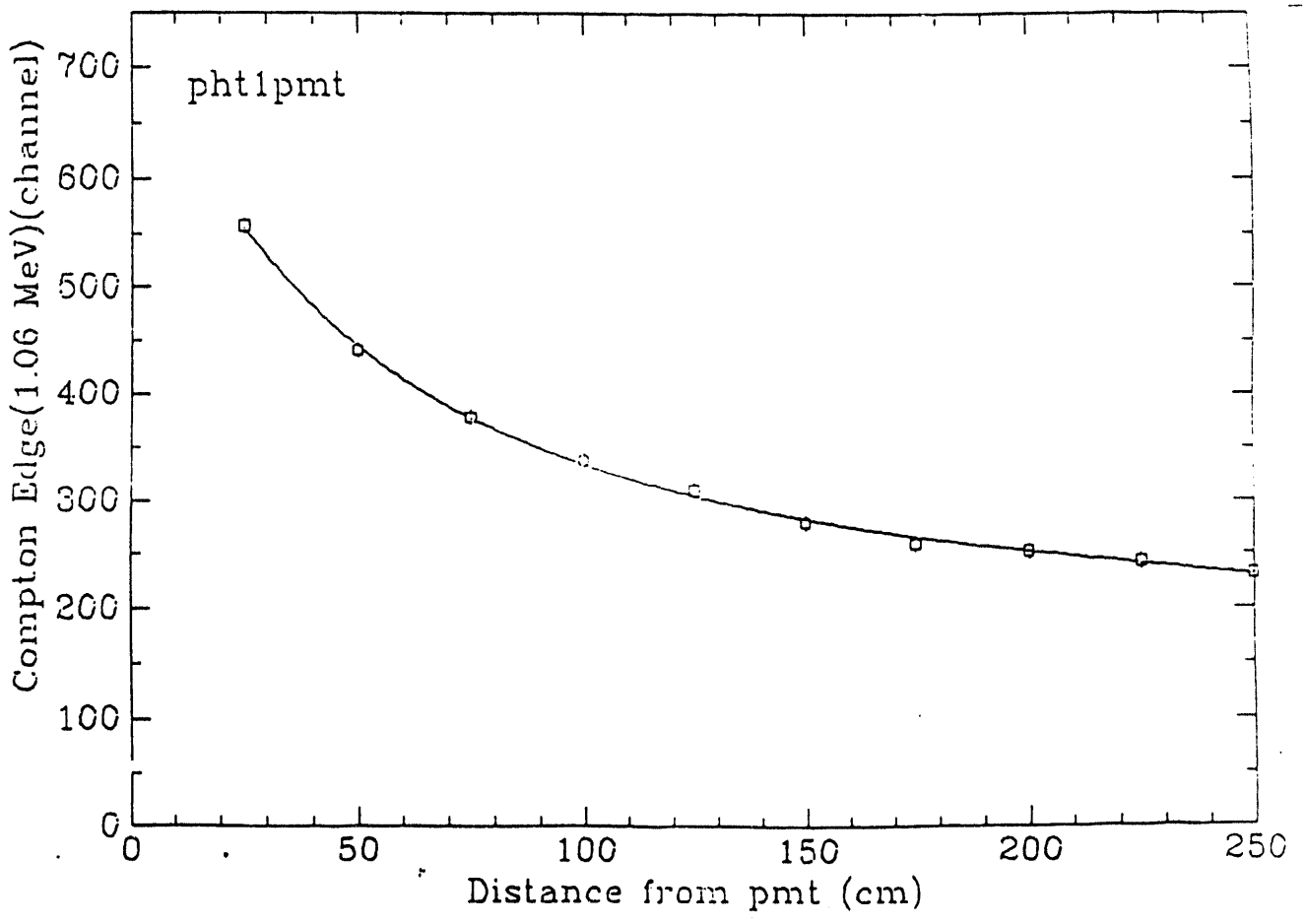

Figure 2

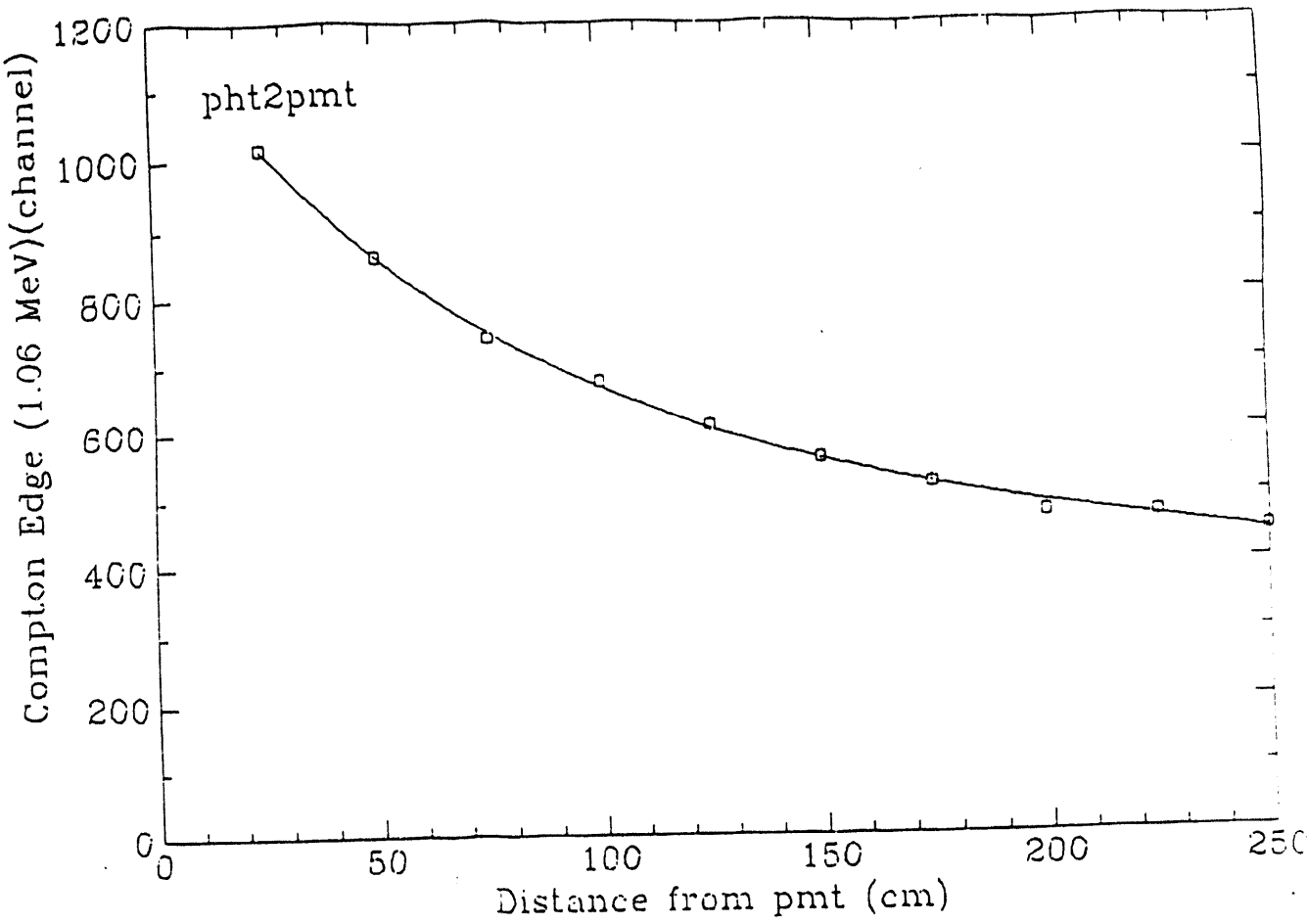

Figure 3

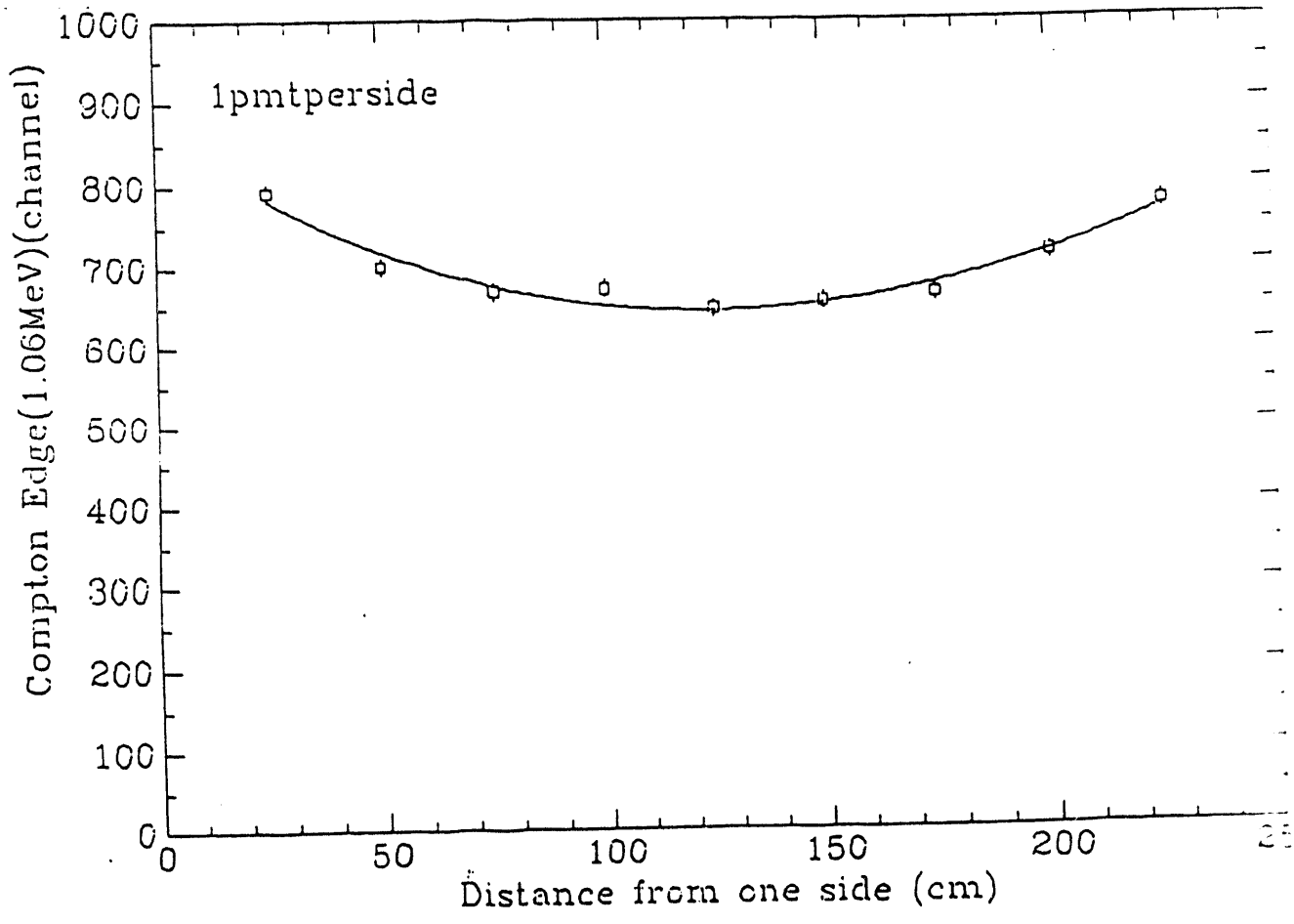

Figure 4

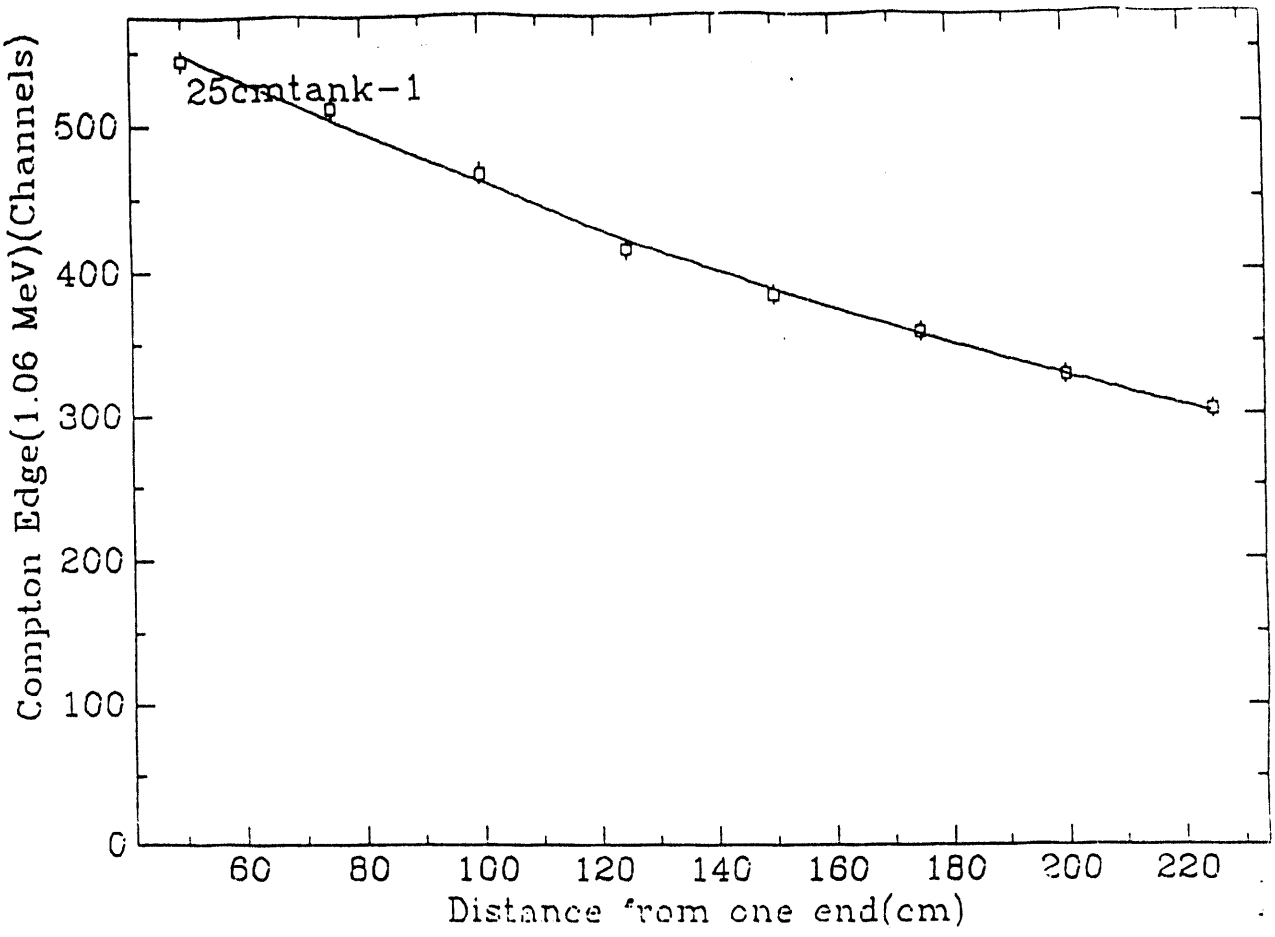

Figure 5

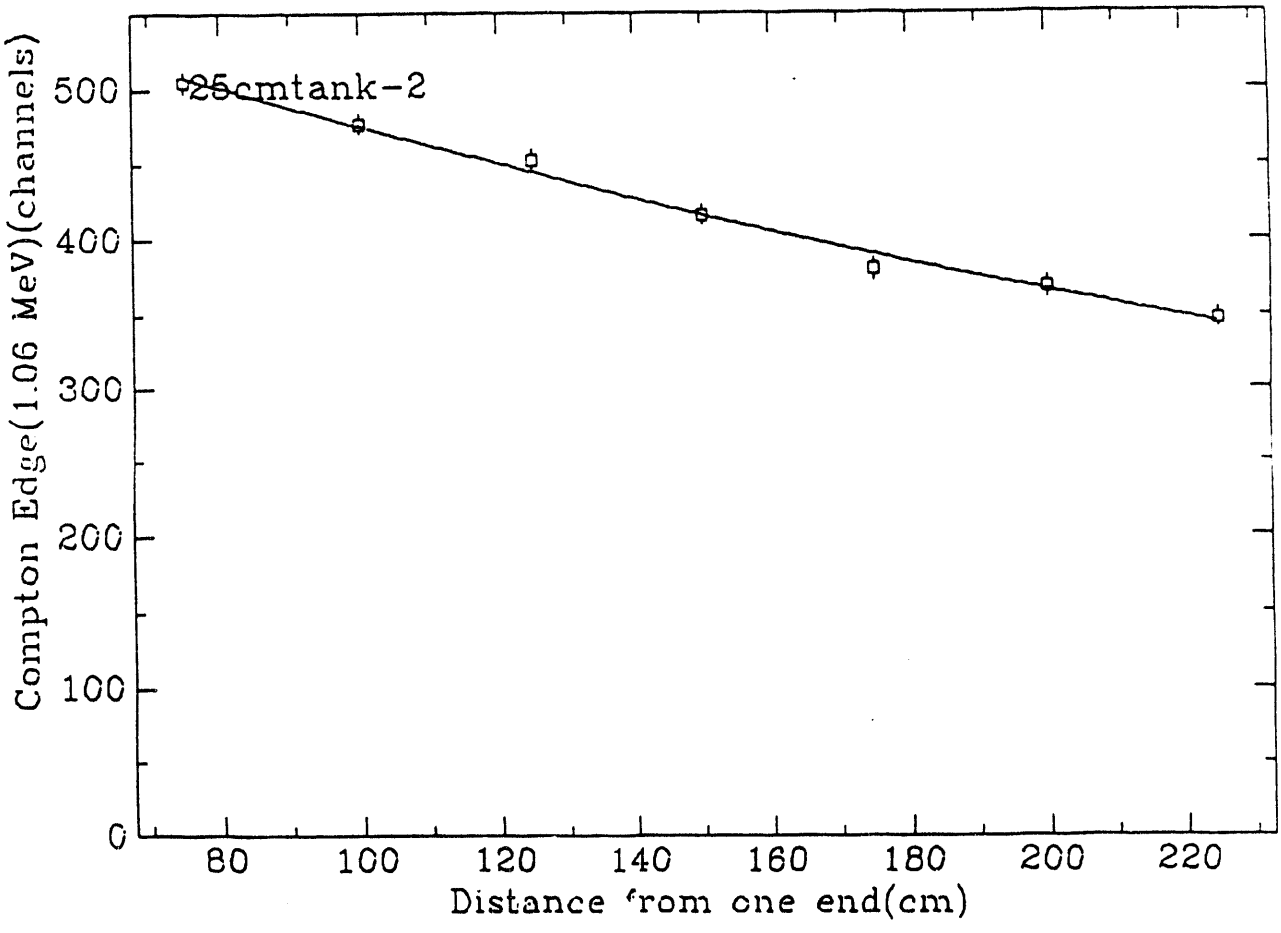

Figure 6

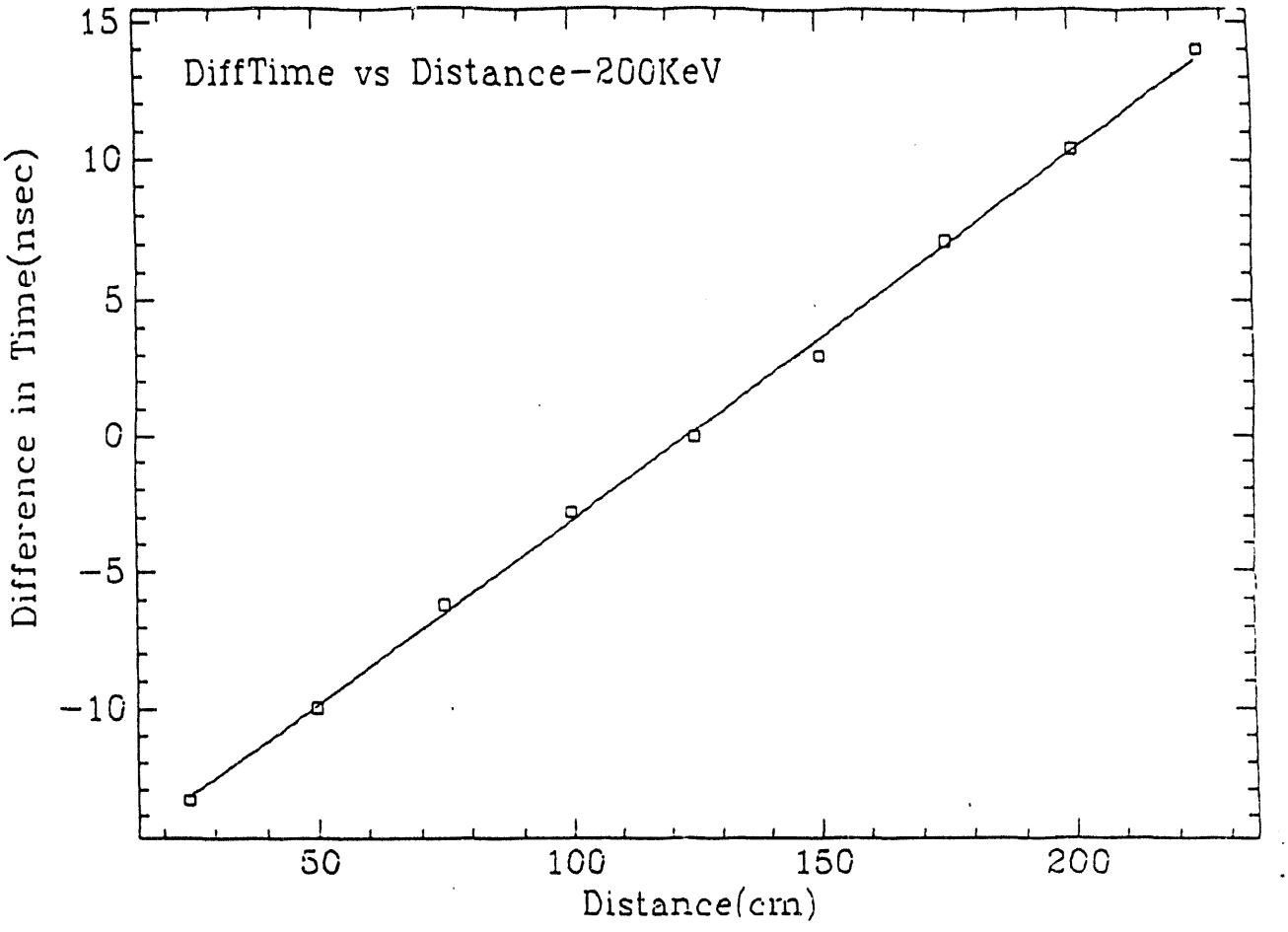
DiffTime vs Distance-200KeV
Difference in Time(nsec)
15
10
5
0
-5
-10
50
100
150
200
Distance(cm)

Figure 7

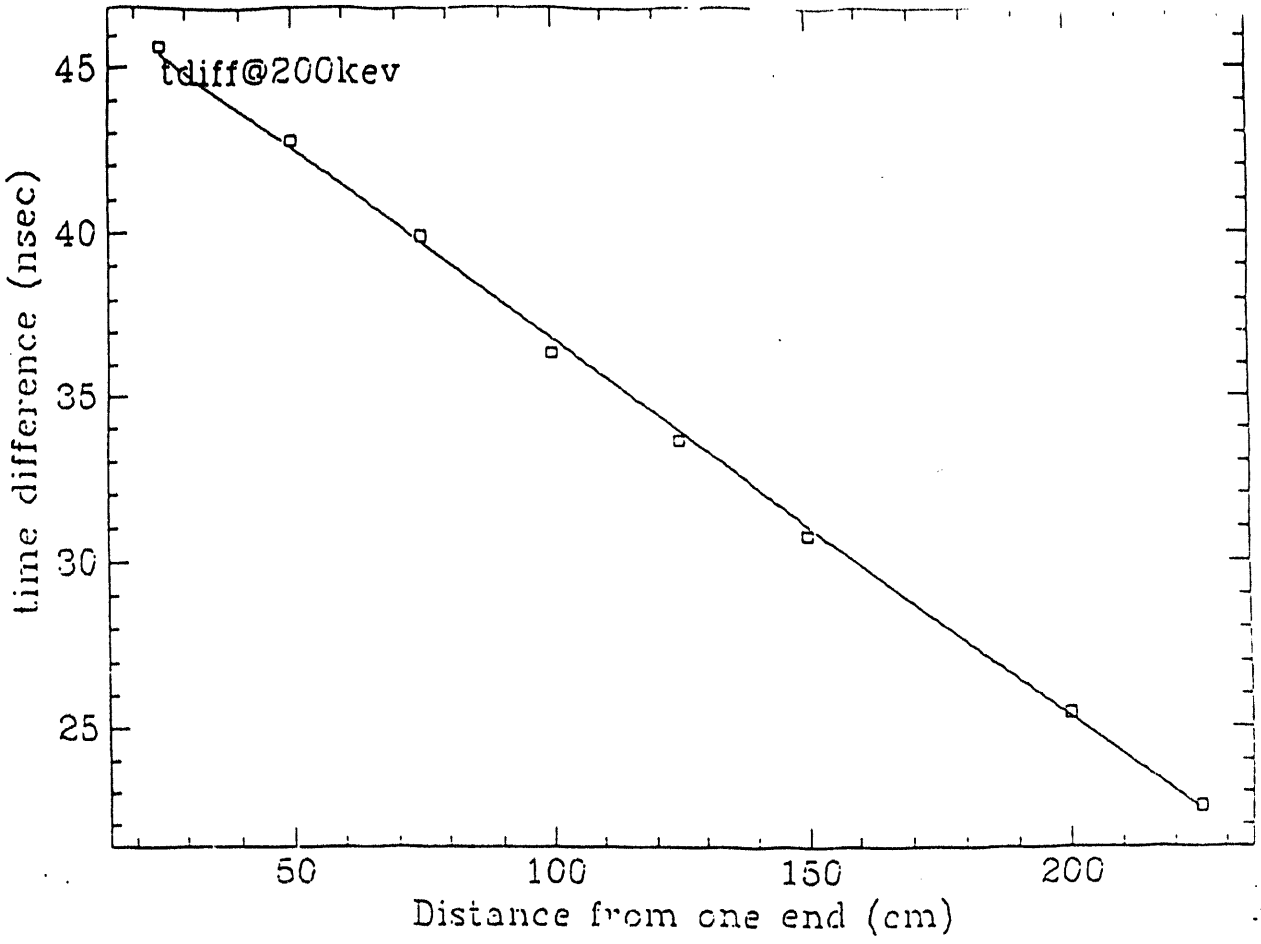

Figure 8

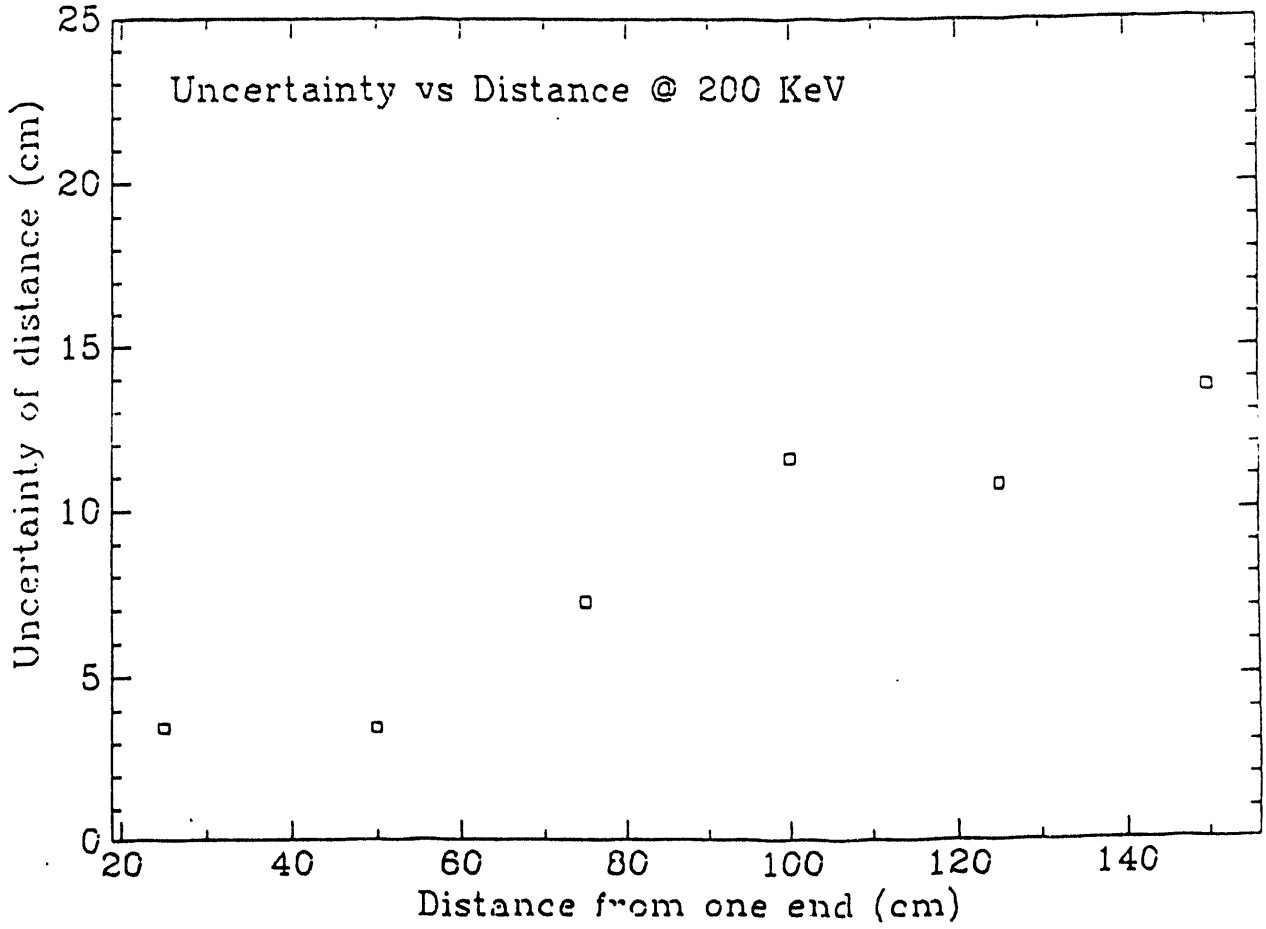

Figure 9

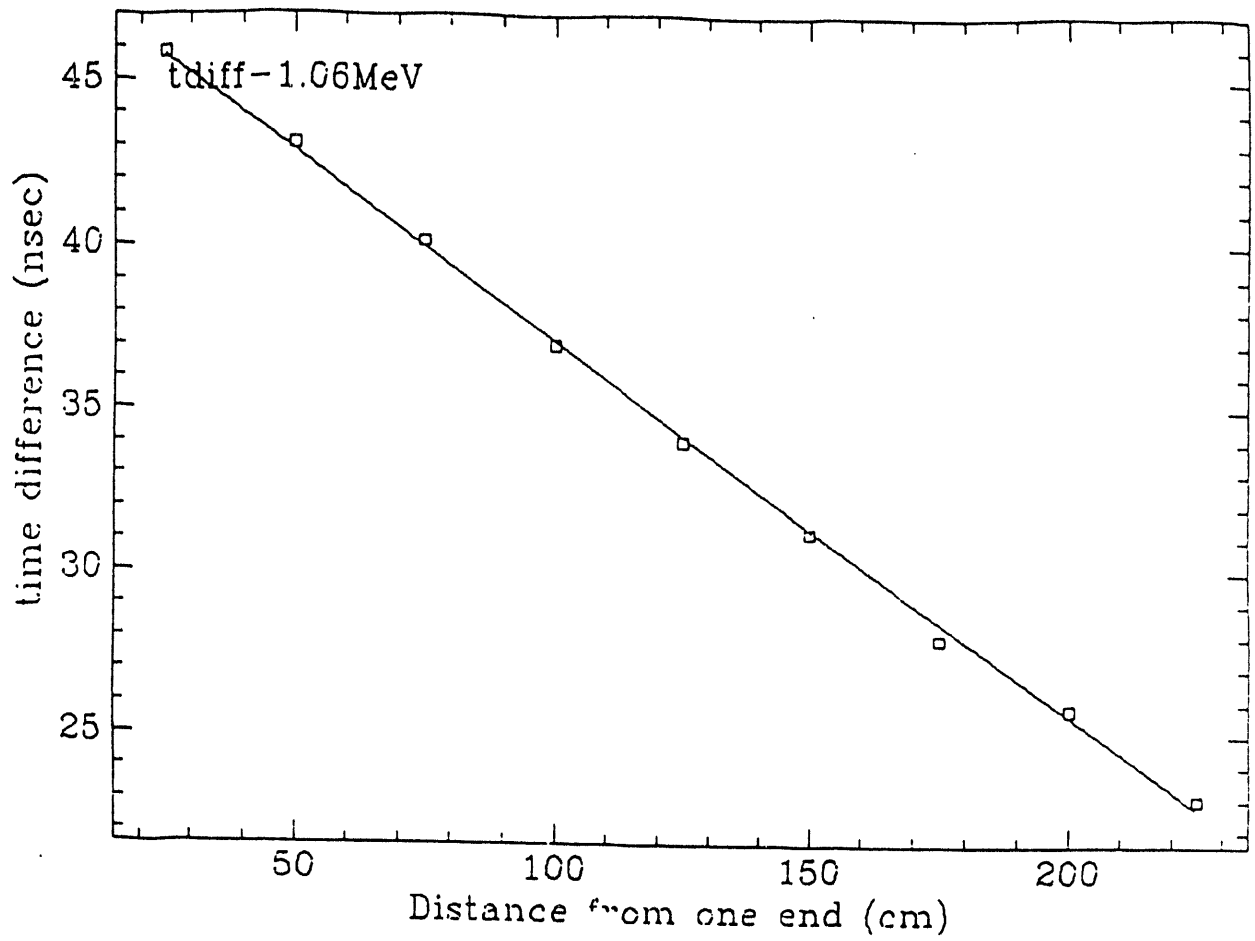

Figure 10

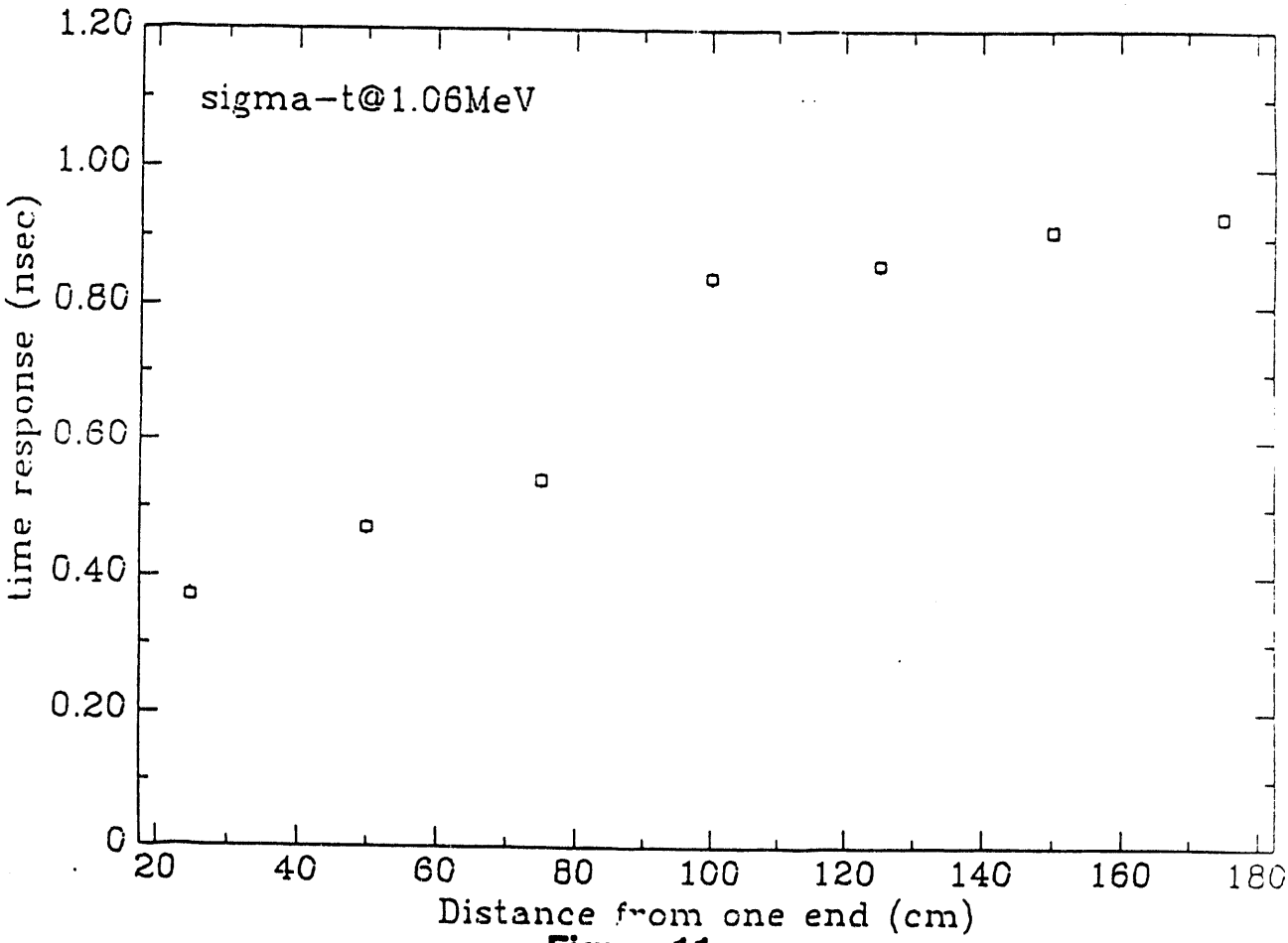

Figure 11

APPENDIX 2

Part 2

Light Attenuation Length of Some Liquids

V. Novikov
(April 8, 1993)

All measurements were performed with 440 nm filter. Most results in Table 1 were obtained recently; some old data are presented for comparison. Approximately, errors do not exceed 5% of the value for $\lambda \leq 5$–10 m and smaller for higher attenuation length.

	Liquid	λ, m
	Min. oil (M.O.), Pseudocumene (PC)	
1	M.O. Britol 6NF	19.5
2	M.O. Carnation	3.6
3	PC	5.1
4	M.O. 6NF + 15% PC	17.5
	M.O. + 15% PC + "x" g/l of PMP	
5	PMP original (3 g/l)	10.
6	PMP via US Merck (3 g/l)	4.7
7	US Merck PMP purif. by Gusten (3 g/l)	7.5
	Gd scintillators	
8	Sample A	3.7
9	Sample B	2.2
10	Sample C	2.2
11	NE 344a, "opened"	2.9
12	NE 344a, "sealed"	4.7

Table 1. Attenuation length of some liquids.

Mineral oil **Carnation** was considered as alternative to Britol 6NF; this is not good idea due to its small attenuation length. Attenuation length of the mixture of **M.O. + 15% PC** droped to 11.1 m in 10 days (presumably, due to poisoning caused by presence of PC). Gd-loaded scintillators **Sample A, Sample B, Sample C** were prepared in the laboratory ~3 years ago (content of Gd is unknown). Gd-loaded scintillators **NE344a "opened"** and **NE344a "sealed"** were prepared by dilution in 3 times of NE344a scintillator by mixture M.O. 6NF + 15% PC (i.e., Gd content was reduced from 0.3% to 0.1%); NE344a scintillator was taken from opened and sealed bottles, respectively.

Data always fit well to exponential function; Figs.1-3 show results of measurements of some liquids.

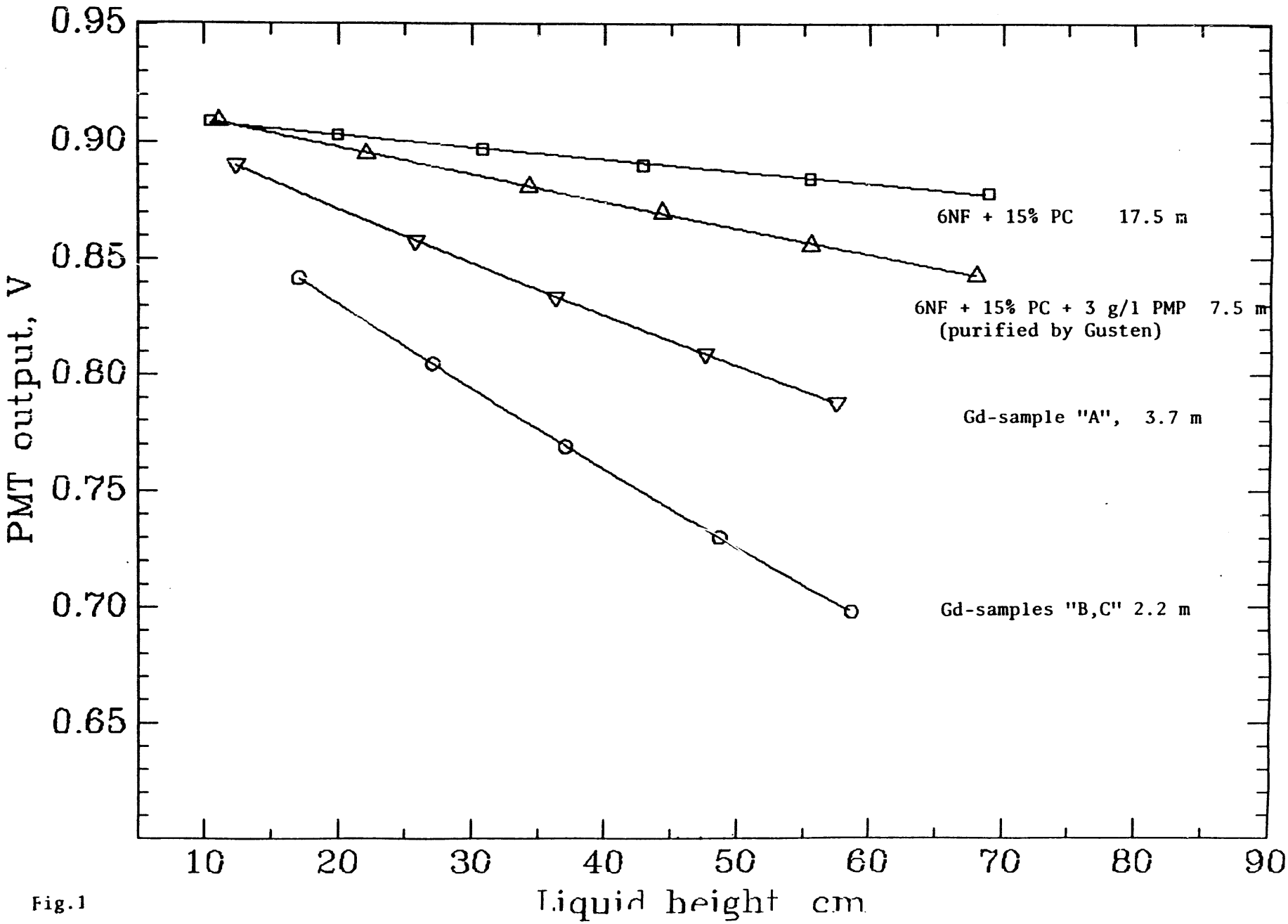
0.95
0.90
0.85
0.80
0.75
0.70
0.65
PMT output, V
10
20
30
40
50
60
70
80
90
Liquid height cm
6NF + 15% PC 17.5 m
6NF + 15% PC + 3 g/l PMP 7.5 m
(purified by Gusten)
Gd-sample "A", 3.7 m
Gd-samples "B,C" 2.2 m

Fig.1

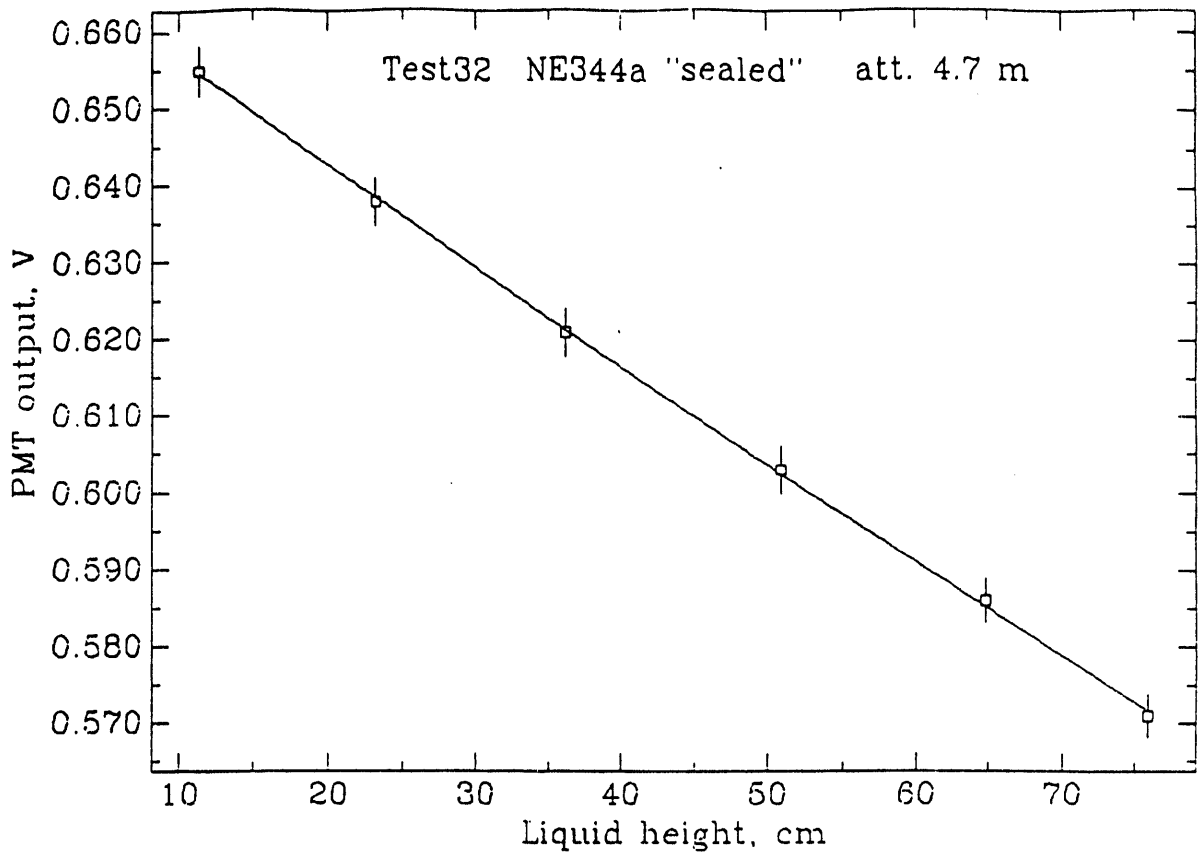
Test32 NE344a "sealed" att. 4.7 m
PMT output, V
0.660
0.650
0.640
0.630
0.620
0.610
0.600
0.590
0.580
0.570
10
20
30
40
50
60
70
Liquid height, cm

Fig.2

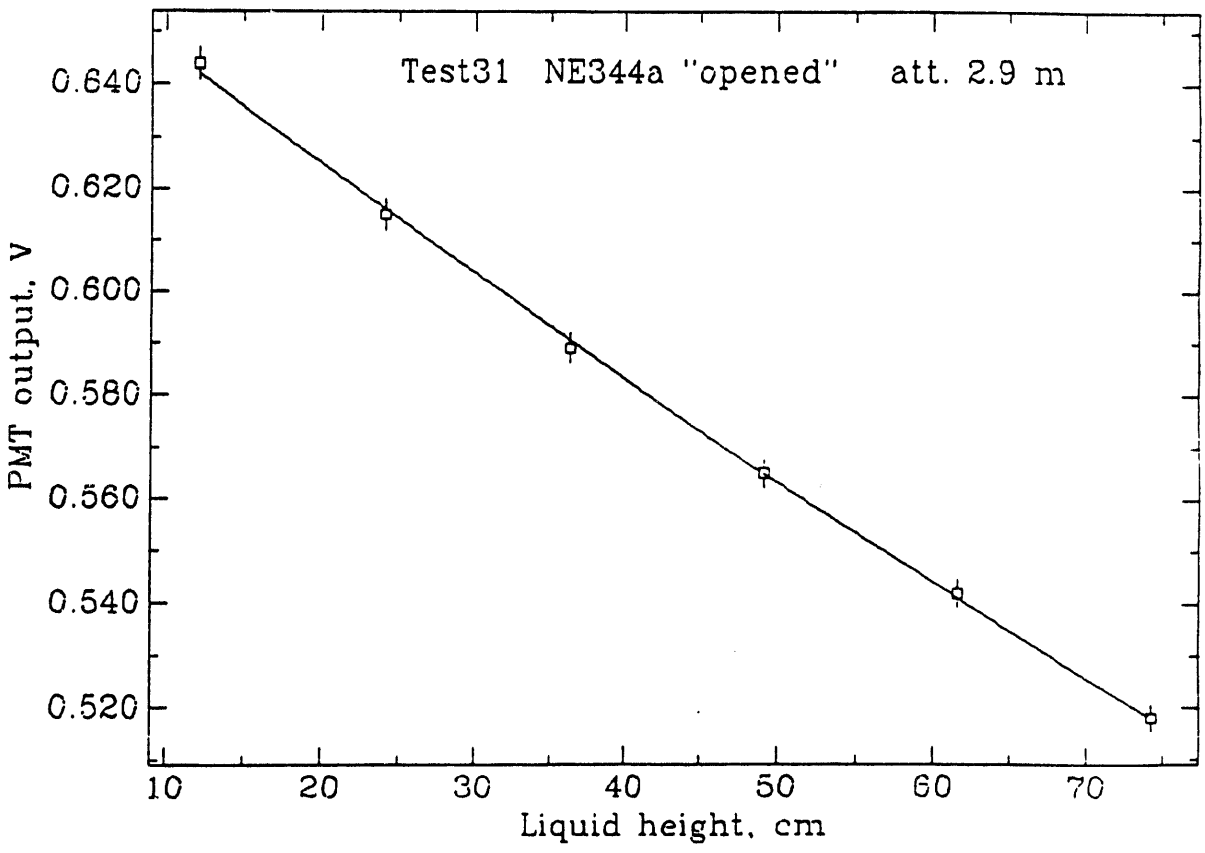
Test31 NE344a "opened" att. 2.9 m
PMT output, V
0.640
0.620
0.600
0.580
0.560
0.540
0.520
10
20
30
40
50
60
70
Liquid height, cm

Fig.3

APPENDIX 2

Part 3

Light-yield and attenuation length of a mineral oil based scintillator

Nicholas Mascarenhas and Vladimir Novikov

Light Yield (N. Mascarenhas)

A measurement of the light-yield of scintillator mix prepared in our laboratory shows that a candidate scintillator can be prepared with good light yield ~ 60 % of anthracene using 2 types of wavelength shifters 1)PPO, Bis Msb 2) PMP.

The apparatus

We prepared about 100 ml of scintillator mix in a glass beaker. The components: Britol 6NF hi purity mineral oil, Bicron scintillation grade pseudocumene and the shifters were mixed as follows.

The required mount of pseudocumene and shifter were measured and placed in a thoroughly clean glass bottle. The mixture was placed on a magnetic stirrer and mixed for 3 hours with a stir bar. When no powder was visible in the mix we allowed it to stand for 6 hours to come into equilibrium.

The light-yield apparatus consisted of a glass beaker optically cemented to a 3 inch photomultiplier tube. A mu metal shield covered the PMT assembly. After thoroughly cleaning the glass beaker we filled it with 15 ml of the mix under study. A ^{207}Bi source was placed at a fixed distance above the liquid level. The position of the half maximum of the compton distribution was recorded.

This experiment used a relative calibration, i.e. we compared the light yield of a given mix to a reference: the best sample of NE235 C. This sample is reported to have a light output 60% of anthracene (calibrated to 460 channels on the pulse height analyser). The error in our measurements are about 15%.

The results for 15% pseudocumene, 85% Britol 6NF hi purity as a function of PMP concentration are shown in Table 1.

Table 1

concentration of PMP	pulse height
1 gm/l	410
2 gm/l	476
3 gm/l	500
5 gm/l	507

next, we optimized the concentration of Bis-Msb for a PPO, Bis-Msb scintillator

for 3 gm/l PPO, 15% pseudocumene and 85% Britol 6NF hi purity

Table 2

concentration of Bis-Msb	pulse height
5 mg/l	393
10 mg/l	436
15 mg/l	447
20 mg/l	452
25 mg/l	458
30 mg/l	465

The light yield did not increase beyond 30 mg/l of Bis-Msb

next we measured the variation in light yield with pseudocumene concentration

for 3 gm/l PPO, 30 mg/l Bis Msb and Mineral oil

Table 3

concentration of pseudocumene	pulse height
6%	400
12%	444
15%	490
18%	480
22%	514

Conclusion

We have prepared a mineral oil based scintillator with good light yield ~ 60% of anthracene (and better than the NE 235 C sample) with the following mixes

1) 3 gm/l PMP, 15% pseudocumene and 85% Britol 6NF hi purity mineral oil
2) 3 gm/l PPO, 30 mg/l Bis-Msb, 15% pseudocumene and 85% Britol 6NF hi purity mineral oil .

Attenuation length report from Indiana University

We sent 1 gallon of each mix of candidate scintillator to Chuck Bower of Indiana University. He measured the attenuation length using the same apparatus used to determine the attenuation length of Macro scintillator. His results are given in Table 4 below. V. Novikov developed our own apparatus to measure the attenuation length at Caltech. His results are summarized in Part 2 of this report.

Table 4

scintillator	atten length at 436nm	419 nm
PPO+Bis-Msb	6.01+/-.004m	1.72+/-0.01m
PMP	9.53+/-0.14m	5.84+/-0.05m

APPENDIX 3

APPENDIX 3

Part 1

EFFICIENCY of the SAN-ONOFRE DETECTOR

M. Chen, R. Hertenberger, N. Mascarenhas, and V. Novikov

(May 5, 1993)

Introduction

The four-fold neutrino signal in the San Onofre detector consists of a fast triple-coincidence created by a positron and its two annihilation gamma rays followed by a delayed neutron capture signal (being either a 2.2 MeV gamma from capture on H or a gamma-burst of 8 MeV from capture on Gd). When considering the efficiency of the detector, it is useful to divide the discussion into two parts: the positron efficiency and the neutron detection efficiency.

a) Positron Detection Efficiency

Two independent experiments were performed to characterize the efficiency of the detector to register the triple coincidence signal generated by a positron. Two separate codes were employed in three independent studies to Monte Carlo the positron signal in the detector. The results of all of these studies are in agreement with each other. We believe we have a solid understanding of the positron efficiency of the detector.

Measured Efficiency

The first measurement was performed by V. Novikov. The purpose of this experiment was to measure the detection efficiency of 511 keV annihilation gammas in a prototype detector, with cells much smaller than the cells of the San Onofre true design. Such a measurement would be useful as a check against the Monte Carlo calculations with similar dimensions.

This experiment employed two Gösgen cells and a Na-22 source (Fig. 1). One can tag the annihilation of the positron by detecting, with a NaI detector, the 1.27 MeV gamma that accompanies the decay. Care must be taken to correct for the branching fraction that includes both the positron and 1.27 MeV gamma as 9.5% of the Na-22 decays are via electron capture, while still emitting a 1.27 MeV gamma.

The schematic of the apparatus appears in Fig. 2. One looks for the coincident detection, in the two Gösgen cells, of the two 511 keV gammas, with a lower threshold of 0.1 MeV. If both cells fire in coincidence above the lower threshold, one then looks to see if a 1.27 MeV gamma accompanied the event. The efficiency is then given by:

$$\text{efficiency} = \frac{\text{(rate of coincidence w/source - false coincidence rate w/o source)}}{\text{(rate of 1.27 MeV in NaI - background rate in NaI)*0.9049}},$$

where the last factor corrects for the branching fraction. Second order corrections that were not included are the false coincidence rate between a true positron and a false 1.27 MeV signal, the false coincidence rate between a false positron and a true 1.27 MeV

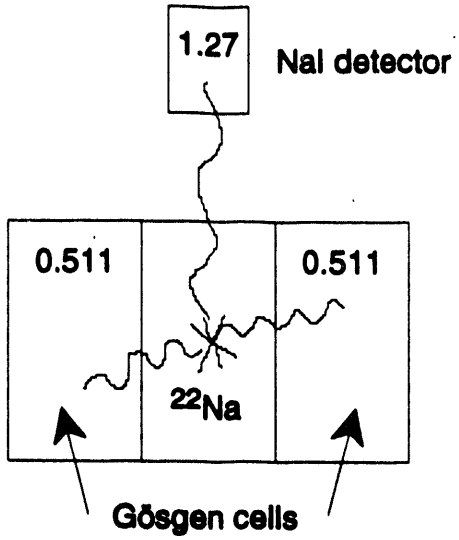

Figure 1. Basic setup for measurement of positron detection efficiency

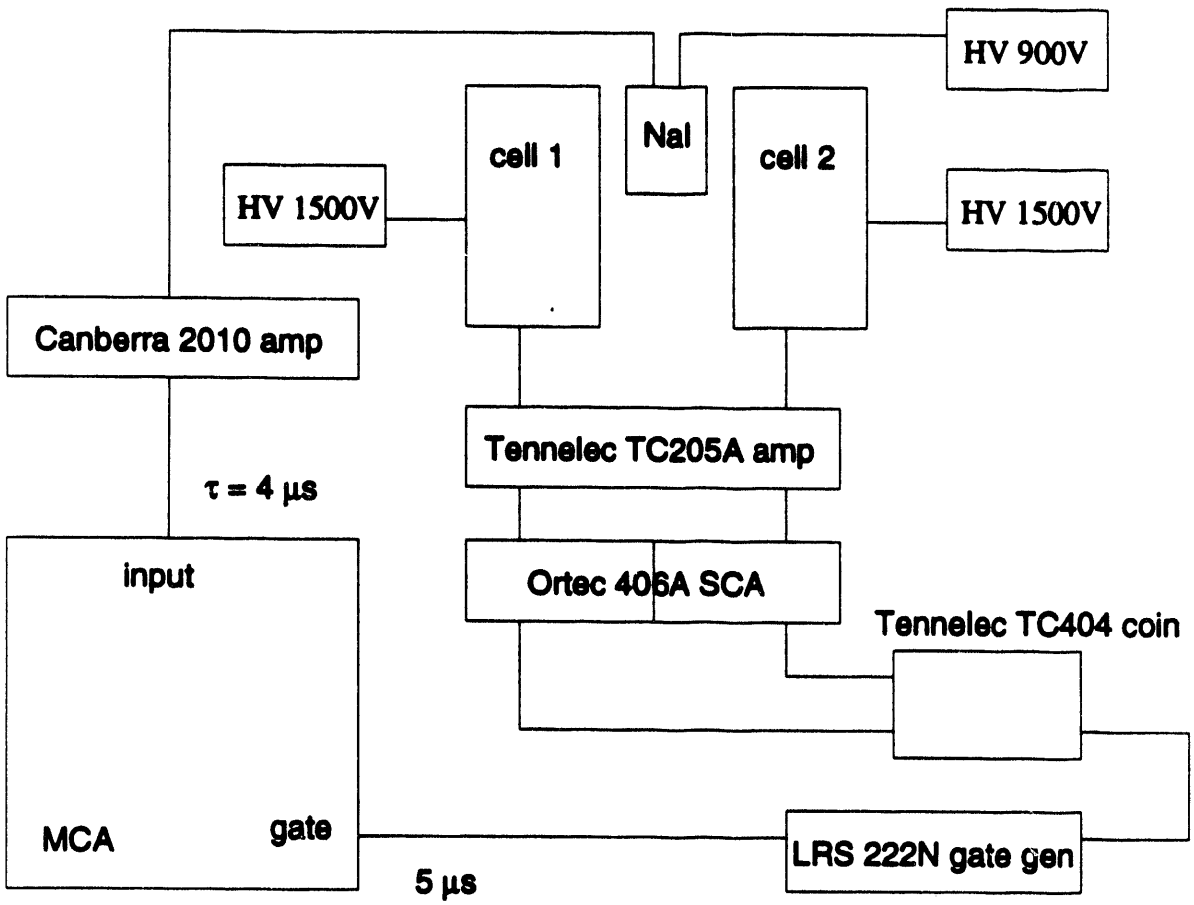

Figure 2. Schematic of the apparatus

signal, and the tiny probabilities that the 1.27 MeV gamma incorrectly triggered the two Gösgen cells or that the annihilation radiation falsely triggered the NaI detector with energy around 1.27 MeV (i.e. in-flight annihilation).

The experiment was performed in the three configurations shown in Fig. 3. The third configuration, C, included paraffin bricks around the Na-22 source to simulate the absorption of the annihilation gammas within the scintillator (in which they would be produced in a real event). Configuration A studied the upper limit counting efficiency and configuration B gave information on the geometry factor. The counting rates in the experiment for all the configurations are given in Table 1. The measured efficiencies for the three configurations, as computed by the formula (given above) are:

configuration A	22%
configuration B	10.8%
configuration C	5.9%,

all with errors less than 10%. For comparison, the Monte Carlo of configuration C gave an efficiency of 6.4% - more detail on the Monte Carlo calculations will follow.

The second experiment was performed by N. Mascarenhas, C. Delany and S. Banerjee. This measurement employed various arrangements of Gösgen cells to more closely simulate the dimensions of the designed cells for the San Onofre detector. In addition, the efficiency was studied as a function of trigger threshold; different triggering criteria and schemes were examined. A Na-22 source was used in these measurements to provide coincident 511 keV gammas for detection in the Gösgen cells. The 1.27 MeV signal in a NaI detector tagged the event. A complete discussion of these measurements appears in a separate section following this chapter.

Monte Carlo Calculations of the Efficiency

Two codes exist for modelling positrons in our detector - an independent code written by V. Novikov and the EGS4 code (ported to Fortran-77 by P. Skensved). The following factors are important when considering the positron detection efficiency - the status of the Monte Carlo codes with regards to how each factor was modelled is indicated beside:

1) random distribution of events in the detector
2) shape of positron spectrum
3) cell thickness (12 cm in EGS4, 13 cm in independent)
4) acrylic cell walls (not in EGS4 MC, 0.635 cm included in independent)
5) energy resolution (sigma = 25%@1 MeV in EGS4, fwhm = 25%@1MeV independent)
6) fiducial volume (must not include edge cells, similar treatment in both MC)
7) positron escape (included in EGS4, not in independent)
8) annihilation in-flight of positron (included in EGS4, not in independent)
9) trigger criterion (various criteria were studied in both MC).

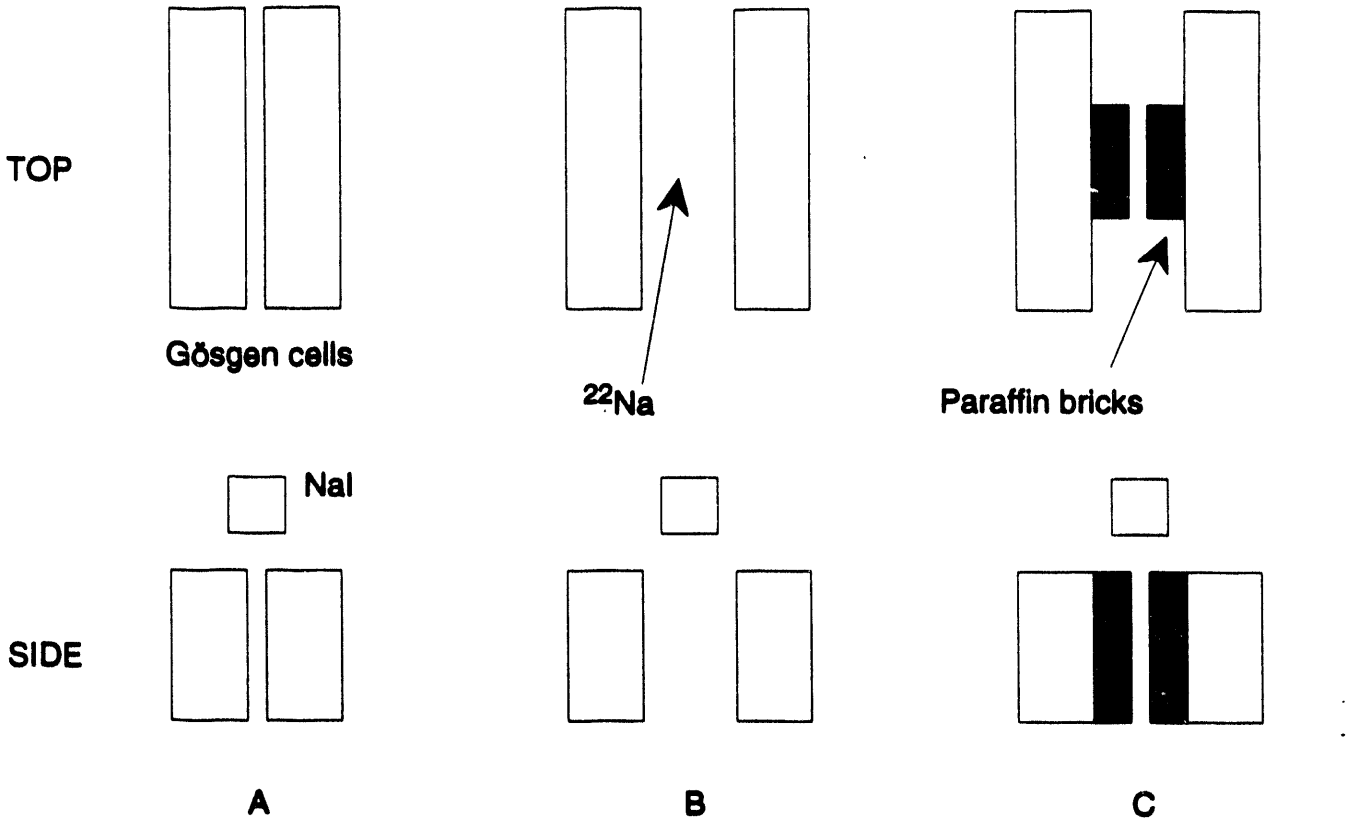

Figure 3. Three configurations used in the measurements.

	Configuration A	B	C
NaI rate of 1.27	25.51 ± 0.16	21.49 ± 0.15	38.54 ± 0.44
NaI bkgnd near 1.27	1.62 ± 0.04	1.60 ± 0.04	1.47 ± 0.04
Gösgen coincidence rate	5.67 ± 0.08	2.43 ± 0.05	2.65 ± 0.05
Gösgen false coin. rate	0.92 ± 0.03	0.50 ± 0.02	0.66 ± 0.01

Table 1. Counting rates in the positron efficiency measurement, for the three configurations [Hz].

a) different errors for similar measurements are due to different accumulation times.

b) the counting rate of the 1.27 MeV gamma differ in the three measurements due to different distances between source and NaI detector.

What is desired from the Monte Carlo calculations is the efficiency for detection of a triple coincidence produced by a positron. The "classical" triple looks for the positron with energy > 1 MeV and looks for the annihilation gammas in the nearby adjacent cells with energy > 0.1 MeV but less than 0.6 MeV. One can increase the signal efficiency by accepting "extended" triples - looking not only at the cells adjacent to the 1 MeV trigger but at additional neighbouring cells further away. This can be accomplished either by summing the energy deposition in the extended cells or by applying a logical OR criteria. The table below (Table 2) gives the results of the EGS4 Monte Carlo simulations of the positron detection efficiency for various possible trigger criteria and with different lower energy trigger thresholds for the annihilation gammas. Novikov's independent Monte Carlo calculated a "classical" triple probability of 9.8% which is in agreement with the value for "Classical triple", at 100 keV, listed in the table below.

In these simulations, the utility of an anticoincidence was examined. One could perhaps employ the remaining cells of the detector, those not of interest for the triple, in anticoincidence, attempting to reject backgrounds from penetrating neutrons leaving energy in many cells along the way before creating a false triple in the designated cluster. Employing such an anticoincidence may lower the positron detection efficiency; the results of the Monte Carlo are contained in Table 2 annotated by "w/anti". Note that the specific geometry and implementation of the anticoincidence is important (i.e. whether one begins to reject events with energy one cell away or two cells away from the triple and at what energy, etc.). The inclusion of an anticoincidence is not finalized from these results.

It is useful to compare the results from the Monte Carlo codes with the two measured results which employed Gösgen cells. As mentioned above, Novikov's Monte Carlo gave a good agreement with his measurement of the Gösgen cell positron efficiency (5.9% measured versus 6.4% Monte Carlo). The second set of measurements can be compared with results from EGS4 configured to simulate the geometries measured. A comparison table (Table 3) is shown below. The agreement is good between both sets of measurements and both codes.

A combined look at the results of the positron efficiency studies leads to the following conclusions. First, the efficiency can be increased by pushing to a lower detection threshold for the 511 keV gammas. Second, the extension of the "event cluster" from the classical three cell triple to an extended arrangement is very beneficial. It is a substantial gain going from three cells to five cells (i.e. inclusion of one extra cell thickness on each side for registering the 511 keV gammas). However, it appears not so worthwhile to increase this to seven cells as the additional gain is smaller. An optimal scheme for triggering the triple coincidence using a five cell event cluster is illustrated below (Fig. 4). One sums the energy of the two "side clusters" to test the upper threshold (energy less than 600 keV) and one employs a logical OR looking for greather than 50 keV energy in either one of the two cells of a given "side cluster".

Type	50 keV	100 keV	200 keV
Classical triple	14.5 ± 0.7 %	9.9 ± 0.6 %	4.7 ± 0.4 %
Extended five sum	19.1 ± 0.9 %	14.4 ± 0.8 %	8.2 ± 0.6 %
Extended seven sum	20.3 ± 1.0 %	15.4 ± 0.9 %	8.8 ± 0.6 %
Extended five OR	21.0 ± 0.9 %	15.4 ± 0.8 %	7.9 ± 0.6 %
Extended seven OR	23.4 ± 1.1 %	16.9 ± 0.9 %	9.1 ± 0.7%
Classical w/anti	7.3 ± 0.5 %	4.9 ± 0.4 %	2.6 ± 0.3 %
Extended five OR w/anti	14.3 ± 0.8 %	10.3 ± 0.6 %	5.9 ± 0.5 %
Extended five OR w/anti sum upper 0.6 MeV	12.8 ± 0.7 %	9.0 ± 0.6 %	5.2 ± 0.5 %
Extended five OR w/anti sum upper 0.8 MeV	15.7 ± 0.8 %	11.7 ± 0.7 %	7.2 ± 0.5 %
Extended five OR no anti sum upper 0.8 MeV	23.2 ± 1.0 %	17.4 ± 0.8 %	9.6 ± 0.6 %

Table 2: Positron Detection Efficiency

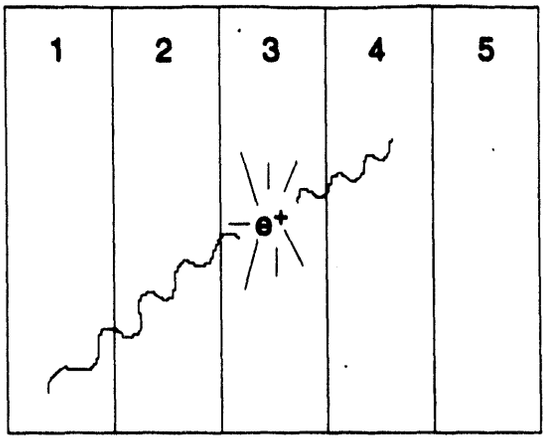

Figure 4. Illustration of extended triple coincidence trigger scheme.

A third Monte Carlo study of the positron efficiency was made by R. Hertenberger. His study employed the EGS4 code with the chief difference being that he tracked electrons and gammas with a lower cutoff of 50 keV. The previous results all employed a lower cutoff (in the EGS4 code) of 100 keV. In this study, the cell thickness employed was 13 cm instead of 12 cm. No cell walls were included.

A comparison between the previous study and this one was made for consistency. The results are shown below:

	50 keV	100 keV	200 keV
Classical triple:			
previous	14.5 %	9.9 %	4.7 %
cutoff 100 keV	15	11	4
cutoff 50 keV	19	10	5
Extended five OR:			
previous	21.0 %	15.4 %	7.9 %
cutoff 100 keV	20	16	7
cutoff 50 keV	24	15	7

With the EGS4 code tracking deposition down to a 50 keV cutoff, we expect more reliable results from the Monte Carlo. The comparison of the two studies shown above exhibits differences only significant for the 50 keV lower threshold case. This makes sense as the code only requires this added accuracy when one needs to consider a threshold as low as 50 keV. Thus, the most accurate value we accept for the positron detection efficiency is 24%, utilizing the extended five OR trigger criteria with a lower threshold of 50 keV.

In Table 3, which compares the second measurement of the positron efficiency with the EGS4 Monte Carlo results, are included additional values which were calculated by Hertenberger using the 50 keV cutoff in the EGS4 code. These calculations simulated the actual geometry employed in that measurement.

An additional factor studied in this Monte Carlo was the effect of varying the cell height (the 50 cm dimension). If this height were reduced to 25 cm, could the efficiency be improved? If we were to employ similar triggering schemes as considered above for the 50 cm height cell, the answer would be no. The smaller 25 cm cell would lose more gammas simply due to the reduced solid angle the smaller cells subtend. Thus, in order to employ these smaller cells, the triggering scheme needs to be modified to utilize entire "blocks" of cells that surround the positron. The block scheme for detecting the annihilation gammas is illustrated below (Fig. 5).

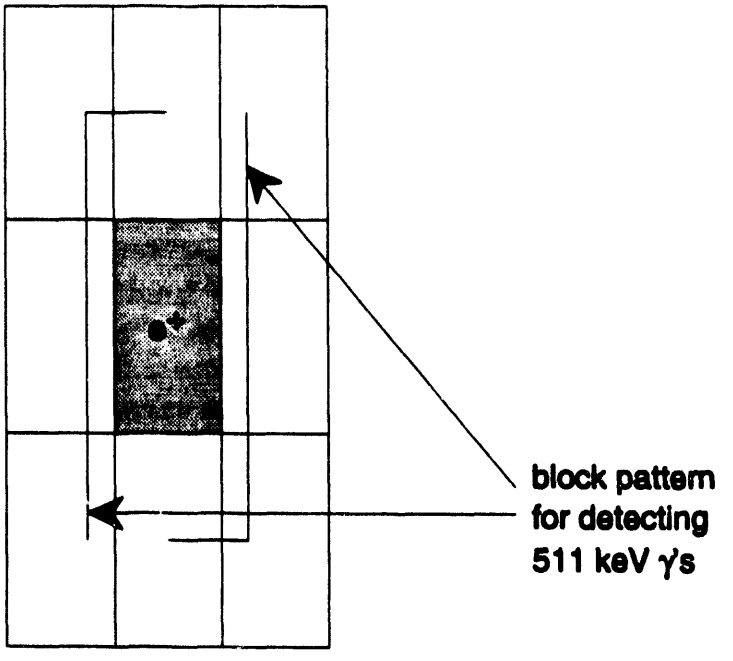

Figure 5. Block arrangement of 25 cm cells.

For a lower threshold of 50 keV and a block arrangement of 25 cm cells, the increase in the detection efficiency (compared to the extended five OR) was a factor 1.65. Of this, as much as half of the increase arises from looking at cells below or above the plane of the positron. The other half of the 65% increase comes from the smaller 25 cm size (this gain coming from reduced self-absorption of the 511 keV gammas emitted up and down). Remember that the increased efficiency of the smaller cells requires the block scheme. Thus, in the experiment, whether 25 cm or 50 cm cells are employed, it will be worthwhile to consider extending the detection of the 511 keV gammas to the planes above (or below) the trigger plane of the positron in the array of cells.

Calibration and Efficiency Monitoring

The task of calibrating the detector and maintaining a stable efficiency for the signal detection is challenging. Our proposal is to initially measure the integrated efficiency of the detector and to continuously monitor the light collection and response of the

photomultipliers with a fixed, installed set of optical fibers.

When we referred to the 50 keV lower threshold for detection of the 511 keV annihilation gamma in our earlier studies, we assumed that our knowledge of the actual energy deposited in the cells to be extremely good. In our studies, we assumed this 50 keV threshold had a negligibly small uncertainty. This is not true in practice. The response at either ends of the long cell to 50 keV actual energy deposition varies considerably with position. If photomultiplier gains and/or response drift, the output might vary from that expected for a true deposition of 50 keV. Such an uncertainty in the 50 keV threshold translates directly into an uncertainty in our signal efficiency. As a consequence of this challenge, we choose to address this uncertainty in a way which will eliminate the neccessity of determining precisely the actual energy deposited in a cell. To reiterate, we will NOT need to 'reconstruct' the energy of a 50 keV deposition to better than 1 keV.

First, we propose to utilize five cells, of identical size and construction as the detector, in a calibration measurement. The five cells will be arranged together as in the experiment. The cells will be energy calibrated with sources at the center of each cell. With just this single position, point calibration, we set our discriminator thresholds.

We will use a calibrated, pure positron source (i.e. no accompanying gamma rays, just positron emission). We will disperse this source in the scintillator of the central cell. Thus, we simulate randomly distributed signal events. With the fixed discriminator threshold optimized and set earlier, we measure the detector efficiency (and subtract the background taken before the source was dissolved in the cell). Thus, we will measure the integrated efficiency of the detector, over all positions in the central cell. As a result, positrons that annihilate away from the center of the cell will emit 511 keV gammas that will interact away from the center of the adjacent cells. With the fixed threshold, we must accept the fact that signals, at one position of the cell, that fire the discriminator thresholds may have different actual energy than signals that fire the discriminator at other positions. We must accept this situation. We can model the varying position response of the detector with the EGS4 Monte Carlo and with our highly successful light collection Monte Carlo. But modelling will not be critical since we will actually measure the integrated efficiency using a calibrated source, with precisely the same arrangement and electronics we will employ in the experiment.

To verify that the light collection and response of the photomultipliers is stable with time, we will employ a system of optical fibers and lasers. Because our efficiency will have been directly measured at a particular set of gains and thresholds, we must ensure that these values are constant throughout the duration of the experiment. We will employ a UV laser and optical fibers to inject photons in numerous fixed positions in every cell such that we can monitor the response of the photomultipliers at both ends of each cell to fixed quantities of light. We will operate this calibration system periodically as it coexists with the experiment.

b) Neutron Efficiency

The main factors affecting the neutron capture portion of the signal efficiency are listed below:

1) containment of the ~20 keV signal neutron within the detector
2) containment of the gamma energy coming from neutron capture (on either H or Gd)
3) energy resolution of the detector (including dead material - cell walls).

The most important factor is the containment of the gammas. Whether we are dealing with a 2.2 MeV gamma or an energetic gamma cascade (with total energy 8 MeV), the long range of the gammas in liquid scintillator necessitates a choice between one of two philosophies for detection. One can either decrease the importance of the energy information and rely mainly on spatial information to identify the neutron capture gammas or one must sacrifice the spatial to gain total energy containment over a large volume, thus allowing one to use the energy to identify the capture. The latter will be considered.

Two Monte Carlo studies were undertaken to estimate the neutron detection efficiency. Novikov's Monte Carlo code was employed to determine the response of the detector to 2.2 MeV gammas coming from neutron capture on H. The EGS4 code was used to estimate the neutron efficiency for a Gd-loaded scintillator.

Capture on H

The Monte Carlo response of the entire 12 ton detector to a single 2.2 MeV gamma is shown in Fig. 6. The total energy deposited in all cells was summed to give the response. The dead layers associated with the acrylic cell walls were included in this calculation. An energy resolution of 25% @ 1MeV fwhm was used. The simulation found that 18.6% of the gammas escaped without a single interaction. The Monte Carlo gave a detection efficiency of 56%, looking in an energy window of 1.8 - 2.4 MeV for the capture gamma.

The energy deposited by the 2.2 MeV gamma is spread outwards from the point of capture. Monte Carlo calculations were performed to determine the spatial extent of the capture signal. Fig. 7 is a plot of the results and shows the fraction of the 2.2 MeV gammas produced which are contained within a sphere of radius R [cm], centered around the point of neutron capture. For the purpose of the Monte Carlo, containment was defined as requiring the gamma to deposit no more than 0.1 MeV energy outside of the event sphere being considered. From Fig. 7, we see that a sphere of radius 85 cm contains 90% of gamma events. Note that the detector geometry and the gammas which escaped without interacting were accounted for. Because of the position uncertainty of the depositions in the x-direction, due to cell discretization, and because of the displacement of the neutron capture from the positron signal, one should use an event radius of 1 m as a realistic value for containment of 90% of the capture gammas.

A simulation of the signal neutron was also performed. The key question is how far from the positron does the epithermal neutron travel before it is thermalized and captured. Fig. 8 shows such a distribution (in arbitrary units). We see that most of the neutrons are captured 10 cm from their point of origin.

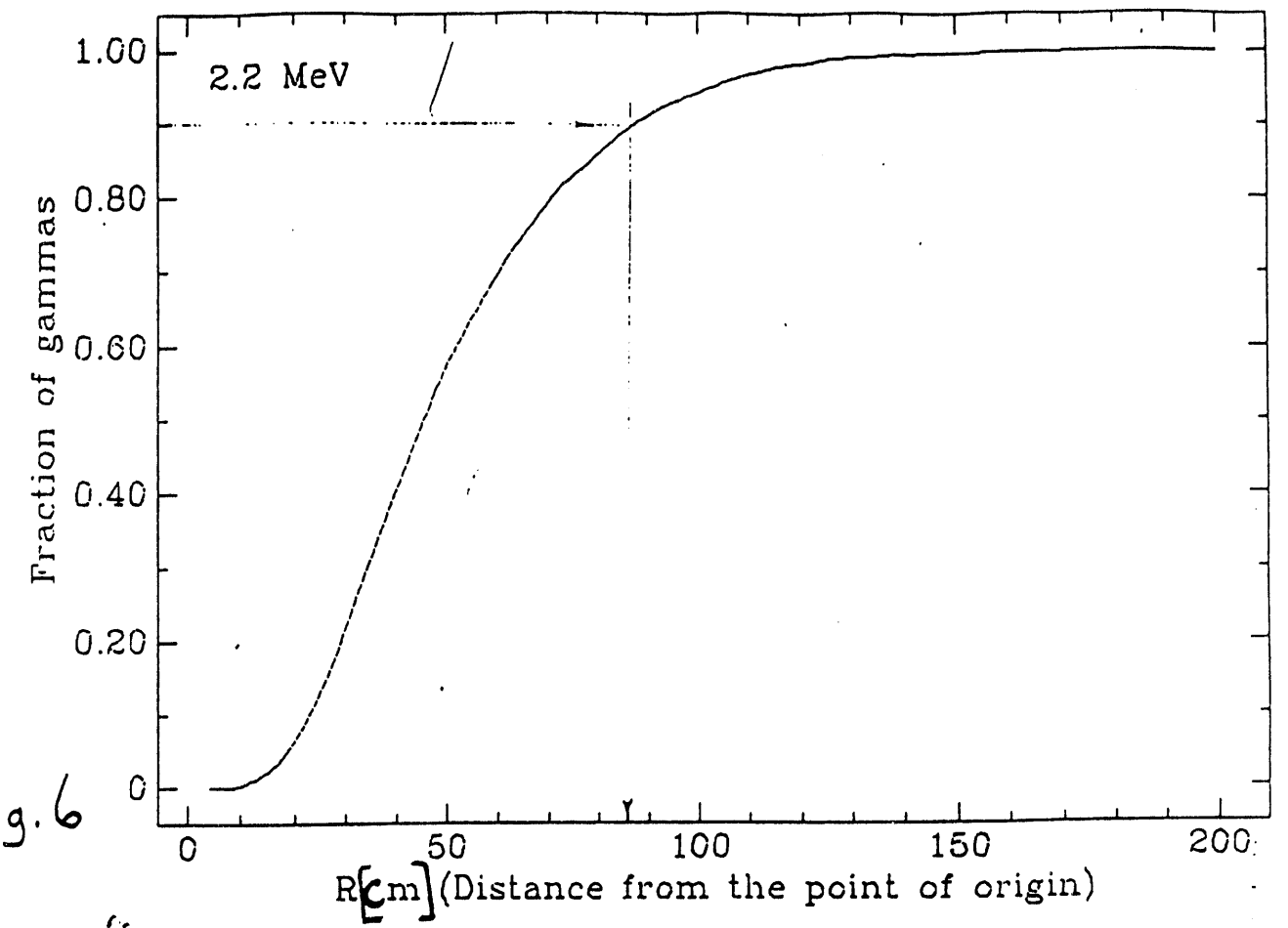
2.2 MeV
Fraction of gammas
1.00
0.80
0.60
0.40
0.20
0
0
50
100
150
200
R[cm] (Distance from the point of origin)

Fig. 6

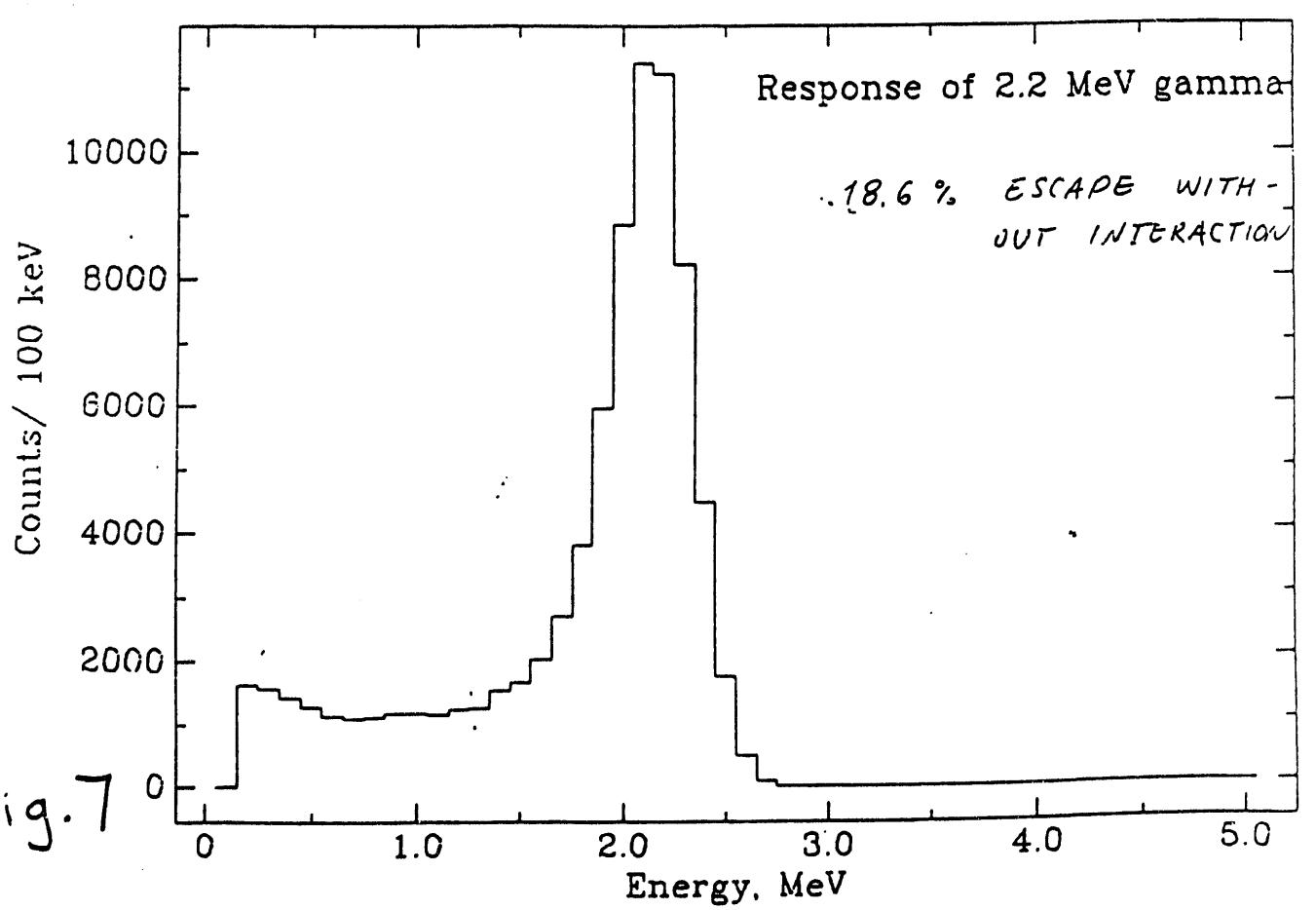
Response of 2.2 MeV gamma
18.6 % ESCAPE WITH-
OUT INTERACTION
Counts/ 100 keV
10000
8000
6000
4000
2000
0
0
1.0
2.0
3.0
4.0
5.0
Energy, MeV

Fig. 7

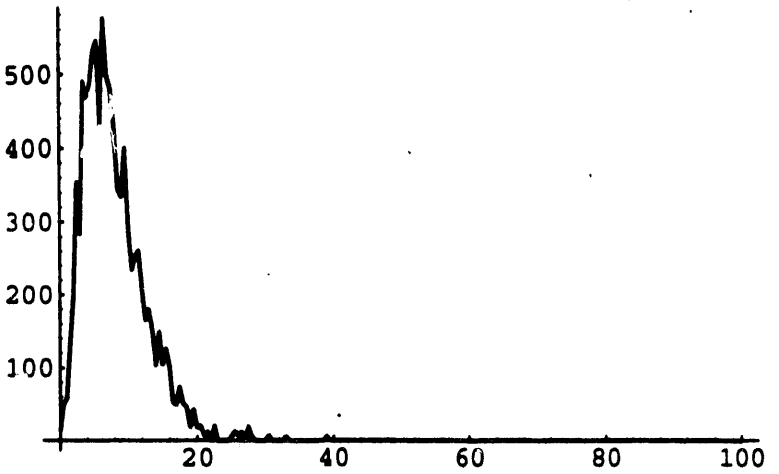

Figure 8. Distance from origin of neutron capture [cm]

The Monte Carlo also showed that 6.7% of the signal neutrons leak out of the detector before being captured (from a random distribution of neutrino events). These neutrons which are not contained will capture on protons in the buffer and produce 2.2 MeV gammas there - some of those gammas will be redirected back into the fiducial volume. But, for the purposes of this Monte Carlo, these signal neutrons are considered lost. In addition, 5.2% of the neutrons that are captured within the fiducial volume do not capture within the allowed 500 μs gate.

Thus, we can combine all of the results to deduce the net neutron detection efficiency. We start with 93.3% probability to contain the neutron and capture it in the fiducial volume. 94.8% of the captures occur within the 500 μs gate. For those gammas that deposit energy in the detector between 1.8 - 2.4 MeV, we take 56% probability. We add the additional factor of 90%, the requirement that the energy be contained in the 1 m event sphere, to get a total neutron detection efficiency of 45%.

Capture on Gd

Simulations were run to study the gamma detection efficiency for capture gammas arising from neutron capture on Gd. The EGS4 code was employed. A separate section follows discussing the efficiency of a Gd-loaded scintillator for neutron detection.

Neutron capture was modelled using a scintillator with 0.05% Gd loading. Note that the neutron capture portion of the efficiency calculation remains essentially unchanged between a Gd-loaded and regular scintillator - there remains still that 93% of the neutrons coming from the signal capture in the fiducial volume and 7% escape. For detection of the gammas signal from capture on Gd, these lost neutrons which capture in the buffer are truly lost this time. They capture on H in the buffer and are not detected above the threshold set for Gd-capture, even if the 2.2 MeV gamma is re-directed back into the fiducial volume. In addition to the fraction of neutrons that capture within the fiducial volume, the Monte Carlo gives the ratio of capture on Gd versus capture on H for the scintillator. For a Gd concentration of 0.05% wt in the scintillator, 77.5% of the neutrons capture on Gd and 22.5% capture on H. This fraction must be included when estimating the net neutron detection efficiency.

Combining the neutron containment probability, capture within the alloted time

window, the capture ratio between Gd and H and the efficiency to detect the gamma-burst of 8 MeV, one arrives at a total net neutron detection efficiency for the Gd-loaded scintillator (0.05% wt conc.) of 50%.

Conclusion

To arrive at an estimate of the net signal detection efficiency, we take a positron detection efficiency of 24%. Note that depending on how the calibration and efficiency monitoring is implemented, the true efficiency may deviate from this somewhat idealized estimate. We accept a neutron detection efficiency of 45% for the regular scintillator and 50% for the Gd-loaded scintillator to arrive at net signal detection efficiencies of 10.8% and 12%, for the unloaded and Gd-loaded scintillators respectively.

APPENDIX 3

Part 2

Measurements of the Positron Annihilation Efficiency with Different Cell Configurations and Energy Threshold

Swagato Banerjee, Chad Delany and Nicholas Mascarenhas

We describe a set of measurements which investigated the positron annihilation detection efficiency as a function of energy threshold and cell configuration. We used a ^{22}Na tagged positron source. The Goesgen cells were configured in different geometries. The readout system employed a personal computer to log the data from the CAMAC ADC's. The coincidence requirements were set with LeCroy NIM discriminators and logic modules. These measurements were carried out between June and October 1992.

The Detector:
The Goesgen cells are 0.6cm thick acrylic boxes 0.86mX 0.20m X 0.1m. Each cell is filled with NE235 C mineral oil based liquid scintillator. Two Amperex 3 inch diameter PMTs view each side of a cell. The signal from both PMTs on an end are ganged, in addition sum each end is analog summed using a linear Fan-In. A NaI scintillation detector tags the 1.27 MeV gamma ray (see Fig 1). A trigger from the NaI detector (set to select the 1.27 MeV only) gates the CAMAC ADC which reads the coincident energy deposited in each of the individual 12 cells, N_t. In a candidate event the two 511 keV gamma rays deposit some energy in the surrounding cells. Offline energy cuts are placed to obtain a positron annihilation events N_p. A schematic of the readout system is shown in Fig 1.

The Experiment:
The energy scale was calibrated using the Compton edge (1.06 MeV) of the ^{22}Na1.27 MeV gamma ray line as well as the 511 keV line. This calibration has an error of about 20% because compton edge is not sharp. The calibration was repeated for each cell configuration. The gate for the 12 cell ADC was 100 ns wide, this was somewhat larger than necessary to detect a coincidence but it ensured the different signals fell well inside the window. Polyethylene bricks were placed in the middle to simulate the scintillator of the missing central cell. Our analysis employed the following energy cuts:

upper threshold for the 511 KeV gamma:	600 keV.
lower threshold for the 511 keV gamma:	25 keV to 200 keV.
1.27 MeV gamma	+/- 80% of the photopeak(1.27 MeV)

It is possible that some triggers in the NaI detector are due to background gammas

(from the K, U, Th in the PMT's and surrounding concrete). The data (N_t)was corrected by removing the source and placing the NaI detector far away from the Goesgen cell. Background was accumulated for the same time as the signal. The background subtraction correction was small, about 12% of the total signal N_t. We also corrected the data for the branching factor of the 511keV gammas (0.9) compared to the 1.27MeV. The efficiency for a given threshold is N_p/N_t.

Configurations:
We studied the following arrangements of cells.
set 1: one 0.18m tall Goesgen cell on either side (see fig 2)
set 2: two 0.18m tall Goesgen cell on either side (see fig 2)
set 3: one 0.54m tall cells on either side (see fig2)
set 4: two 0.54m tall cells on either side (see fig2)
set 5: 0.18m cells, Block structure (see fig3)

Results:
It is observedthat the detection efficiency is a strong function of energy threshold (see Table 1). These experiments demonstrate conclusively that there is considerable gain in efficiency in going to a low energy threshold for the 511keV gamma rays. It confirms experimentally the improvement in efficiency in adding additional cells (two on each side) to the triple coincidence earlier proposed. The set-up (set 4) resembles the configuration we intend using at San Onofre (0.5 m tall tank), hence the efficiency determined here is directly applicable to our proposed detector. The efficiency for positron annihilation detection for this set-up is 22.39 +/- 0.47% at 50keV threshold.

FIG 1

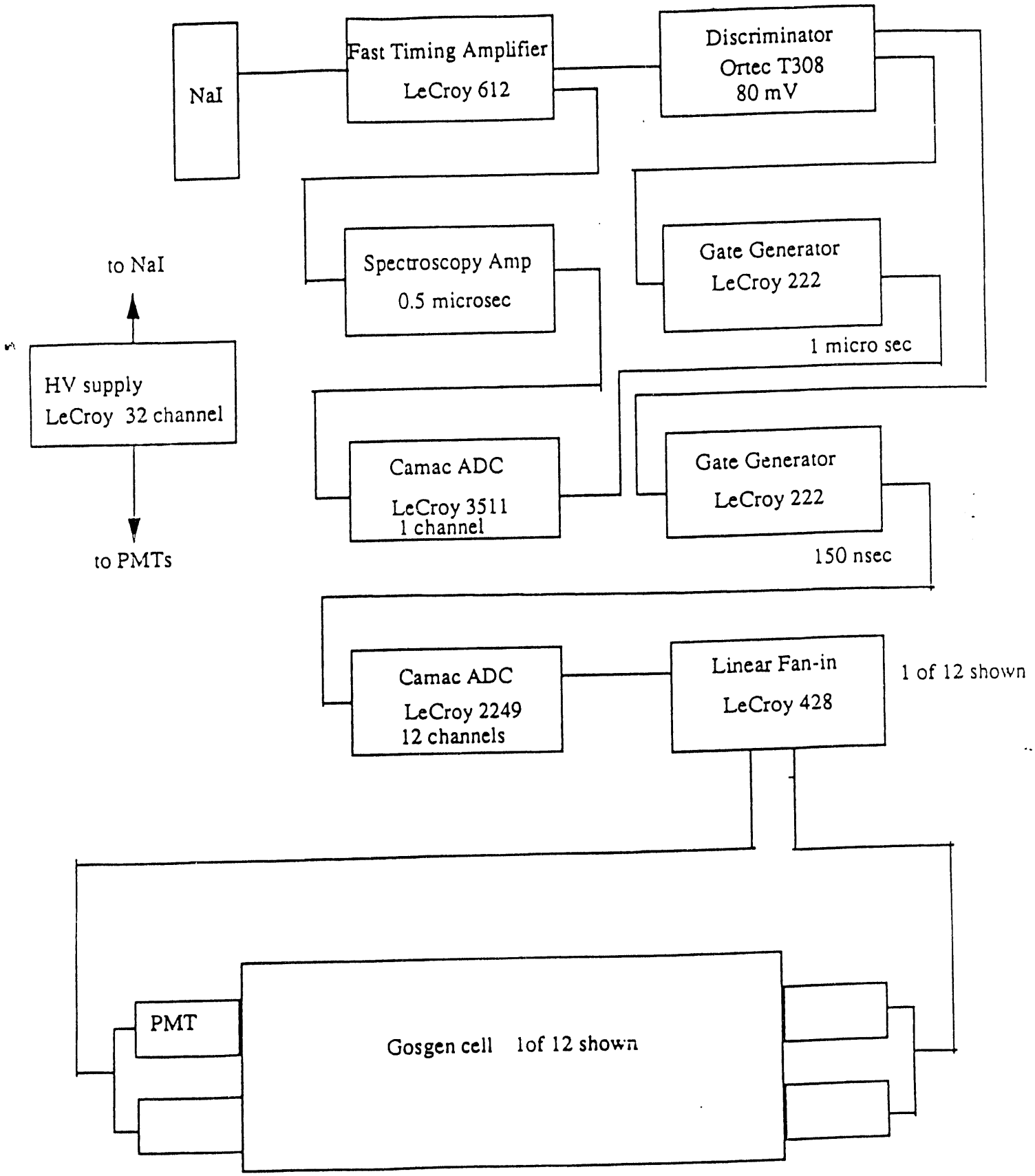
NaI
Fast Timing Amplifier
LeCroy 612
Discriminator
Ortec T308
80 mV
to NaI
HV supply
LeCroy 32 channel
to PMTs
Spectroscopy Amp
0.5 microsec
Gate Generator
LeCroy 222
1 micro sec
Camac ADC
LeCroy 3511
1 channel
Gate Generator
LeCroy 222
150 nsec
Camac ADC
LeCroy 2249
12 channels
Linear Fan-in
LeCroy 428
1 of 12 shown
PMT
Gosgen cell 1of 12 shown

Fig. 2

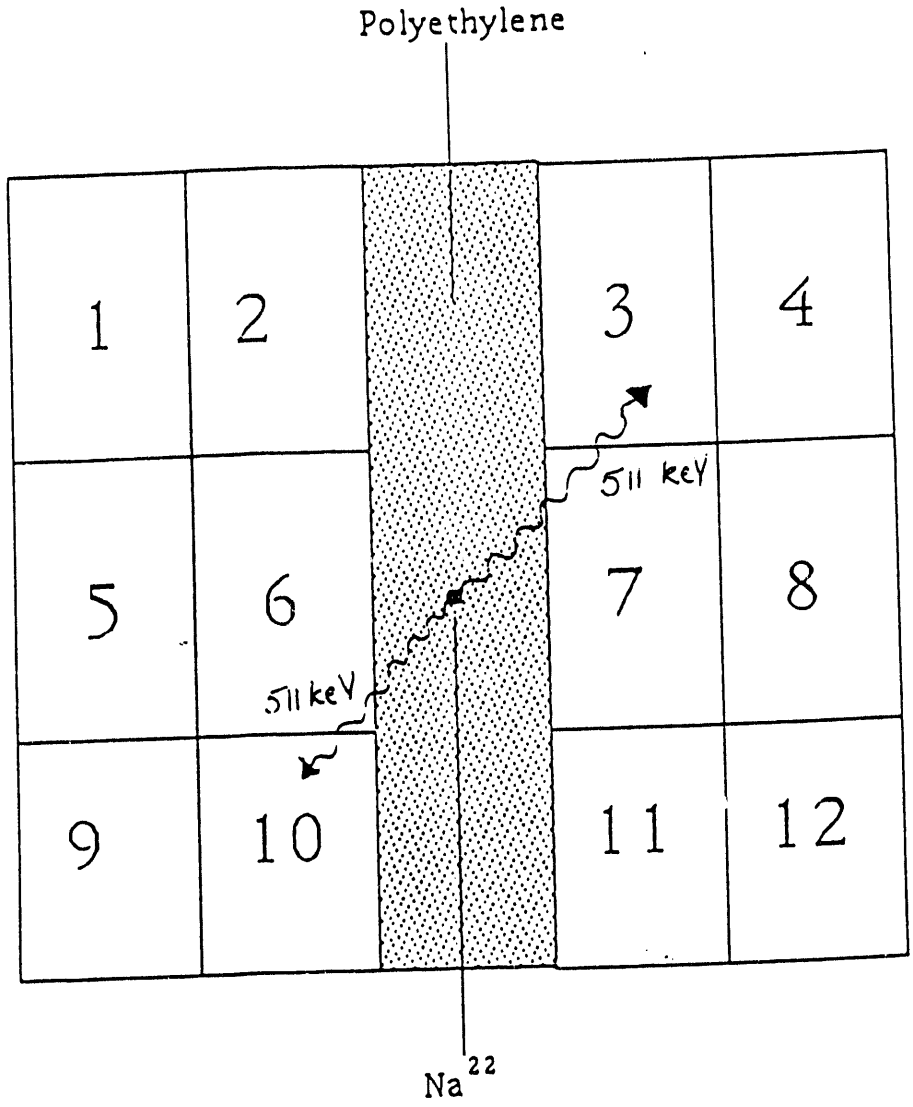

Set 1 - Cells 6 and 7

Set 2 - (Cells 5 or 6) and (Cells 7 or 8)

Set 3 - (Cells 2, 6, or 10) and (Cells 3, 7, or 11)

Set 4 - (Cells 1, 2, 5, 6, 9, 10) and (Cells 3, 4, 7, 8, 11, or 12)

FIG 3

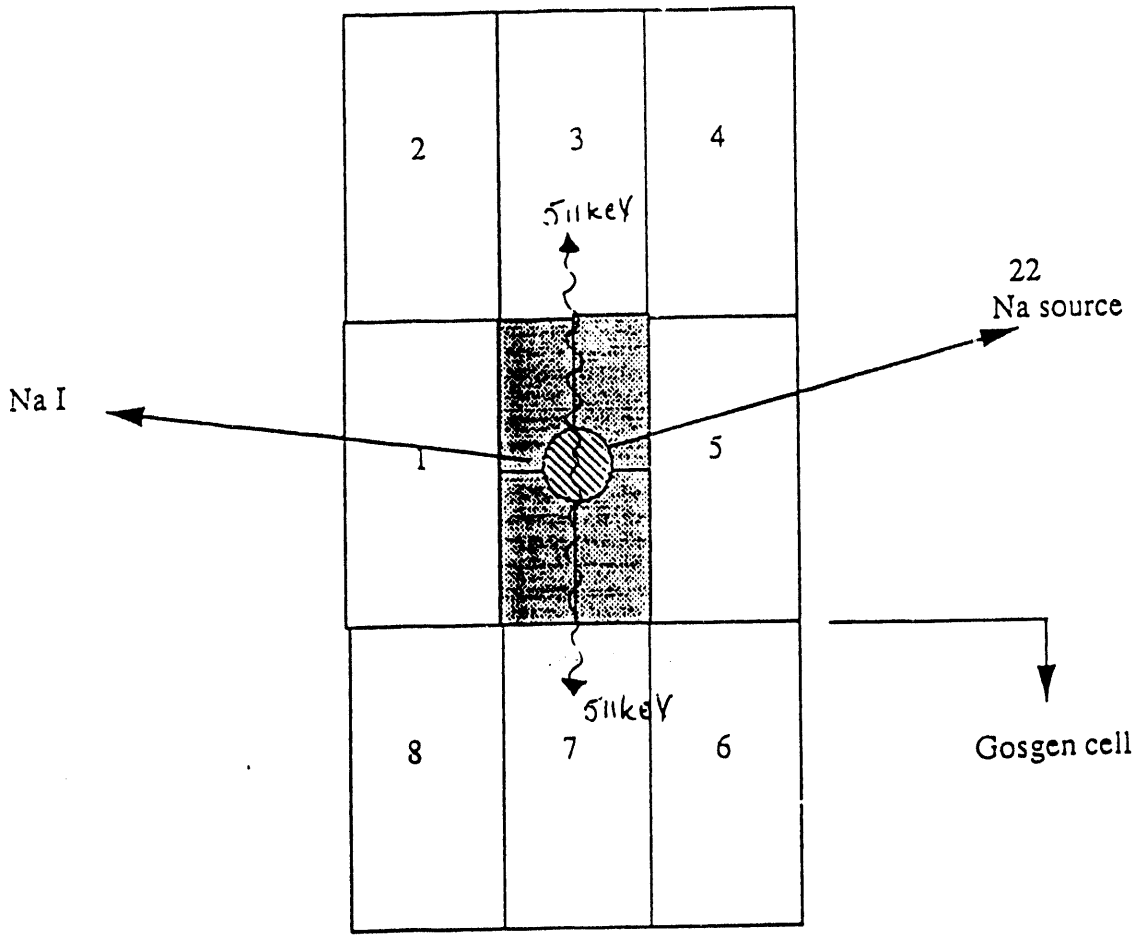

TABLE 1

POSITRON ANNIHILATION DETECTION EFFICIENCY (%)

	configuration	25keV	50keV	75keV	100keV	150keV	200keV
set 1	0.18m cell on each side (cell 6+7, fig2) %	10.23+/-.30	6.64+/-.24	4.76+/-.20	3.59+/-.18	2.16+/-.14	1.09+/-.10
set 2	2, 0.18m cells on each side (cell 5or6+7or8, fig2) %	15.25+/-.37	10.40+/-.30	7.84+/-.27	6.10+/-.24	3.83+/-.18	1.97+/-.13
set 3	0.54m cell each side (cell 2or6or10+3or7or11, fig2) %	23.91+/-.49	14.53+/-.37	9.68+/-.29	6.67+/-.24	3.47+/-.18	1.64+/-.11
set 4	2, 0.54m cells each side (cell 2,6,10,1,5,9+3,7,11,4,8,12, fig2) %	34.10+/-.61	22.39+/-.47	16.00+/-.38	11.55+/-.33	6.20+/-.23	2.26+/-.15
set 5	0.18m cells block structure (fig3)%	36.57+/-.46	21.13+/-.38	13.71+/-.30	10.22+/-.32	4.86+/-.32	3.12+/-.30

APPENDIX 3

Part 3

ADVANTAGE AND NEUTRON-EFFICIENCY OF A GD-LOADED SCINTILLATOR

M. Chen, R. Hertenberger
Physics Department, California Institute of Technology
Pasadena, CA, 91125, USA

May 18, 1993

1. Introduction

The use of a Gd-loaded scintillator could considerably reduce both correlated and uncorrelated background in the 12 ton neutrino oscillation detector for the San Onofre experiment. The advantages of the Gd-loaded scintillator compared with an unloaded scintillator are related to the huge neutron-capture cross-section of ^{nat}Gd (48,000 barns against 0.33 barns for protons) and the high energy and multiplicity of the γ's emitted after the neutron capture ($E_{total} \approx 8MeV$, $M \approx 3-4\gamma$'s).

2. Consequences of the higher cross-section

The high cross-section shortens considerably the capture time of neutrons created by the neutrino interaction in the scintillator. At concentrations of .05% Gd (by weight) the neutron capture time is reduced from 166 μsec (value for unloaded scintillator) to 46 μsec and at concentrations of .1% Gd to 27 μsec fig.[1] and ref.[1]. The coincidence window for the four-fold coincidence will therefore be decreased by a factor of 3 to 5 from 500 μsec (for the unloaded scintillator) to 150 μsec or 90 μsec, respectively and, as a consequence, uncorrelated backgrounds will be reduced by the same factor.

The shorter capture-time will also influence the timing-efficiency of the muon-veto, reducing considerably correlated backgrounds from neutrons created by muon-spallation or muon-capture.

2.1. The influence of the shorter neutron capture time on the veto efficiency

At depths of 25 mwe veto times of 100 μsec are possible without excessive dead-time losses for through-going muons passing the fiducial volume. We expect a rate of 900 Hz for these events. Through-going muons passing only the buffer without entering the fiducial volume ($\approx$ 1100 Hz) will be vetoed for 10 μsec and for muons stopped in the whole detector ($\approx$ 20 Hz) the veto time will be 500 μsec. The dead-time of the detector will be about 10%.

Using scintillators loaded with .05% or .1% Gd, the 100 μsec veto will quench the

amount of spallation neutrons created by through-going muons in the fiducial volume by factors of 8.8 ($= (exp^{-100/46})^{-1}$) or 40, respectively. The number of double-neutrons created by spallation in the fiducial volume will be reduced even more, as the characteristic time to veto one of the two created neutrons will be reduced by a factor of two. Therefore, veto-reduction factors of 77 and more than 500 seem to be reachable. The equivalent reduction-factors for the unloaded scintillator would be 2 for single neutrons and 3 for double neutrons. Neutrons from muon-capture will be suppressed much more, due to the longer veto-time. Reduction factors of 20 for hydrogen and 50,000 or 10^8 for the two Gd-loaded scintillators can be reached.

Per day about 130,000 neutrons and about 13,000 double-neutrons will be created by muon-spallation in the fiducial volume itself (ref.[6]). The related numbers for muon-capture are about 40,000 neutrons and 10,000 double neutrons. Double neutrons are especially dangerous. They are created at the same place and at the same time and therefore, they are able to fake a neutrino signal in a correlated way. The γ burst produced by the capture of the first neutron on Gd will fake the triple coincidence with a relatively high probability of 10 % (see table 3) and the capture-γ of the second neutron will fullfill the 4-fold coincidence with the correct timing behaviour (see ref.[2]). The high energy of the spallation and capture muons is responsible for two further reductionfactors leading to an additional reduction factor of 3.5: With a 30 % probability one of the two fast neutrons will escape the detector and the reaction centers of triple and single events will be displaced in space. Together with the efficiency for the γ detection ($\approx$ 50 %) correlated background from double-neutrons will be suppressed by a factor of 70 ($= 10 \times 3.5 \times 2$) ref.[3]. Including the veto, the final reduction factor for the .05% Gd-loaded scintillator will become 5,400 for spallation-neutrons and more than 3.5×10^6 for capture-neutrons leading to less than 4 correlated background events per day, compared to about 15 for the unloaded scintillator. The use of a scintillator loaded with .1 % of Gd would reduce this background to less than 1 per day, because of its 6 times better veto reduction factor. The final reduction factor for the unloaded detector will be about 850. In this case, the pobability of the 2.2 MeV γ to fake a triple coincidence via multiple compton scattering is $\simeq$ 3 %. Double neutrons created in the buffer are negligible, due to the squared additional reductionfactors (opening angle and absorption). It should be remarked, that all single neutrons living longer than 100 μsec are only contributing to accidental background named neutron-soup. This is investigated in detail in ref.[2].

The following consideration holds for both sorts of scintillators - Gd-loaded or unloaded - in the same way. It is introduced here only for reasons of completeness. In principle, also single neutrons could fake the neutrino signal in a correlated way: the multiple fast neutron recoil signal on protons could simulate the triple coincidence and the succeeding capture γ would lead to the final four-fold coincidence. Alternatively, the fast neutron could scatter inelastically on a ^{12}C nucleus and the 4.4 MeV deexcitation γ could fake the triple coincidence. To suppress completely these fast processes ($\tau \ll$

100 nsec) veto times of 10 μsec are sufficient. All veto times are larger than 10 μsec and therefore, the detection inefficiency of the muon-veto (< .1 %) becomes the limiting factor for this sort of correlated background.

The production rate of neutrons in the buffer will be 770,000 per day from spallation and 210,000 per day from capture. As an upper limit, 980 of them will not be vetoed. Opening angle (factor 5) and buffer absorption (not considered here) reduce this number by another factor greater than 5 to less than 200 per day. In the fiducial volume, about 170,000 neutrons are produced and less than 170 will not be vetoed. The fiducial volume itself acts as an additional muon veto. Therefore, the 170 events will be reduced by at least another factor of 100. Together with the coincidence-reduction factor of 500 ref.[2] for both processes mentioned above, the background rate from these correlated events will become less than 1 per day. Taking into account a reasonable value for the neutron absorption in the buffer leads to the number of .2 per day given in ref.[6].

Fast neutrons created outside the veto are dangerous for the same reason and are indeed one of the main sources of background. They are suppressed by the 80 cm thick boron loaded buffer, but they will contribute with about 3.5 background events per day (ref.[6]).

2.2 Shorter coincidence time

The influence of Gd on the uncorrelated background was studied in detail in ref.[2]. At a given homogeneous rate N_t of events [per sec] faking a triple coincidence and at a homogeneous rate N_s [per sec] of single events in the correct energy window the accidental background-rate per day will be:

$$N_{bckg} = N_t \times N_s \times \tau \times 86400 \qquad (1)$$

As the backgroundrate N_{bckg} depends on the coincidence time τ the use of a Gd-loaded scintillator will reduce accidental background by more than a factor of 3 compared to the unloaded scintillator.

Gd influences negatively the triple-coincidence rate. There are two main effects: The amount of radioimpurities might increase. Taking the Gd sample from ref.[4] and assuming a concentration of .05% Gd, the ^{232}Th concentration in the scintillator will roughly double. As a consequence also the triple rate from the 2.6 MeV γ's doubles. On the other hand, a different Gd sample investigated by our group was considerably cleaner than the sample from ref.[4]. The total amount of ^{238}U and ^{40}K is in both samples nearly not affected. The probability of the γ cascade produced by the neutron capture on Gd to fake a triple coincidence is a factor of 4 larger than the probability of the 2.2 MeV γ from the proton capture (see table 3). In ref. [2] it is pointed out, that both effects result in a slightly enhanced triple rate for the Gd loaded scintillator (.5 → .6 per sec).

This shortcoming will be more than compensated by the much smaller single-event rate of the Gd loaded scintillators. It will be decreased by the high energy of the γ-cascade ($\approx$ 8 MeV) following the neutron capture on Gd. The γ-energy from capture of a neutron by a proton in the unloaded scintillator is only 2.2 MeV.

3. Higher energy and multiplicity of the neutron-capture-γ's

The neutron cross-section of Gd is strongly dominated by the isotope ^{157}Gd having a cross-section of 254,000 barns. Its abundance in natural Gd is 15.7%. The other contributing isotope is ^{155}Gd having a similar abundance of 14.7 %. But its cross-section is only 61,000 barns. All other isotopes have negligibly small cross-sections. In the following only ^{157}Gd will be taken into account. All arguments given for ^{157}Gd will hold in a similar way for ^{155}Gd. The final nucleus ^{158}Gd is highly excited (7.939 MeV) and deexcites via emission of a γ cascade. According to ref.[5] primary γ's are emitted in the range between 7.857 MeV and 3.700 MeV, the latter being the lowest energetic primary γ detected. Strong lines appear at 5.903 MeV and at 6.750 MeV. (In ^{156}Gd the primary γ's reach from 3.900 MeV to 8.450 MeV without outstanding intensities.) Secondary γ's range from 2.200 MeV to very small energies, indicating that in the average more than 2 γ's are created after a capture.

The high energy of the primary γ's helps reducing the accidental background coming from radio impurities. It enables one to work at thresholds above 3 MeV for the neutron signal. The dominating part of the γ-background from radioactive nuclei has energies well below this threshold. Only the $^{208}Tl \rightarrow {}^{208}Pb$ transition from the ^{232}Th decay-chain contributes, as well as the decay of low mass radioactive isotopes created by neutron induced transfer reactions or μ interaction on ^{12}C or ^{16}O. The background correlated with these events was studied in ref.[2]. The singles contribution of γ's from U, Th and K is reduced by a factor of 4 (U and K are important for the unloaded scintillator), the number of singles correlated with μ induced radioactive nuclei is reduced by a fator of 5.5 and these of the "neutron soup" by a factor of 2.

4. Monte-Carlo Calculations for neutron efficiency and triple probability

Monte-Carlo calculations have been performed to determine the influence of the high γ-energy and γ-multiplicity on the neutron-efficiency of the 12 ton detector. The following assumptions were used:

- The decay spectrum of ^{158}Gd was used to determine the energies of the γ's released in the detector.
- Only two γ's are created at the same random origin equally distributed across the whole detector. The direction of both γ's was determined randomly. The energy-sum of both γ's was 8 MeV. Four descrete energy-combinations were calculated: 7 - 1, 6 - 2, 5 - 3 and 4 - 4 MeV. For each combination 50000 2-γ events were calculated. The resulting spectra were normalized and summed up.

- To produce only one spectrum, which contains all information about the γ's emitted from Gd the four discrete spectra were summed up. As the intensity of the emitted primary γ's varies strongly over the spectrum, the four spectra obtained for the four energy cuts must be normalized individually. For these normalisation coefficients the intensities given in ref.[5] for the individual primary γ-rays were summed up in energy intervalls of 1 MeV $\pm$ .5 MeV. The normalisation factors were normalized itself by a factor of 100/66, as the sum of all primary gammas from ref.[5] is only 66% of all neutron captures taken into account.
- No acrylic cell-walls have been introduced in the calculation.
- The resolution of the detector was set to 25% FWHM @ 1 MeV.

Fig. 2 shows the results of the calculation. Table 1 gives the γ efficiency for the detector. The detector efficiency depends on the threshold used for the neutron signal. To reduce background, one attempts to raise this threshold; to maximize efficiency a low threshold is desirable. In this respect 3.5 MeV seems to be an optimum. Additionally, in this energy range the efficiency is very stable and nearly independent of small electronic drifts. In ref.[2] it is shown, that already for a threshold of 3 MeV accidental background is suppressed sufficiently.

The Monte-Carlo calculation gives an efficiency of 75+-3 % for a threshold of 3.5 MeV. This value is clearly dominated by the high energetic primary γ's. Table 2 gives the efficiency for only one primary γ as a fuction of the threshold. The calculation was performed for one 7 MeV, 6 MeV, 5 MeV or 4 MeV γ. The efficiency was 67 % for the 7,6 and 5 MeV γ and 62 % for the 4 MeV γ indicating, that the secondary γ is contributing only weakly. This also indicates, that neglegting additional γ's is a good assumption, their influence is surely smaller than 3 %.

A further problem might be the disregard of the acrylic cell walls, which have been substituted by active scintillator material. But due to the fact, that both acrylic and mineral oil are consisting of low Z material only, and because of the high γ-energy, this is probably of minor influence.

A similar calculation has been performed to study the probability of the Gd induced γ cascade to fake a triple coincidence. A real triple coincidence is given if there is a high energetic positron signal (> 1 MeV) detected in one cell and if there are two .511 MeV positron annihilation γ's detected in adjacent cells. We plan to look for the .511 MeV signals in two adjacent cells on each side, respectively. The following 5 cell signal structure was simulated in the γ Monte Carlo: In the central cell an energy larger than 1 MeV had to be deposited and in the two neighboring cells left and right an energy larger than 50 keV and smaller than 600 keV had to be observed. An additional anti-coincidence in the surrounding cells was not required. The results are summarized in table three. Two energy cuts have been calculated assuming the emission of three γ's with 6 + 1 + 1 MeV or 4 + 2 + 2 MeV. Both calculations yield probabilities of $\simeq$ 8

%. In the writeup above a pessimistic upper limit of 10 % is assumed being a factor of 4 larger than the probability for a 2.2 MeV γ to fake a triple coincidence via multiple Coulomb scattering. Introducing a veto condition by looking for the energy of 8 MeV deposited in the total detector could probably reduce the given probability by a factor of 2. But even with the pessimistic assumption of 10 % the neutron induced background is not limiting the experiment.

4.1 Total neutron efficiency

The total efficiency for the neutron capture signal consists of 4 individual efficiencies:

$$\epsilon = \epsilon_\gamma \times \epsilon_n \times \epsilon_\tau \times \epsilon_{Gd} \tag{2}$$

ϵ_n and ϵ_{Gd} are the probabilities, that the neutrons will be captured within the fiducial volume ($\epsilon_n = 93 \pm 5$ %) and the probability of a neutron to capture on a Gd nucleus and not on a proton ($\epsilon_{Gd} = 72 \pm 4$ %). ϵ_n and ϵ_{Gd} have been determined in additional Monte-Carlo calculationsfor the .05 % loaded scintillator. The results are presented in fig.3. They are in agreement with a different Monte-Carlo calculation of Steinberg et al., ref.[4] giving values of 77 % and 23 %. ϵ_τ is the efficiency of the coincidence time ($\epsilon_\tau \approx 95$ %). The overall efficiency becomes herewith

$$\epsilon = .75 \times .93 \times .72 \times .95 = .48 \tag{3}$$

and has to be compared with the efficiency for the unloaded scintillator:

$$\epsilon = .56 \times .92 \times 1.0 \times .95 = .49 \tag{4}$$

The excellent γ efficiency of the Gd loaded detector (75 %) is compensated by the relatively bad capture probability ($\epsilon_{Gd} = 72$ %). Using a Gd-loaded scintillator of .1% Gd by weight would increase ϵ_{Gd} considerably. As we are not at all restricted by accidental background from radio impurities the additional increase of ^{232}Th is unimportant. The considerably shorter coincidence time would additionally compensate this shortcoming.

5. Conclusion

The advantages of a .05% Gd-loaded scintillator over the unloaded scintillator are obvious. Accidental background will be substantially reduced by the shorter coincidence time (factor 3) and by the high threshold applicable for the neutron like event (another reduction factor of 7). The correlated background from double neutrons will be suppressed by a factor of 3.5. An overall background rate of about 10 events per day can be reached.

For a more efficient suppression of background a Gd concentration of .1 % per weight would be necessary. At this concentration the background will be dominated by fast neutrons produced outside the detector, which enter the fiducial volume by passing

the 80 cm thick Boron loaded buffer. This background is independent of the amount of Gd and would limit the background rate to about 5 events/day. Additionally, the higher Gd concentration of .1 % would increase the detector efficiency. Values larger than 85 % seem to be reachable for the capture probability ϵ_{Gd}. Together with a 100 % timing efficiency reachable by the very short capture time of less than 30 μsec the total neutron efficiency will increase from 50 % to 60 %.

6. Acknowledgement

One of the authors, R. H., was supported by the Alexander von Humboldt foundation as Feodor-Lynen-Fellow when composing this manuscript.

References

[1] F.Boehm et al., NIM A300 (1991) 395-402

[2] V.Novikov, Appendix ? - Accidental Background of the San Onofre Detector

[3] M.Chen et al., Appendix 3 - Efficiency of the San Onofre Detector

[4] R.Steinberg, private communication

[5] NDS 56,2 (1989)

[6] F.Boehm et al., The San Onofre Neutrino-Oscillation Detector

number of calculated events 50000

energy first gamma 7.0 6.0 5.0 4.0
energy second gamma 1.0 2.0 3.0 4.0
branching ratios:
bra7_1 = .147
bra6_2 = .410
bra5_3 = .285
bra4_4 = .158

Results: Threshold in [MeV]

thresh	content	%
0.0	47668	.95
0.5	47124	.94
1.0	45435	.91
1.5	44552	.89
2.0	41937	.84
2.5	40561	.81
3.0	38623	.77
**********	**********	**********
3.5	37386	.75
**********	**********	**********
4.0	35674	.71
4.5	34275	.69
5.0	32626	.65
5.5	31135	.62
6.0	29053	.58
6.5	27022	.54
7.0	24623	.49
7.5	19191	.38
8.0	5690	.11

Table 1: Result of the Monte-Carlo calculation for the Gamma efficiency of the neutron capture on Gd. Four different calculations have been performed for four energy-cuts of gamma pairs. The gamma-energies used are:

7 + 1 MeV 6 + 2 MeV 5 + 3 MeV 4 + 4 MeV

For each energy-cut 50000 double gamma events have been calculated. The normalisation factors given above as branching ratios have been used to normalize the individual spectra of the four calculations. Then the four spectra were summed up and the summed content of the final spectrum is presented here as a function of the cut-off threshold.

number of events 100000

thresh	Gamma Energies 4 MeV	5 MeV	6 MeV	7 MeV
0.0	.81	.78	.77	.76
0.5	.79	.77	.75	.74
1.0	.77	.76	.74	.73
1.5	.76	.74	.73	.72
2.0	.74	.73	.72	.71
2.5	.71	.71	.70	.70
3.0	.68	.69	.69	.69
3.5	.62	.67	.67	.68
4.0	.20	.64	.66	.67
4.5	.00	.59	.64	.66
5.0		.21	.61	.64
5.5		.00	.55	.62
6.0			.20	.60
6.5			.01	.53
7.0			.00	.21
7.5				.01
8.0				.00

Table 2: Threshold dependent efficiencies for high energetic gammas released in the 12-ton detector. In the Monte-Carlo calculation only one gamma of respective energy was released into the fiducial volume. The different columns refer to the energy of the gamma. The threshold is given in MeV.

Triple probability for neutron capture on Gd:

triple gamma:	6 + 1 + 1 MeV	7.0 (.5) %
	4 + 2 + 2 MeV	8.5 (.5) %
double gamma:	5 + 3 MeV	4.9 (.5) %
	6 + 2 MeV	5.8 (.5) %
	7 + 1 MeV	3.9 (.5) %

Table 3: The following assumptions enter in the determination of the probability of the gamma-burst to fake the three fold coincidence:

Three gammas with the given energies are emitted.

The energy deposited in the "center" cell had to be larger than 1 MeV. The energies observed in two adjacent cells on each side of the "center" cell respectively, had to lie between 50 keV and 600 keV.

No anti-coincidences using the energy deposited in the additional cells of the detector have been applied.

As a test case, the emission of only two gammas was investigated.

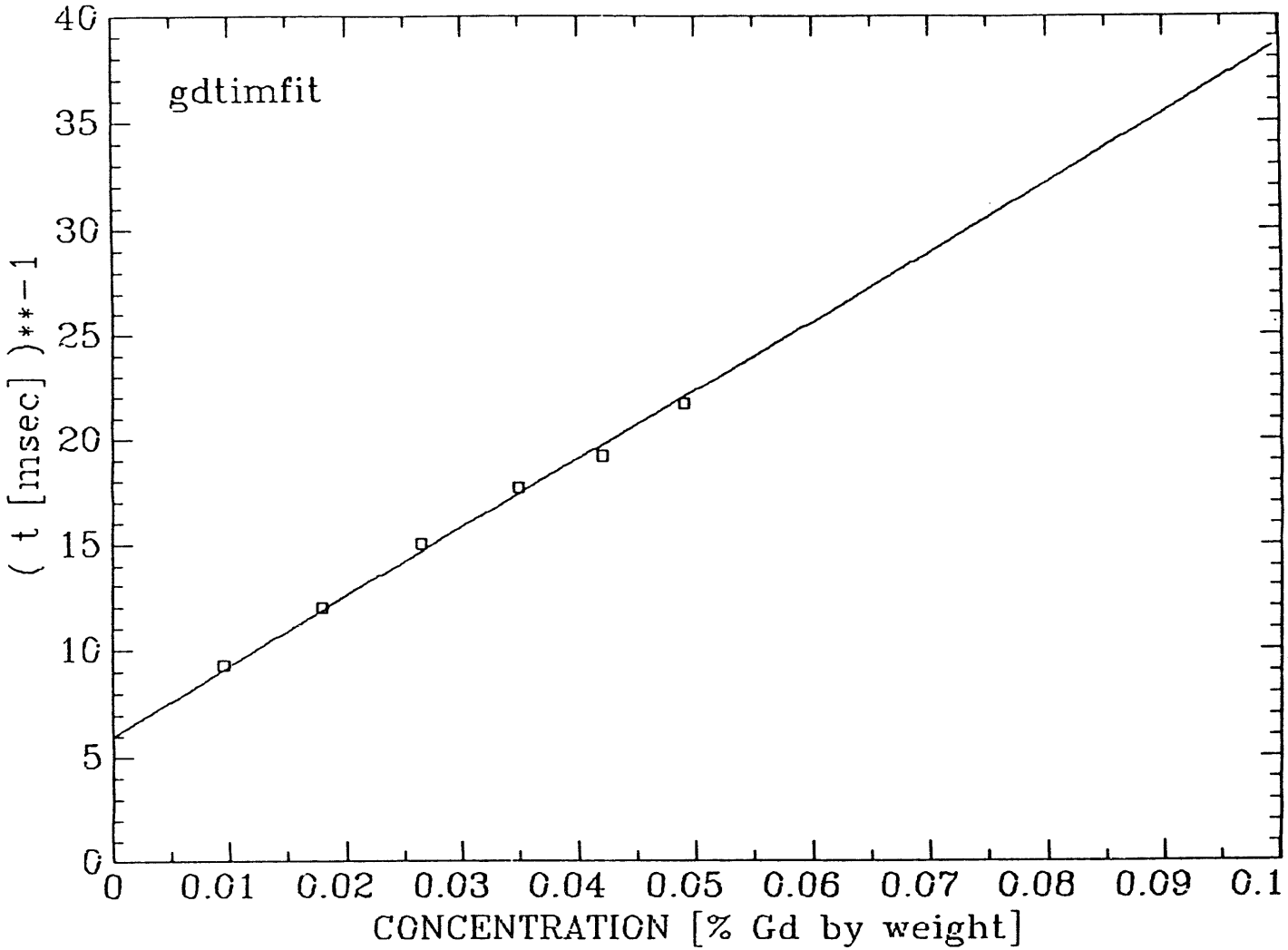

Figure 1: Measured capturetimes for Gd-concentrations ranging from .01 to .05 % by weight from ref[1]. The linear interpolation was obtained by fit:

t[msec] = 1 / (6 + 327.6 * C) ; C := Concentration of Gd by weight

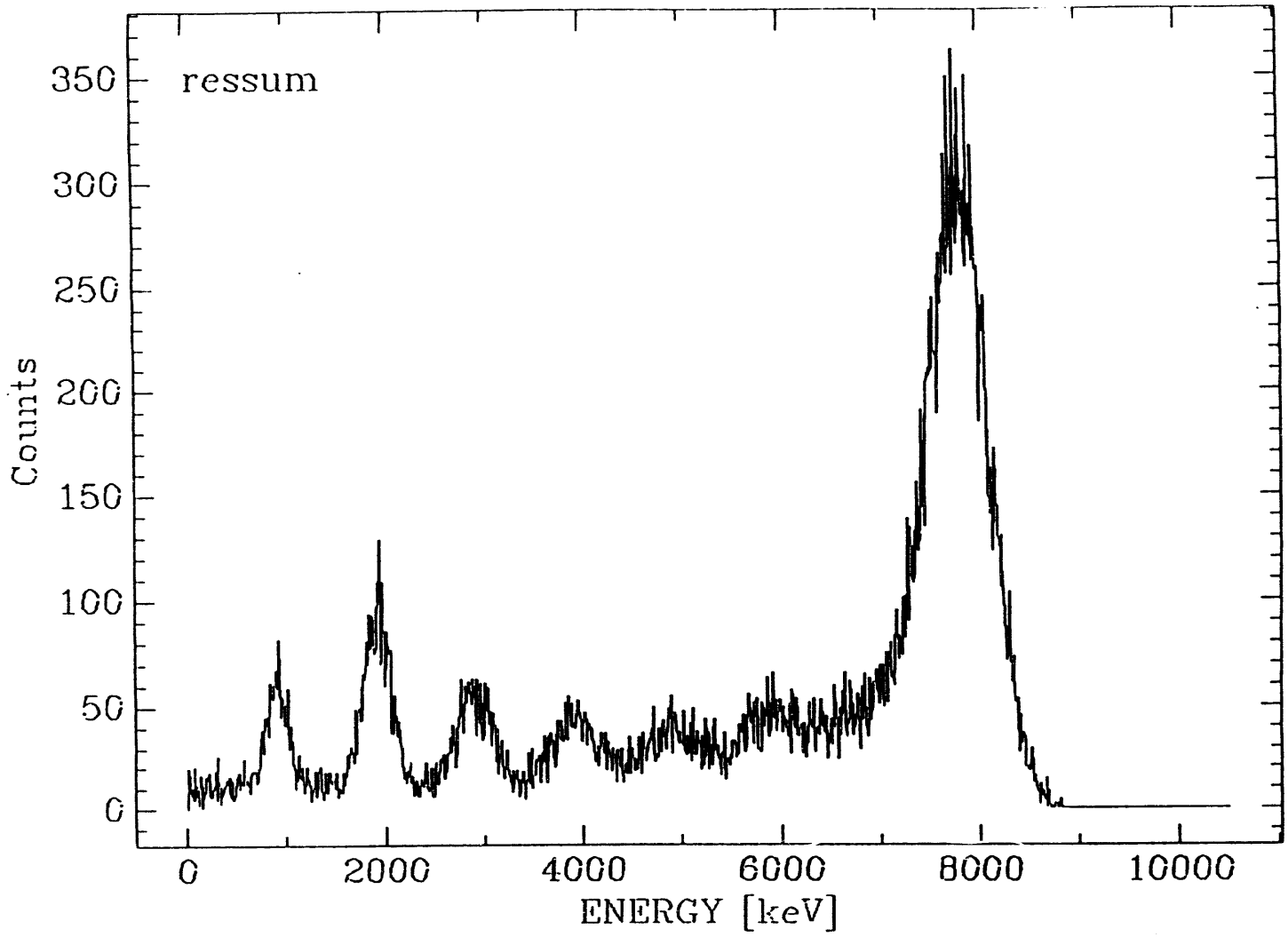

Figure 2: Gamma spectrum obtained from Monte-Carlo calculations for double-gamma emission in the fiducial volume of the 12-ton detector. Four discrete energy-cuts have been calculated, normalized and summed up. The procedure is explained in the text as well as in the subscript of Table 2. The peak-structures appearing at energies smaller than 6 MeV originate from the discrete energy-cuts made. In the experimental spectrum these structures will be smeared out.

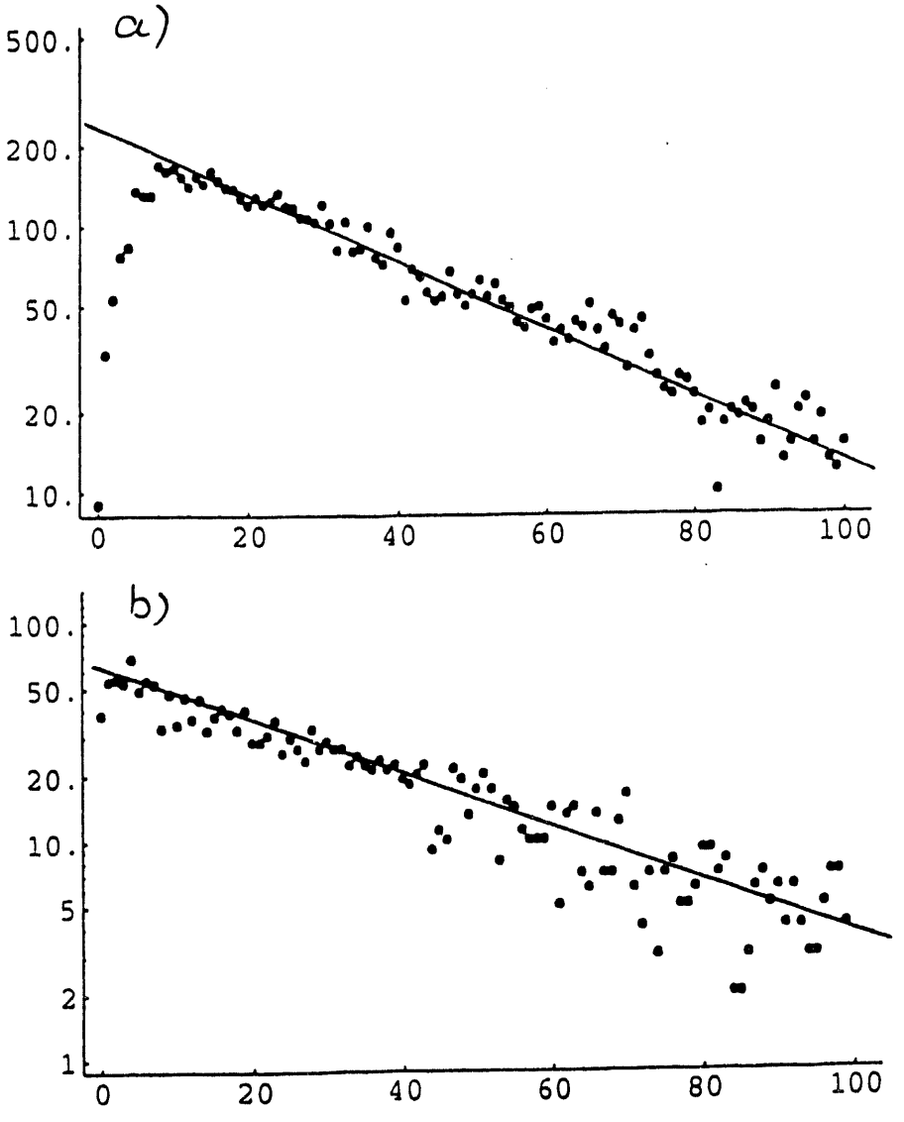

Figure 3: Calculated capture time and capture probability for a .05 % Gd-loaded scintillator.

a) Capture on Gd:
eps(Gd) = 72 %
tau(Gd) = 39+-5 musec

b) Capture on H
eps(H) = 28 %
tau(H) = 38+-5 musec

The measured capturetime from fig.1 is 45+-2 musec. An alternative Monte-Carlo mentioned in ref.[4] gives capture probabilities of 77 % and 23 %, respectively.

APPENDIX 4

Appendix 4

Part 1

Monte Carlo Studies of the Backgrounds in the San Onofre Detector

M. Chen, V. Novikov

May 18, 1993

Introduction

When considering the trigger criteria for identifying the signal from a neutrino interaction in the San Onofre detector, it is important to understand the potential sources of background. The goal, when selecting a signal detection scheme, is to maximize signal efficiency while maintaining the highest possible background rejection. Thus, we would like to know what the likelihood is of a given background to mimic the signal. Monte Carlo studies were undertaken to estimate the susceptibility of our detector design and trigger criteria to backgrounds from gammas and neutrons.

Background from Gammas

Triple Probability from Gammas

Gammas from natural and muon-induced radioactivity are an important background. An estimate of the magnitude of this background is found elsewhere in this appendix. Gammas can imitate the triple coincidence signal of a positron. They can do so via multiple Compton scattering, in many adjacent cells, leaving just the correct amount of energy in the cells (within the selected trigger thresholds) to simulate a triple coincidence. Energetic gammas can also undergo pair-production. A positron is produced in this process and its subsequent annihilation can indeed produce a triple coincidence which resembles a positron.

The probability of a single gamma to fake a triple coincidence in the detector was studied twice with two different Monte Carlo codes. One study was performed by V. Novikov. His independent code (first discussed in Appendix 3 - Efficiency) tracked gammas randomly distributed over the surface of the detector fiducial volume, isotropically incident into this volume. The specific factors important to the simulation and particular to this code (as discussed in Appendix 3, regarding the efficiency) were identical to those used in simulating the background. Figure 1 (duplicated here and discussed in a separate part of this appendix, "Accidental Background...") presents the probability of single gamma to imitate a triple coincidence. The triple coincidence criteria used here was a central cell with energy > 1 MeV and adjacent cells (in a classical triple configuration) with energy between 50 and 600 keV. No anti-coincidence was included (though earlier studies found that inclusion of an anti-coincidence greatly increases the background rejection).

The other study was performed by M. Chen using the EGS4 code. In this study, the simulation factors particular to this code were again identical to those used in simulating the efficiency (study of M. Chen in Appendix 3). Isotropic gammas were distributed randomly throughout the fiducial volume. Four gamma energies were simulated - the four most important gammas being:

1.46 MeV from ^{40}K (PMT glass)
2.2 MeV from neutron capture on H and from ^{238}U chain
2.614 MeV from ^{232}Th chain
4.4 MeV from excitation of ^{12}C nucleus (via fast neutron).

The probability to fake a triple for various trigger criteria (similar to those studied in Appendix 3 - Efficiency) are displayed in Table 1. Note that the lower threshold trigger for detection of the annihilation gammas was set to 50 keV, unless otherwise noted in the table. Note also that the anti-coincidence does have a large effect and greatly suppresses the background. An examination of Table 1 and Figure 1 reveals that the triple probability from single gammas is approximately 2%. Both Monte Carlo studies yielded this value - the results from the EGS4 study were slightly higher due to the extended acceptance criteria for triple coincidences and the lack of cell walls in the simulation.

Single Probability from Gammas

Using the independent code of V. Novikov, the probability for a single gamma of a given energy to complete a four-fold coincidence was calculated. This required that the gamma deposit energy between 1.8 and 2.5 MeV (energy resolution of the detector taken into account) and that the deposition occur near the hypothetical origin of the positron (i.e. a spatial cut factor of 6 was included). Figure 2 (duplicated from "Accidental Background...") plots the single probability as a function of gamma energy. Taken together with the triple probability from single gammas, one can compute the accidental background rate in the detector, given an estimate of the amount of radioactive contamination present. Further discussion of the accidental background appears in the separate section, "Accidental Background...".

Background from Multiple Gammas - Gd-loaded Scintillator

When considering a Gd-loaded scintillator, one must be aware that the neutron capture signal presents itself as a unique background to be considered. Following a neutron capture on ^{157}Gd is a gamma burst with 8 MeV total energy. Typically three or more gammas are emitted - two or three of them are energetic. Thus, coincident gammas can be created in the detector. The probability for this process to simulate a triple coincidence is likely to be higher than the triple probability from single gammas.

A Monte Carlo study was performed with the EGS4 code. Gd-capture events were simulated, randomly distributed in the detector. Five emission schemes were simulated:

7 + 1 MeV (two gammas simulated)
6 + 2 MeV

5 + 3 MeV
6 + 1 + 1 MeV (three gammas simulated)
4 + 2 + 2 MeV.

In the simulation of a Gd-capture event, the direction of each decay gamma was distributed isotropically. In this Monte Carlo study, the same factors as considered in the EGS4 efficiency and single gamma background were employed. One exception, however, was that energy resolution was accidentally omitted - this shouldn't have a very large effect. Additionally, the EGS4 code was run with a lower tracking cutoff for electrons and photons of 50 keV (i.e. giving greater accuracy for low energies). For the trigger criteria known as "extended five OR with summed upper threshold, no anti-coincidence" (please see Appendix 3 for an explanation of this trigger scheme), the probability for a Gd-capture event to imitate a triple coincidence (50 keV lower threshold) is given in below, for the emission schemes considered:

emission scheme	triple probability
7 + 1 MeV	3.9 %
6 + 2 MeV	5.7%
5 + 3 MeV	4.9%
6 + 1 + 1 MeV	6.9%
4 + 2 + 2 MeV	8.5%.

We see that in the worst case, the triple probability is ~4 times greater than that for single gammas.

If one were to employ an anti-coincidence, this triple probability would be reduced significantly. Thus, one should look at all the other cells excluding the cluster of five cells that triggered triple coincidence. There would probably be excess energy deposited in these cells, as the total energy of the Gd-capture gammas sums to 8 MeV. One would use this excess energy to reject the triple, attributing it to this background. A high rejection threshold could be employed, minimizing the effect of the anti-coincidence criterion on the signal efficiency.

Because the total energy of the Gd-capture event is so great, the background from natural radioactivity is practically zero. However, the large spatial extent of the Gd-capture signal decreases the importance of a spatial cut in rejecting background. Thus, when considering the single probability for Gd-loaded scintillator, one is essentially considering just the "neutron-soup" capture background, with no spatial rejection. The four-fold probability is equal to that of the neutron capture portion of the signal efficiency. These issues are discussed in "Accidental Background...".

With regards to correlated backgrounds from multiple neutrons, the increased triple probability from the Gd-capture signal is important. In the "two-neutron" correlated background, both neutrons created by a muon survive the muon veto and are both captured in the fiducial volume on Gd, The first capture event fakes the triple coincidence with increased probability. The second capture event completes the four-fold coincidence. Using the worse possible result from the Monte Carlo, an 8% probability to fake a triple by a Gd-capture event, one arrives at a total two-neutron background rate of 3.6 per day, for a Gd-loaded scintillator.

Correlated Backgrounds from Single Neutrons

Fast neutrons are a correlated background in the detector. They may penetrate to the fiducial volume (un-vetoed) and may interact in a cluster of cells, leaving recoil protons with equivalent energy just in the right amount to fake a triple coincidence. Alternatively, the neutron might interact with a carbon nucleus in the scintillator, exciting it. The first excited state of ^{12}C decays with a 4.4 MeV gamma - this gamma may trigger a triple coincidence as described earlier. In both of these processes, the neutron remains in the detector, possibly thermalizing and capturing completing the four-fold coincidence. Thus, single neutrons can be the source of correlated background events.

Monte Carlo simulations of fast neutrons in the detector were performed. An independent neutron transport code was employed (code originated with SNO, written by R. Heaton and modified by T. Radcliffe and M. Chen). Fast neutrons of various energies were simulated, isotropically incident into the detector and randomly distributed on the surface of the fiducial volume.

The following factors are important in the simulation of neutrons in the detector. Multiple interactions were allowed. Both elastic and inelastic scattering cross-sections were included (inelastic process on C). The thermalization and capture of neutrons on H and on Gd is treated in the Monte Carlo. Capture gammas and gammas arising from the excitation of ^{12}C are created but not tracked by the neutron code. The time of each interaction is available. For recoiling protons, the equivalent-electron energy as a function of the proton energy was deduced using the parameterization of Maier and Nitschke [1]. For elastic scattering off carbon or gadolinium, the equivalent-electron energy is negligible.

Monte Carlo results exist so far only for the classical triple trigger criteria. Here, we require that the central cell register over 1 MeV (no upper threshold imposed in this simulation). The adjacent cells must fire between 50 and 600 keV energy. Energy resolution was simulated as 25% @ 1 MeV fwhm.

For the probability that a fast neutron produces a complete triple coincidence via multiple recoil protons and captures within fiducial volume of the scintillator, the Monte Carlo gave 1.6×10^{-3} for 14 MeV neutrons and a probability of 1.2×10^{-3} for 24 MeV neutrons. Note that the requirement that the neutron capture in the fiducial volume is important in the case of a Gd-loaded scintillator and less important in the case of unloaded scintillator. For an unloaded scintillator, if the offending neutron escapes the fiducial volume, it will most likely be captured in the buffer. If it captures on H in the buffer (here a boron-loaded buffer would assist), it might re-direct the 2.2 MeV capture gamma back into the detector. Thus, those neutrons that "escaped" the fouth requirement of the coincidence might still be registered in the detector. This is not so for Gd-loaded scintillator in the fiducial volume.

A neutron might produce a correlated background signal through the excitation of the 4.4 MeV gamma. Figure 3 shows the probability that a neutron of a given energy entering the detector will excite a 4.4 MeV gamma. The detector is quite large and energetic neutrons have a long way to go as they slow down and lose energy. The top curve of Figure 3 reveals that the probability to produce a 4.4 MeV gamma is as large as 40% for a 20 MeV neutron. This seems a little too high - we should be a little skeptical

of this result. However, we will use it in our estimate. We demand that the same neutron that excited the 4.4 MeV gamma also capture in the fiducial volume. The lower curve in Figure 3 displays the cumulative probability (4.4 MeV excitation plus capture). Finally, we include (manually) the triple probability from a single 4.4 MeV gamma, which has been Monte Carlo'ed separately (we must do this as the neutron code does not track gammas). Figure 4 gives the total probability for a fast neutron to simulate a triple coincidence and to capture. This probability is approximately 2×10^{-3}.

Thus, to determine the complete four-fold coincidence probability from a single neutron one should include the probability arising from multiple recoil protons, the probability arising from 4.4 MeV excitation and the detection probability of the 2.2 MeV capture gamma (discussed in Appendix 3 - Efficiency). As the detection probability of the capture gamma (in the case of H or Gd) is approximately 50%, we can take the sum of 2×10^{-3} and 1.6×10^{-3} and multiply by 50%. The total four-fold coincidence probability from single neutrons (of energy between 8 - 24 MeV) is 2×10^{-3}. Thus, our segmented detector design and "classical" triple coincidence criteria are able to suppress the background from neutrons by a factor of 500.

Conclusions

Monte Carlo studies have given the following important rejection factors for neutrons and gammas. For neutrons, the four-fold coincidence requirement gives a factor 500 rejection. For gammas, the triple coincidence requirement includes a probability of 0.02 to trigger a triple coincidence (thus reducing the accidental background). For coincident gamma bursts coming from neutron capture on Gd, the triple probability has an upper limit value of 8%.

References

[1] K.H. Maier and J. Nitschke, *Nucl. Instr. and Meth.*, **59** (1968) 227.

Type	1.46 MeV	2.2 MeV	2.614 MeV	4.4 MeV
Classical triple 50 keV lower	92 ± 10	167 ± 13	166 ± 13	159 ± 13
Classical triple 100 keV lower	57 ± 7	118 ± 11	114 ± 11	111 ± 11
Extended five OR 50 keV lower	115 ± 12	241 ± 17	258 ± 17	247 ± 17
Extended seven OR 50 keV lower	131 ± 14	272 ± 20	293 ± 21	277 ± 20
Classical w/anti 50 keV lower	79 ± 9	121 ± 11	120 ± 11	91 ± 10
Classical w/anti 100 keV lower	49 ± 7	84 ± 9	83 ± 9	69 ± 8
Extended five OR w/anti	103 ± 11	193 ± 15	209 ± 16	170 ± 14
Extended five OR w/anti sum upper 0.6 MeV	102 ± 11	183 ± 15	184 ± 15	136 ± 13
Extended five OR w/anti sum upper 0.8 MeV	106 ± 11	236 ± 17	238 ± 17	186 ± 15
Extended five OR no anti sum upper 0.8 MeV	118 ± 12	297 ± 19	293 ± 19	261 ± 18

Table 1: Triple Probability from Single Gammas ($\times 10^{-4}$)

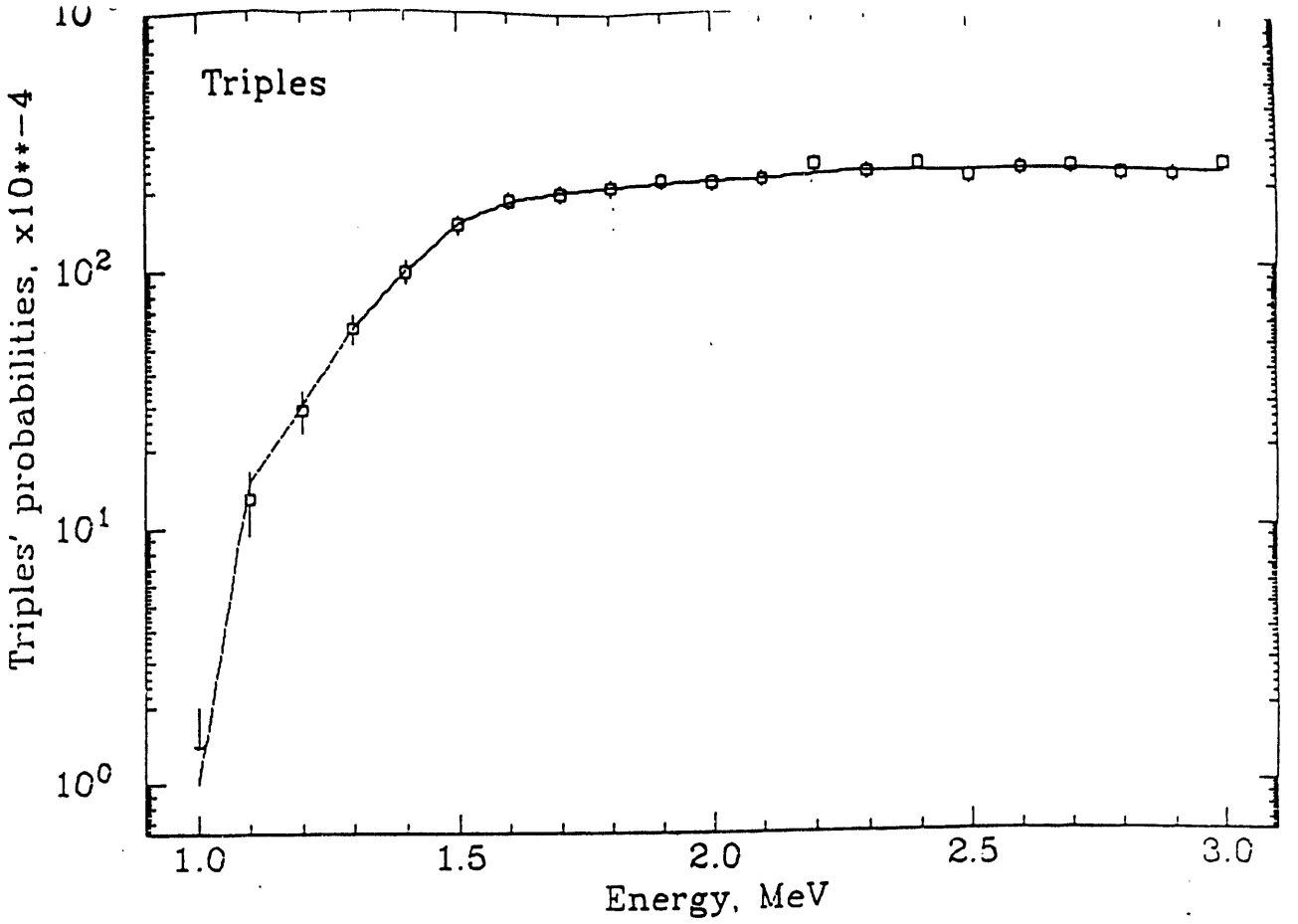
Triples
Triples' probabilities, x10**-4
10^2
10^1
10^0
1.0
1.5
2.0
2.5
3.0
Energy, MeV

FIG. 1

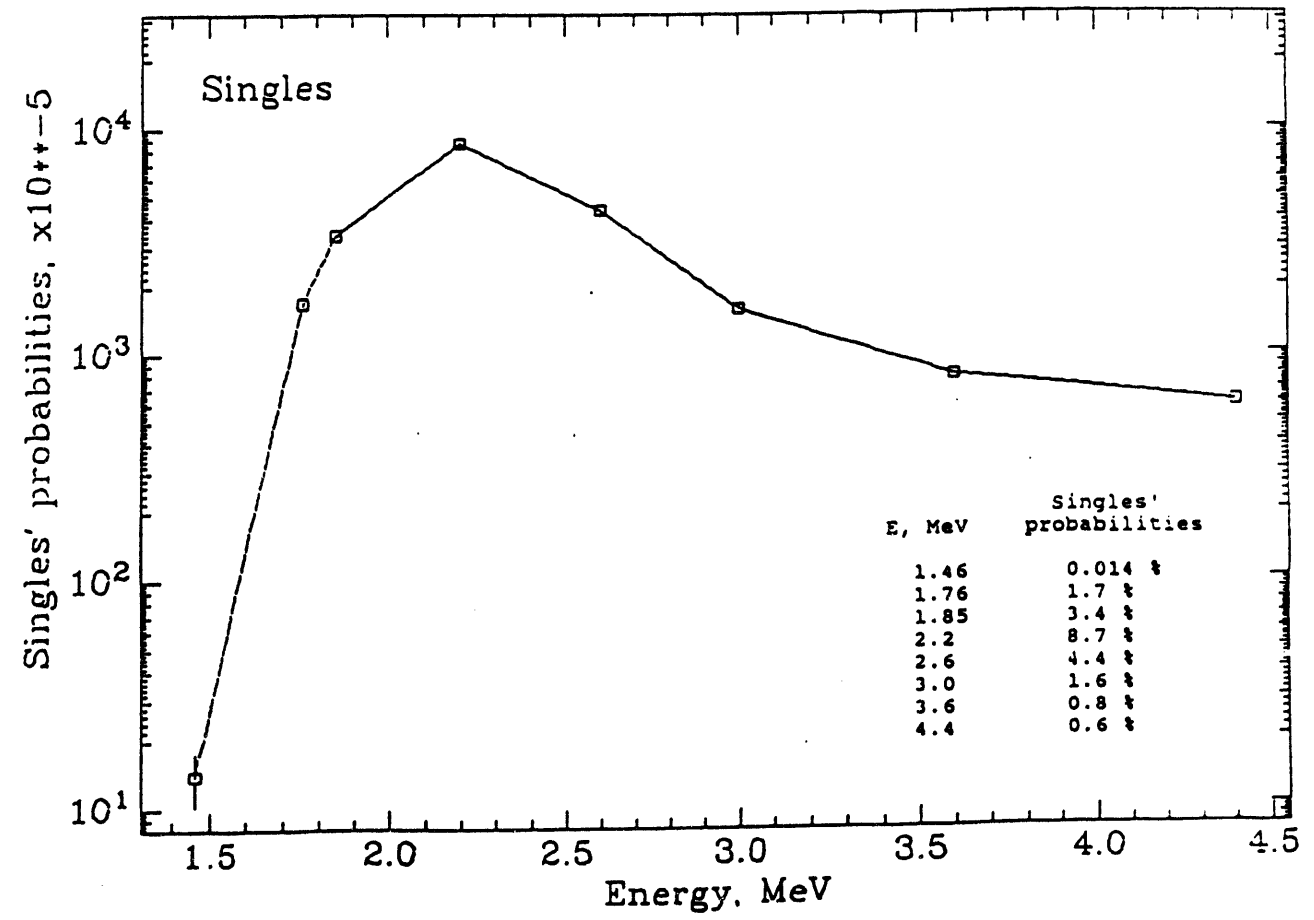
Singles
Singles' probabilities, x10**-5
10^4
10^3
10^2
10^1
1.5
2.0
2.5
3.0
3.5
4.0
4.5
Energy, MeV
E, MeV
Singles' probabilities
1.46 0.014 %
1.76 1.7 %
1.85 3.4 %
2.2 8.7 %
2.6 4.4 %
3.0 1.6 %
3.6 0.8 %
4.4 0.6 %

FIG. 2

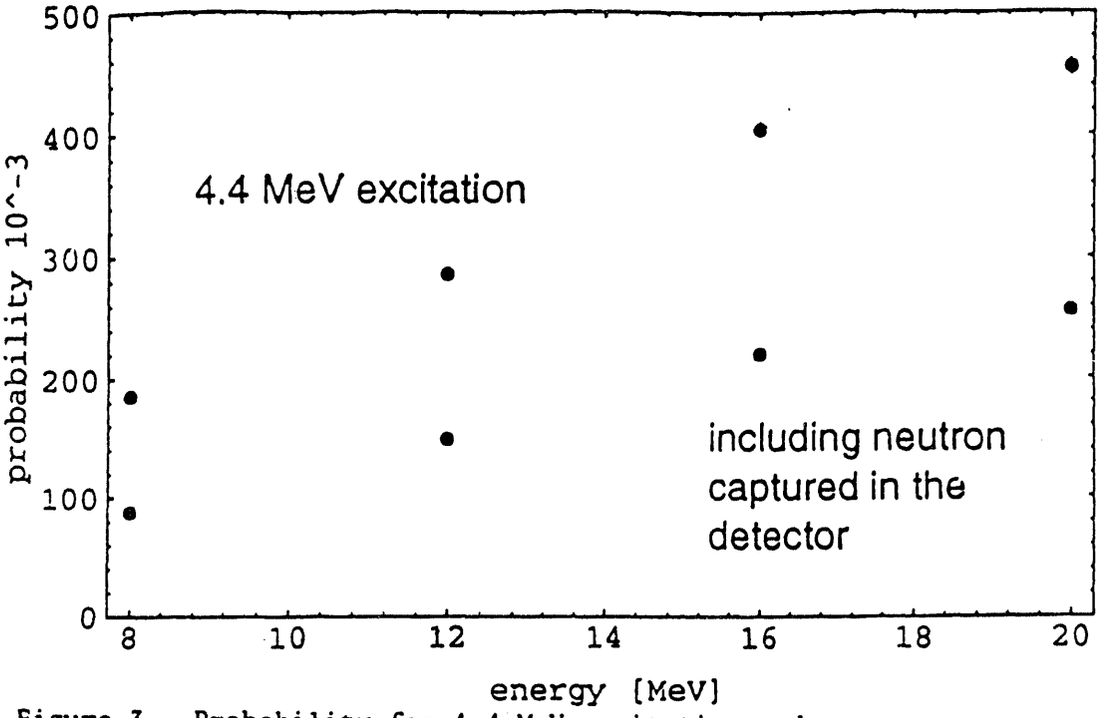

Figure 3. Probability for 4.4 MeV excitation and neutron capture

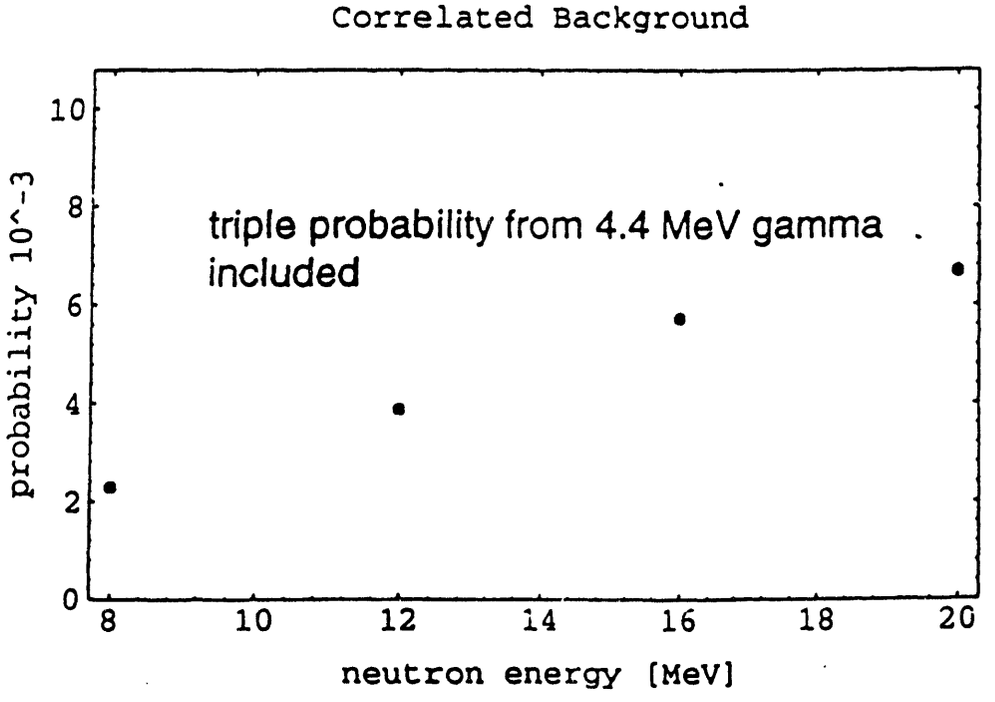

Figure 4. Probability for four-fold coincidence

APPENDIX 4

Part 2

ACCIDENTAL BACKGROUND of the SAN ONOFRE DETECTOR

V.M.Novikov

April 12, 1993

Preface.

In Chapter 1 estimation of accidental background for the scintillator without gadolinium is given; in Chapter 2 background is adjusted for the case of a Gd-loaded scintillator (0.05 % by weight). From time to time, some parameters were changed; this is why the following notes are important.

Important conventions.

Detector location. The detector was assumed to be at 25 mwe underground.

Detector mass. As a target for production of μ-induced radioactive nuclei as well as neutrons in fiducial volume, detector was supposed to consist of 12 t of carbon (in scintillator) and 0.7 t of oxygen (in acrylic).

Muon flux of 28 $sec^{-1}m^{-2}$ at 25 mwe is accepted.

Muon trigger rate is 2000 sec^{-1} for veto counters, 900 sec^{-1} for the fiducial volume of the detector.

Muon veto time is 500 μsec for stopped muons, 100 μsec for muons going through the fiducial volume of the detector and 10 μsec for muons which hit only veto counters (the latter trigger rate is 1,100 sec^{-1}).

Neutron capture time is 170 μsec for the scintillator without gadolinium and 50 μsec for the Gd-loaded scintillator (0.05% of Gd).

Coincidence window for the neutrino signal is 500 μsec for the scintillator without gadolinium and 150 μsec for the Gd-loaded scintillator.

CHAPTER 1. Scintillator without Gadolinium.

1.Why γ's are dangerous ?

Gammas likely produce both triples and singles in the San Onofre detector (whenever here, unless explanation is given, termin "single" means probability for a gamma with given energy to complete, together with preceding triple, 4-fold background event; this probability includes both energy and spatial cuts). For gammas randomly distributed over the detector volume their probabilities to create a triple and a single can be found in [1] and [2], respectively. Since most gammas are supposed to be external ones, one has to know probabilities to produce triples by such gammas,- see Fig.1; these values are very similar to those for gammas randomly distributed in the detector. Probabilities of gammas of different energies to produce singles are shown on Fig.2 [2] (to create single, no difference between external gammas and randomly distributed ones was assumed).

In order to give an idea on the order of gamma flux we should start to worry about, let us suppose for the gammas of energy of $\geq$1.4 MeV to have (somehow averaged over the spectrum) probability of 2% to create both triples and singles. Then, taking into account coincidence window of 500 μsec, we come to equation

$$R_{bkg} = 1.7 \times (\frac{R_\gamma}{10})^2, \qquad (1)$$

where R_γ is a number of gammas entering the fiducial volume of the detector, sec^{-1}, R_{bkg} - background of the San Onofre detector, day^{-1}. In other words, the flux of gammas of 10 sec^{-1} with $E_\gamma \geq$ 1.4 MeV give rise to background of 1.7 day^{-1}.

It is not easy to achieve the level as low as 10 γ's sec^{-1} in 12 t detector; for example, in LVD experiment the counting rate of γ's with $E_\gamma \geq$1.5 MeV is 100 sec^{-1} in inner single module of mass of 1 t and surface of 7 m^3 [3]; scaling by surface to the San Onofre detector ($\sim$ 8 times larger) gives rate of 800 sec^{-1}. In LSD experiment similar inner module has rate of 20 - 30 sec^{-1} for $E_\gamma \geq$0.8 MeV [4] which approximately corresponds to the rate of $\sim$ 100 sec^{-1} in San Onofre detector after scaling by surface and having some idea on the γs' energy spectrum.

2.Sources of gammas from natural radioactivity.

^{238}U and ^{232}Th chains and ^{40}K are the main sources of gammas from natural radioactivity. Table 1 shows mean number of high energy gammas released per decay of each isotope, including daughters.

Isotope	$\geq$.6 MeV	$\geq$1.4 MeV	$\geq$2.0 MeV
^{238}U	1.357	0.410	0.088
^{232}Th	1.283	0.483	0.359
^{40}K	0.107	0.107	0.00

Table 1. Number of high energy gammas per decay of ^{238}U, ^{232}Th and ^{40}K.

In ^{238}U chain high energy gammas ($E_\gamma \geq .6$ MeV) with relative intensities $\geq 10^{-5}$ are coming from four isotopes [5]: ^{214}Bi (138 lines), ^{234m}Pa (81 lines), ^{214}Pb (3 lines) and ^{214}Po (1 line). ^{214}Bi is much more relevant than other isotopes.

In ^{232}Th chain γ's are shared more or less uniformly by three isotopes: ^{208}Tl (19 lines), ^{228}Ac (113 lines) and ^{212}Bi (11 lines).

In 10.7 % of ^{40}K decays 1.46 MeV γ is released.

Figs.3–4 demonstrate "importance" each of isotopes of U and Th series mentioned above.

3.Where γ's are coming from to the San Onofre detector ?

3.1 Passive shielding.

It is very important to make a right choice of the passive shielding. It looks that combined shielding consisting of low radioactive concrete ("sulfurcrete", [6]) and mineral oil buffer is appropriate.

3.1.1 Sulfurcrete shielding.

Compare to lead, sulfurcrete contains U and Th of the similar level as lead (in weight %, see Appendix 1 and [6]), produces much smaller fast neutron flux and is supposed to be much cheaper. The latter allows sulfurcrete to be used as a constituent of the walls of the laboratory which significantly simplifies the construction of the experiment. The thickness of sulfurcrete should be $\sim$ 60 cm or more; if so, we can assume that γ flux from the walls is coming mostly from the radioactivity in the sulfurcrete itself.

To calculate γ flux from the sulfurcrete surface, the following relevant numbers were used: mean values of A=20 and Z=10 were taken, i.e. one–element medium instead of compound *; density ρ=2.44 g/cm^3; weight fractions of ^{238}U, ^{232}Th and ^{40}K are 9 *ppb*, 11 *ppb* and 86.8 *ppm*, respectively (see the table of Appendix 1); all γ–lines mentioned in the Chapter 2 were taken into account.

Resultant γ spectrum, in terms of $cm^{-2}sec^{-1}$, is shown of the Fig.5. Scaling to the detector's surface (50 m^3) gives integral number of gammas of 930 sec^{-1} with $E_\gamma \geq$1.4 MeV. This is a lot (equation (1) gives background of $\sim$15,000 day^{-1}), i.e. necessity of additional passive shielding is obvious.

3.1.2 Muon veto, buffer.

The muon veto and the buffer are supposed to consist mainly of acrylic and mineral oil. I'll assume that they do not give rise to γ ray flux. There are two requirements needed to be satisfied: 1. Thickness should be enough to reduce flux of γ's from concrete, 2. At least buffer should be loaded with boron; this shifts energy of neutron's capture gammas from dangerous 2.2 MeV (capture on ^1H) to safer 0.7 MeV (capture on ^{10}B) as well as reduces flux of thermal neutrons into detector's volume.

The buffer+μ–veto thickness of 63 cm required for effective moderation of fast neutrons [7] still allows $\sim 20 sec^{-1}$ of γ's with $E_\gamma \geq$1.4 MeV enter the fiducial volume of the detector. Let's choose 80 cm (which is logic, at least, because such a thickness is required for the

* The validity of this assumption was verified to be correct by comparison with Monte Carlo calculations using EGS code. Thanks to Mark and Ralf providing me result of γ transportation in concrete.

scintillator's dead layer for reduction of 1.46 MeV γ flux from PMTs to the level of 5 sec^{-1}–see next chapter). This reduces γ flux to the level of 8.8 sec^{-1} of $\geq$1.4 MeV γ's. Convolution of the γs' energy spectrum (see Fig.6) with energy–dependent triples' and singles' probabilities (Figs.1,2) gives expectation of 0.121 sec^{-1} of triples and 0.156 sec^{-1} of singles.

3.2 Photomultipliers.

Photomultipliers XP4512B contain a lot of potassium (see Appendix 2): 7 % of K_2O in the window (312.5 gramms of S80151 glass per each photomultiplier). This is 2.2 kg of potassium from 120 photomultipliers. As a result, $\sim$ 7,300 sec^{-1} of 1.46 MeV γ's are coming into 4π (or 3,700 sec^{-1} in direction of the fiducial volume of the detector while from the sulfurcrete the flux of 1.46 MeV γ's is 685 sec^{-1} per 50 m^2). There is a contamination of PMTs by ^{238}U and ^{232}Th also but I'll presume most part of such gammas coming from walls.

For initially proposed dead layer of thickness of 50 cm the counting rate behind it will be $\sim$ 50 sec^{-1} which is not acceptable. Reduction up to the level of 6 sec^{-1} (or 0.075 sec^{-1} of triples and 0.001 sec^{-1} of singles, respectively) requires 80 cm of scintillator to be a dead layer. Probably we should start to think about using PMTs with smaller content of potassium.

3.3 Radon.

Not radon is dangerous itself but its decay product ^{214}Bi. There are not so many high energy gammas in its decay, but, instead, cascade of γ's is very usual for ^{214}Bi which is often even more dangerous for us than just a single γ. For further discussion I'll accept equality of a ^{222}Rn decay to a 2.2 MeV γ in meaning of probability to produce a triple and a single (one should calculate probability to produce a triple and a single per 1 decay of ^{214}Bi).

Usually outdoor radon concentration varies in range of 0.1–0.4 pCi/l (4–15 Bk/m^3) with, depending on the location, sometime significantly higher or lower values [8]. Measured at the same location, indoor concentration is always higher than outdoor one. Table 2 show radon concentrations at three underground sites [9].

Site	Windsor	Mont Blanc	Sudbury
^{222}Rn, Bk/m^3	2.	74.	37.

Table 2. Radon activity in different underground sites [9].

All values listed in Table 2 were measured when ventilation was "ON". With ventilation "OFF" radon concentration is icreasing rapidly by hundreds times [10].

For 12 t San Onofre detector location we should use ^{222}Rn concentration numbers given for Mont Blanc or Sudbury rather than Windsor's one (in the latter case extremely low radon concentration is explained by the location of the laboratory in salt mine, with very low content of ^{238}U in salt). Moreover, it is known that radon concentration varies very significantly in time (for example, in Mont Blanc site it varies in the range of 1 to 4 pCi/l, or 40 to 150 Bk/m^3, [10]).

In the San Onofre detector radon is located in air gaps between detector's cells; full volume of air is estimated to be $\sim$ 0.5–1 m^3. Obviously, special care should be made to eliminate flux of radon into detector's cavity. For example, assuming radon activity of 40 Bk/m^3 and "active" air volume of 0.5 m^3, from (1) one get backgroung in San Onofre detector $\sim$ 30 day^{-1} – just from the radon!

The (only) possibility to reduce such a background is to place the whole detector (including buffer and μ veto) into housing with permanent flow of radon–free air inside it. In this case concentration of radon in detector's cavity will be govern, presumably, by radon coming from PMTs, resistors, cables, etc. Hopefully, we can reach the level of 0.1 pCi/l, or $\sim$ 2 sec^{-1} (in 0.5 m^3 of air), or, in another words, 0.046 and 0.174 sec^{-1} of triples and singles, respectively.

3.4 Active volume of the detector.

Fortunately, relatively cheap components which constitute inner part of the detector can be found (mineral oil, acrylic). Nevertheless, some background is also coming from the detector itself; part of it is due to natural radioactive contamination while muon induced activity is also not negligible.

3.4.1 Natural radioactivity in acrylic and scintillator.

I'll suppose here 0.3×10^{-12} g/g of ^{238}U and $0.3\times^{232}Th$ [11], $\leq 41.\times10^{-9}$ of ^{40}K [12] in mineral oil, $21.\times 10^{-12}$ of ^{238}U and $17.\times10^{-12}$ of ^{232}Th in acrylic [13]. The corresponding number of decays of ^{238}U and ^{232}Th in mineral oil (12 t) is 0.066 and 0.022 sec^{-1}, correspondently, in acrylic (2.16 t) is 0.561 and 0.148 sec^{-1}, correspondently. From ^{40}K there are 2.3 sec^{-1} 1.46 MeV γ's in the fiducial volume from the scintillator (upper limit).

Again, one should perform calculations in order to interpret 1 decay of ^{238}U or ^{232}Th in terms of "triples" and "singles". Here I'll again will presume that 1 such a decay in acrylic (both for triples and singles) and in scintillator (for singles) is equivalent to 2.2 MeV γ while such a decay in scintillator has two times higher probability to produce a triple.

After all, one can get that 0.049 sec^{-1} of triples ($\sim$60 % of them are from ^{40}K) and 0.070 sec^{-1} of singles ($\sim$ 0.4 % are from ^{40}K) are coming from components of the inner detector itself.

3.4.2 Muon induced radioactivity.

3.4.2a Capture and spallation products. ^{12}C (12 t in scintillator) and ^{16}O (0.7 t in acrylic) are main producers of μ-induced radioactive nuclei. For stopped muons, I'll suppose 8% and 25% of nuclear capture probability for ^{12}C and ^{16}O, respectively [15]. I accept also neutron multiplicity of 0.8, i.e. $\sim$20% μ captures without neutron emission. This means (for μ-stopping rate at 25 m w.e. of 50 $kg^{-1}day^{-1}$, [15]) production of $\sim10^4$ of ^{12}B and 1.8×10^3 of ^{16}N per day. From μ-spallation (assuming neutron production rate of 11 $kg^{-1}day^{-1}$ and two-to-one neutron emission probability of 0.1 [16]) 1.2×10^5 of ^{11}C, 1.2×10^4 of ^{10}C, 0.7×10^4 of ^{15}O and 0.7×10^3 of ^{14}O per day are formed. ^{15}O is not important (its decay contains no gammas; the positron from its decay is effectively absorbed by acrylic). Taking into account decay scheme of each isotope I accept probabilities for ^{12}B, ^{16}N, ^{10}C, ^{11}C, ^{14}O to create a triple as 0.%, 1.%, 20.%, 10.%, 5.% and probabilities to create a single as 2.%, 2.%, 6.%, 6.%, 6.%, respectively. In other words, this is 0.167

sec^{-1} of triples and 0.095 sec^{-1} of singles.

3.4.2b "Neutron soup". Three main sources constitute "neutron soup": 1.External neutron flux, 2.Neutrons from the buffer, 3.Neutrons produced in fiducial volume.

Our estimation gives expectation of 1,800 day^{-1} of external neutrons with $E_n \geq 5$ MeV. It corresponds to the total number of neutrons not more than 5,000 day^{-1} (even if we accept pessimistic suggestion of μ-capture neutron spectrum as a neutron source spectrum).

The number of capture and spallation neutrons produced in the buffer and entering the detector is estimated to be 15,000 and 70,000 day^{-1}, respectively. Neutrons from μ-capture are effectively vetoed by 500 μsec stopped-muon veto. Of 70,000 spallation neutrons, about 40,000 are produced by muons which hit only veto counters but not the fiducial volume of the detector (i.e., 10 μsec veto time is appllied).

Neutrons produced in fiducial volume from μ-capture are effectively vetoed. Of 130,000 spallation neutrons 72,000 are still alive after 100 μsec.

Total unvetoed "neutron soup" is 117,000 day^{-1}, or 1.354 sec^{-1}. This means .033 sec^{-1} of triples and 0.118 sec^{-1} of singles.

3.5 Construction materials.

Any construction materials aimed to icrease mechanical properties of the detector should be avoided unless they have radioactive purity of $\sim 10^{-10}$ g/g or better in ^{238}U and ^{232}Th. For example, 1 t of material with a very good purity of 10^{-9} g/g brings background nearly 60 day^{-1}.

4.Background estimation.

Table 3 summarizes the accidental background components discussed above. I remind that thickness of buffer (+ μ-veto) as well as scintillator's dead layer were chosen to be 80 cm; sulfurcrete was supposed to be of infinitive thickness.

	Triples, sec^{-1}	Singles, sec^{-1}
Passive shielding	0.121	0.156
Photomultipliers (only ^{40}K)	0.075	0.001
Radon	0.046	0.174
U,Th,K in scintillator and acrylic	0.049	0.070
μ-induced radioactive nuclei	0.167	0.095
"Neutron soup"	0.033	0.118
	0.491	0.614

Table 3. Accidental background components in the scintillator without Gd.

With 500 μsec coincidence window background of the San Onofre detector will be 13 day^{-1}. Further reduction of background is possible by increasing of buffer's thickness. On the other hand, Table 3, of course, is not complete; few unknown inner background components (or underestimation of listed ones) may exist which can sweep out effect of passive shielding.

CHAPTER 2. Gd-loaded Scintillator.

Compare to pure C_nH_{2n}, in Gd-loaded scintillator one has smaller neutron capture time and more energetic neutron sygnal. In general, this leads to better sygnal-to-background ratio; more in details, this means:

1. Reduction of background singles' rate (while the triple rate will be essentially the same);

2. Reduction of accidental part of background: 1.due to smaller coincidence window (for external gammas, inner natural radioactivity and and long-lived μ-induced nuclei); 2.due to better working veto time for through going muons (for "neutron soup");

3. Reduction of correlated part of background – due to better working veto time for through going muons (for background from multiple neutrons).

Below the results of estimations of accidental background counting rate for scintillator without gadolinium (Chapter 1) are revised for the case of Gd-loaded scintillator.

1.Passive shielding.

Gd-loading will not change the rate of triples from external gammas (0.121 sec^{-1}). The rate of singles will be zero; this is because of the fact that even the most energetic γ from natural radioactivity (2.6 MeV, ^{208}Tl) is far from the lower threshold of neutron-sygnal (3 MeV). Yield from the well known cascade 0.583 MeV×2.614 MeV (= 3.2 MeV) is negligible (unbelievable that both gammas will penetrate the buffer).

2.Photomultipliers.

Triple rate will be the same as for the scintillator without Gd (0.075 sec^{-1}) while for the reason mentioned above the single rate will be zero.

3.Radon.

The same argument works for background from radon, i.e. we'll have 0.046 sec^{-1} of triples and no singles (to be more correct, in decay of ^{214}Bi there are transitions in which gammas with $E_\gamma \geq 3.0$ MeV are released - but with summed up yield of $\sim 10^{-4}$ - which is negligible). On the other hand, word "radon" always meant ^{222}Rn here. In some cases, activity of ^{220}Rn (which is much more efficient to produce singles in Gd-loaded scintillator than ^{222}Rn) could be of the order or even higher than that one from ^{222}Rn [8]. However, in our case (radon housing, buffer, sulfurcrete) we are much more safe from ^{220}Rn flux due to its small half-life (~1 min).

4.U, Th and K in acrylic and scintillator.

Radiopurity of liquid scintillator will depend on the purity of Gd. Gd content of 0.05% means that any radioimpurity in Gd will be diluted by liquid scintillator by 5×10^{-4}. Let us accept Gd purity given by Steinberg [17]: 5 ppm of K, 0.005 ppm of ^{232}Th and 0.0007 ppm of ^{238}U. The purity of the scintillator considered in Chapter 1 after loading to it 0.05% of gadolinium will be 0.65×10^{-12} g/g of ^{238}U, 2.8×10^{-12} g/g of ^{232}Th and $\leq 44. \times 10^{-9}$ of K. In other words, compare to the original C_nH_{2n} scintillator, Gd brings almost no effect in K, approximately 2 times worse purity in ^{238}U and almost 10 times worse purity in ^{232}Th.

Corresponding number of decays of ^{238}U and ^{232}Th in scintillator (12 t) is 0.143 and 0.205 sec^{-1}, respectively, in acrylic (2.16 t) is 0.561 and 0.148 sec^{-1}, respectively (numbers for acrylic do not differ from those ones given in Chapter 1). From ^{40}K there are 2.5 sec^{-1} of 1.46 MeV γ's from the scintillator (upper limit).

Again, I'll suppose that the probability to produce triple event by a decay of ^{238}U or ^{232}Th is 2.3 % and 4.6 % from acrylic and scintillator, respectively. After all, triple rate will be 0.070 sec^{-1} (~55 % of them are from ^{40}K).

For singles the situation is different from the case of scintillator without gadolinium. Only decays of ^{208}Tl (from ^{232}Th chain) are important, and they are very efficient to produce singles. In energy, I'll put 50 % and 100 % efficiency that $\geq$3.0 MeV is detected, for acrylic and scintillator, respectively (the difference between acrylic and scintillator is that in the latter case beta particles are counting too). Spatial cut reduces both numbers by a factor 6. We also should take into account branching ratio of 0.36 of ^{208}Tl in ^{232}Th chain. After all, rate of singles will be 0.017 sec^{-1}.

5.Muon induced activity.

5.1 μ-induced radioactive nuclei.

Unlike to 3.4.2a of the previous Chapter, the single rate from this background source will be much less (for production rate of radioactive nuclei and their probabilities to create a triple see Chapter 1). Taking into account decay scheme of each isotope I'll accept probability for ^{12}B, ^{16}N, ^{10}C, ^{11}C, ^{14}O to produce a single as 10.%, 15.%, 1.%, 0.%, 10.%, respectively. In other words, this is 0.167 sec^{-1} of triples and 0.017 sec^{-1} of singles.

5.2 "Neutron soup".

Unvetoed neutron rate of 38,000 day^{-1} is coming from external flux (5,000) and flux from the buffer (~33,000 = 40,000$\times e^{-10./50.}$) – 3.4.2b of the previous Chapter.

Of 130,000 day^{-1} spallation neutrons produced by muons going through the fiducial volume of the detector ~17,000 are still alive after 100 μsec.

Therefore, total unvetoed "neutron soup" rate is 55,000 day^{-1}, or 0.637 sec^{-1}. This means 0.015 sec^{-1} of triples and 0.055 sec^{-1} of singles.

6.Summary of accidental background.

Table 4 summarizes the accidental background components discussed above.

	Triples, sec^{-1}	Singles, sec^{-1}
Passive shielding	0.121	–
Photomultipliers (only ^{40}K)	0.075	–
Radon	0.046	–
U,Th,K in scintillator and acrylic	0.070	0.017
μ-induced radioactive nuclei	0.167	0.017
"Neutron soup"	0.015	0.055
	0.494	0.089

Table 4. Accidental background components in the Gd scintillator.

With 150 μsec coincidence window accidental background of the San Onofre detector

will be $0.494 \times 0.089 \times (150. \times 10^{-6}) \times (8.64 \times 10^{4}) = 0.6\ day^{-1}$.

The important question should be verified:

– Do we have the same spatial background suppression factor for singles as for the scintillator without Gd? (In particular, is it the same 1/6 for gammas from n-capture on Gd as it is for 2.2 MeV γ?).

AIIM

Association for Information and Image Management
1100 Wayne Avenue, Suite 1100
Silver Spring, Maryland 20910
301/587-8202

Centimeter

Inches

MANUFACTURED TO AIIM STANDARDS
BY APPLIED IMAGE, INC.

2 of 2

CONCLUSION.

As a conclusion, it looks that accidental background counting rate of 13 day^{-1} in scintillator without gadolinium and ≤ 1 day^{-1} with Gd-loaded scintillator (0.05% of Gd) is reachable in the San Onofre neutrino detector. As far as detector's design is concern, the following conditions should be satisfied:

– combined passive shielding consisting of sulfurcrete of "infinitive" (at least 60 cm) thickness and mineral oil based buffer of 80 cm thickness;

– only high purity materials should be used for inner detector's part and buffer ($\sim 10^{-12}$ g/g). The latter should be boron loaded;

– 80 cm scintillator's dead layer at the PMT side;

– both inner detector and the buffer should be located inside the housing which prevents from the radon flux.

REFERENCES.

1.M.Chen, "Monte Carlo Studies of the Signal and Background for the San Onofre Neutrino Detector", internal report, August 27, 1992.

2.V.M.Novikov, "Efficiency of the San-Onofre Neutrino Detector and Background from Single Gammas", internal report, August 19, 1992.

3.V.Alpat et al., Presented at Texas/PASCOS'92, Berkeley, 13-18 December 1992, and V.Alpat, Private Communication.

4.O.Saavedra, Private Communication.

5.C.M.Lederer, Table of Isotopes, Wiley-Interscience, 1978.

6.SNO Collection of Annexes, 1987, Annex 9.

7.N.Mascarenhas, "Neutron Background in the San Onofre Experiment", presented at Albuquerque, August 1992.

8.W.Nazaroff, A.Nero, Radon and Its Decay Products in Indoor Air, 1988.

9.J.J.Simpson, "Why are Physicists Going Underground ?", in Proceedings of the WEIN'89 Symposium, Montreal, 1989.

10.M.Aglietta et al., Nuclear Physics B (Proc.Suppl.) **28A** (1992) 430.

11.F.Boehm et al., NIM **A300** (1991) 395.

12.ICP-MS Analysis, Sept. 15, 1992, see Appendix 3.

13.SNO Collection of Annexes, 1987, Annex 14.

14.M.Chen, V.M.Novikov, "Background of the San-Onofre Neutrino Detector from Multiple Neutron Events", internal report, November 19, 1992.

15.S.Chalarambus, Nuclear Physics **A166** (1971) 145.

16.L.B.Bezrukov et al., Sov. J. Nucl. Phys. **17** (1973) 987.

17.R.Steinberg and C.E.Lane, "The Perry Experiment", talk at the meeting at Irvine University, February 19, 1993.

FIGURE CAPTIONS

Figure 1
Probabilities of γs of different energies to create a triple in the San Onofre 12 t detector. Random distribution over the surface; random angular distribution into 2π (in direction of the detector). Central cell lower threshold 1 MeV; "wing" lower and upper thresholds are 0.05 and 0.6 MeV, respectively; no anticoincidece.

Figure 2
Probabilities of γs of different energies to create a single in the San Onofre 12 t detector [2]. For definition of "single" see text.

Figure 3
Intensities of γ lines with $E_\gamma \geq 0.6$ MeV from isotopes of ^{238}U chain.

Figure 4
Intensities of γ lines with $E_\gamma \geq 0.6$ MeV from isotopes of ^{232}Th chain.

Figure 5
γ flux from sulfurcrete, $cm^{-2}sec^{-1}$.

Figure 6
γ flux from sulfurcrete behind the buffer+μ-veto shielding of 80 cm of thickness.

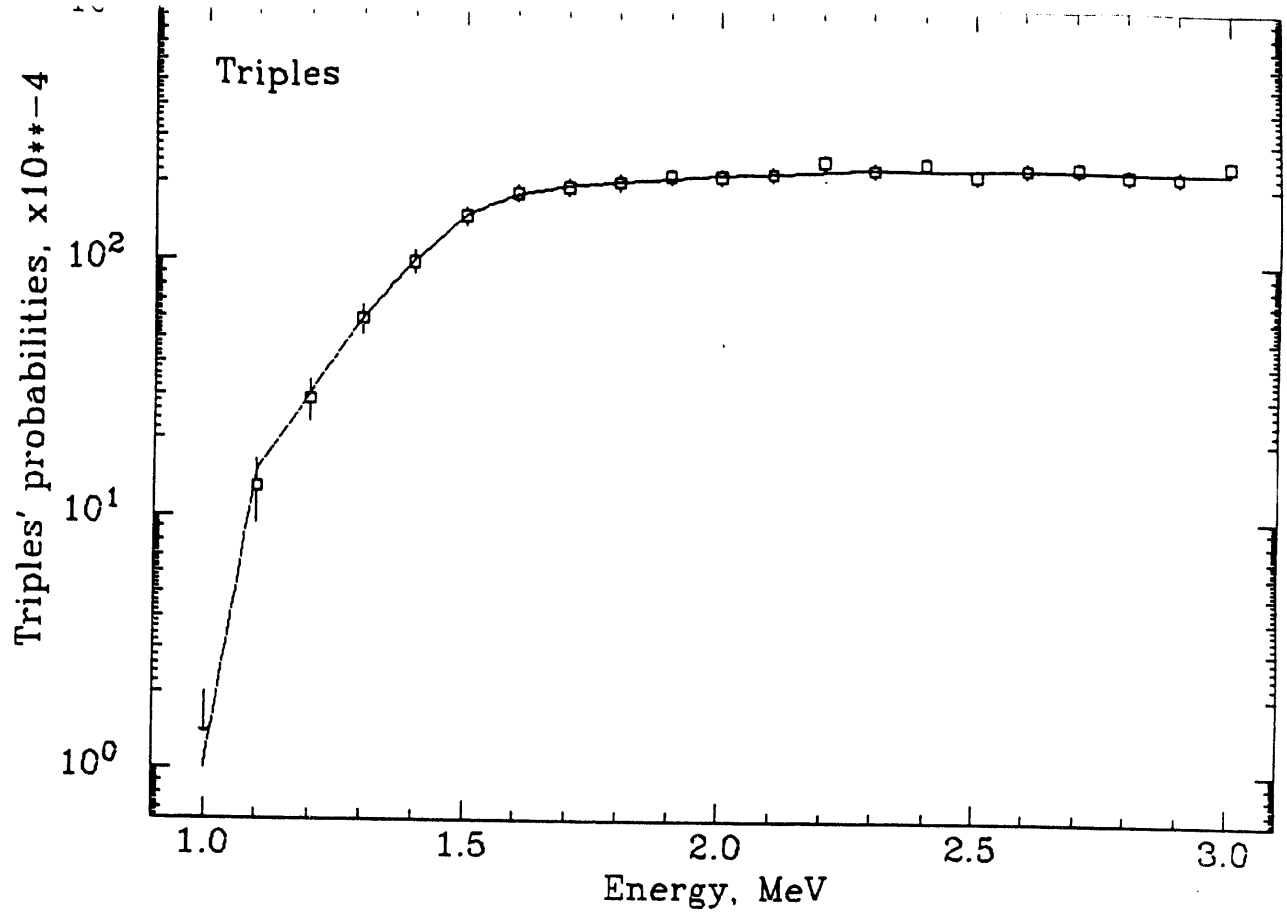
Triples
Triples' probabilities, x10**-4
10^2
10^1
10^0
1.0
1.5
2.0
2.5
3.0
Energy, MeV

FIG. 1

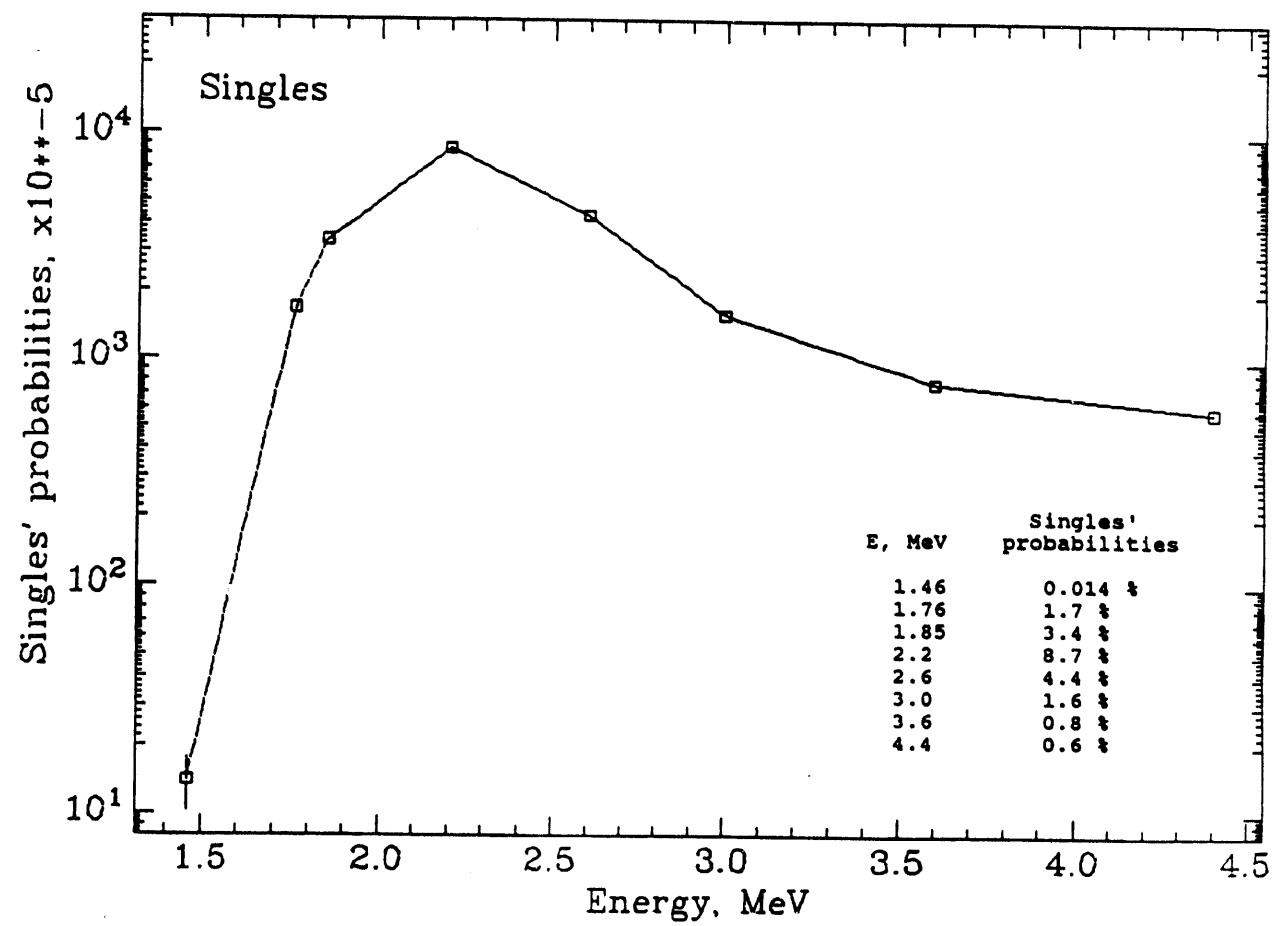
Singles
Singles' probabilities, x10**-5
10^4
10^3
10^2
10^1
1.5
2.0
2.5
3.0
3.5
4.0
4.5
Energy, MeV
E, MeV
Singles' probabilities
1.46 0.014 %
1.76 1.7 %
1.85 3.4 %
2.2 8.7 %
2.6 4.4 %
3.0 1.6 %
3.6 0.8 %
4.4 0.6 %

FIG. 2

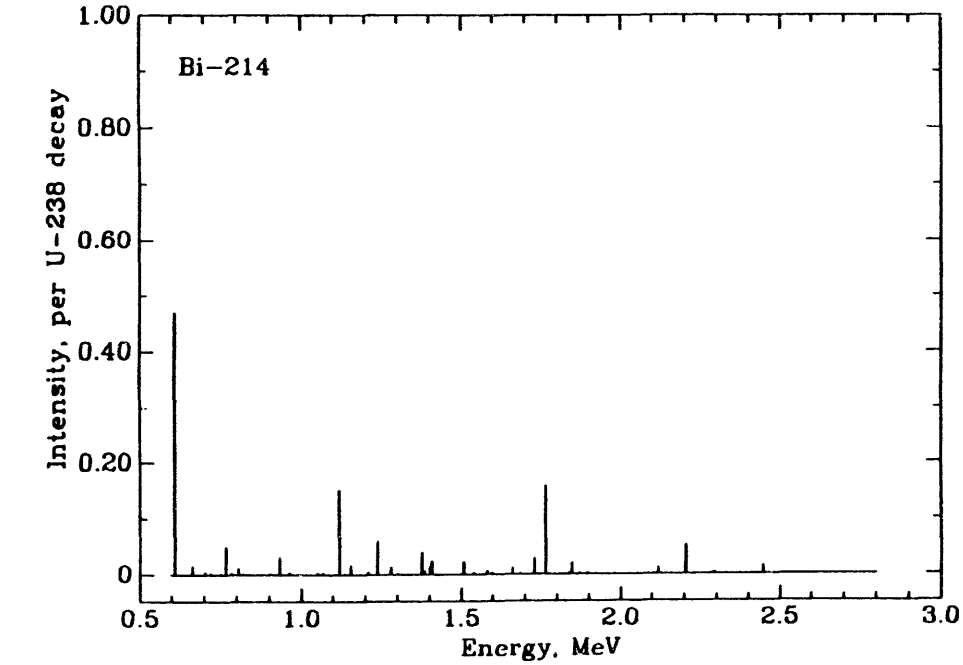
Bi-214
Intensity, per U-238 decay
1.00
0.80
0.60
0.40
0.20
0
0.5
1.0
1.5
2.0
2.5
3.0
Energy, MeV

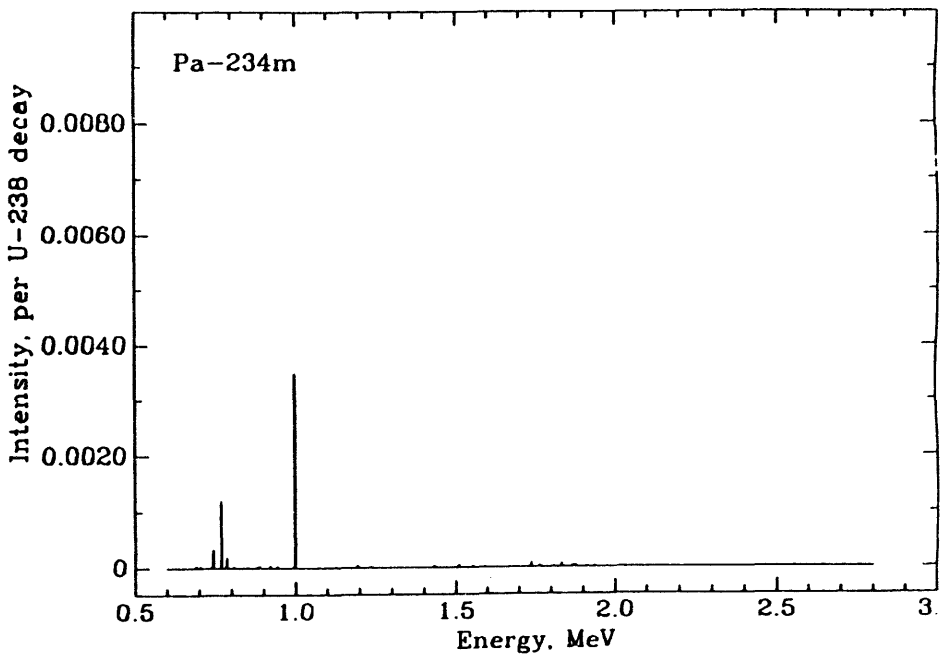
Pa-234m
Intensity, per U-238 decay
0.0080
0.0060
0.0040
0.0020
0
0.5
1.0
1.5
2.0
2.5
Energy, MeV

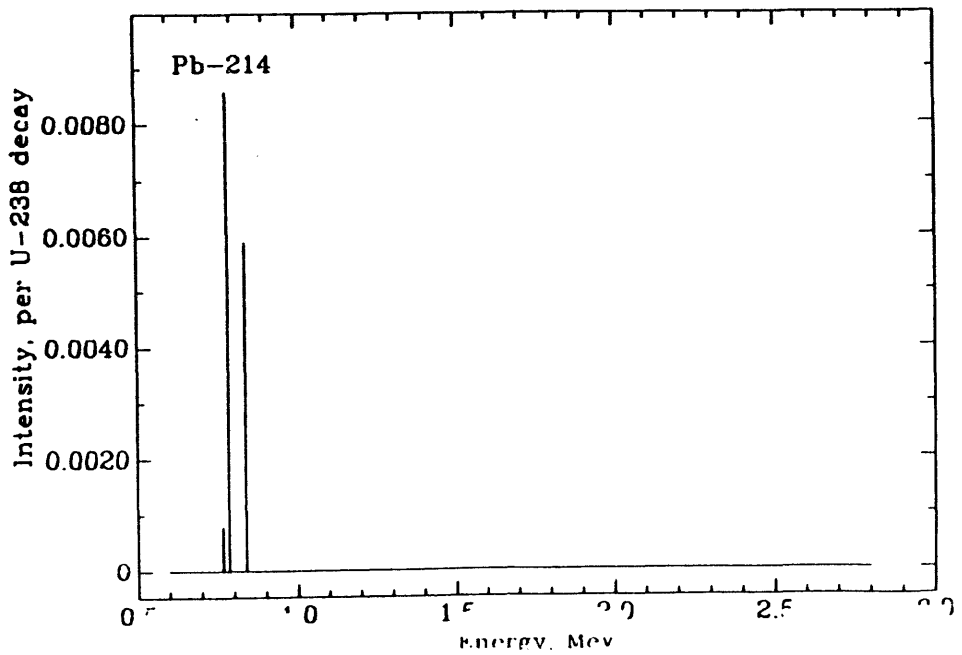
Pb-214
Intensity, per U-238 decay
0.0080
0.0060
0.0040
0.0020
0
Energy, MeV

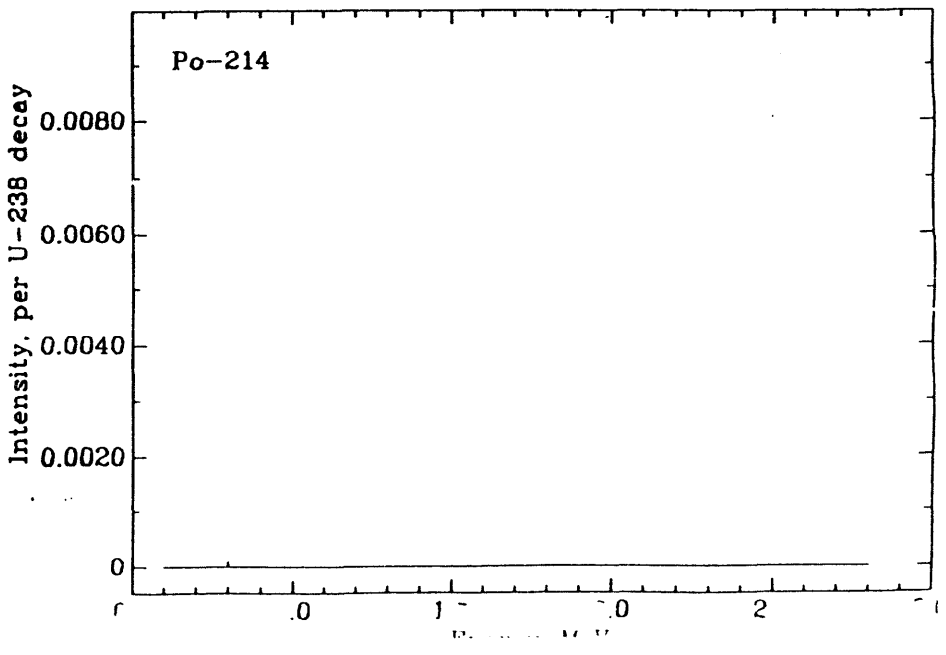
Po-214
Intensity, per U-238 decay
0.0080
0.0060
0.0040
0.0020
0

FIG. 3

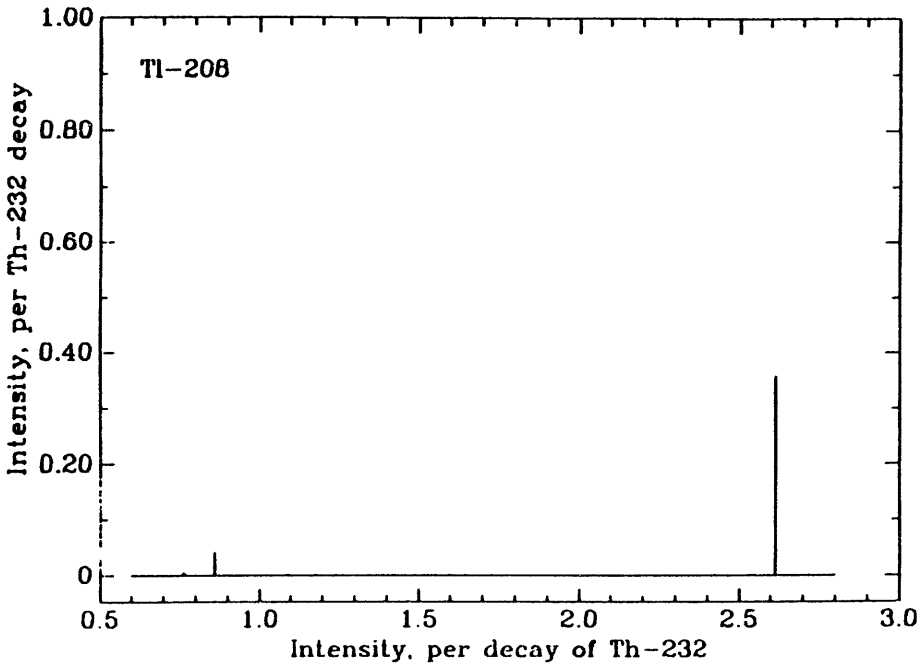
Tl-208
Intensity, per Th-232 decay
1.00
0.80
0.60
0.40
0.20
0
0.5
1.0
1.5
2.0
2.5
3.0
Intensity, per decay of Th-232

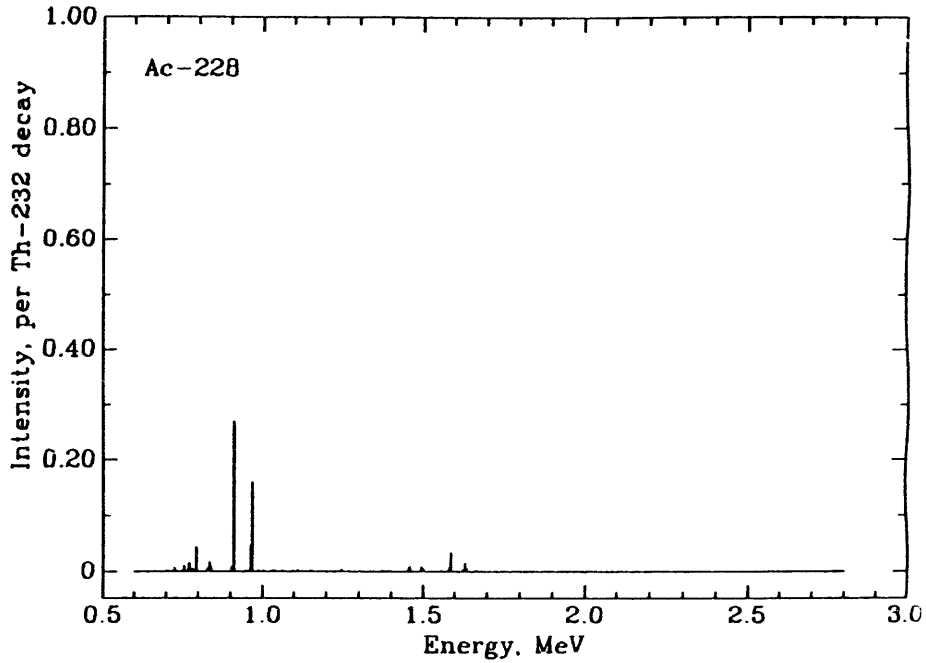
Ac-228
Intensity, per Th-232 decay
1.00
0.80
0.60
0.40
0.20
0
0.5
1.0
1.5
2.0
2.5
3.0
Energy, MeV

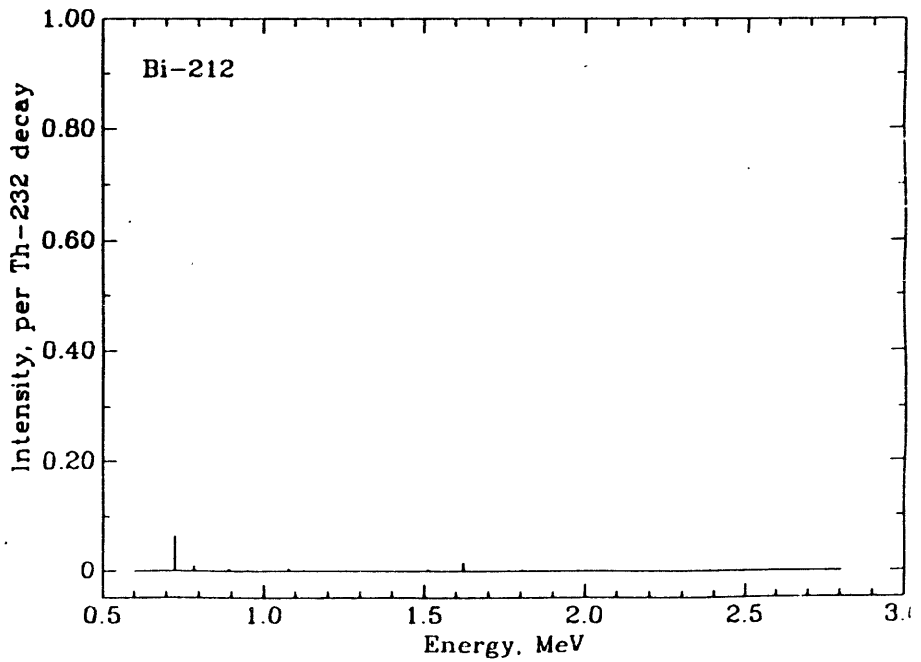
Bi-212
Intensity, per Th-232 decay
1.00
0.80
0.60
0.40
0.20
0
0.5
1.0
1.5
2.0
2.5
Energy, MeV

FIG. 4

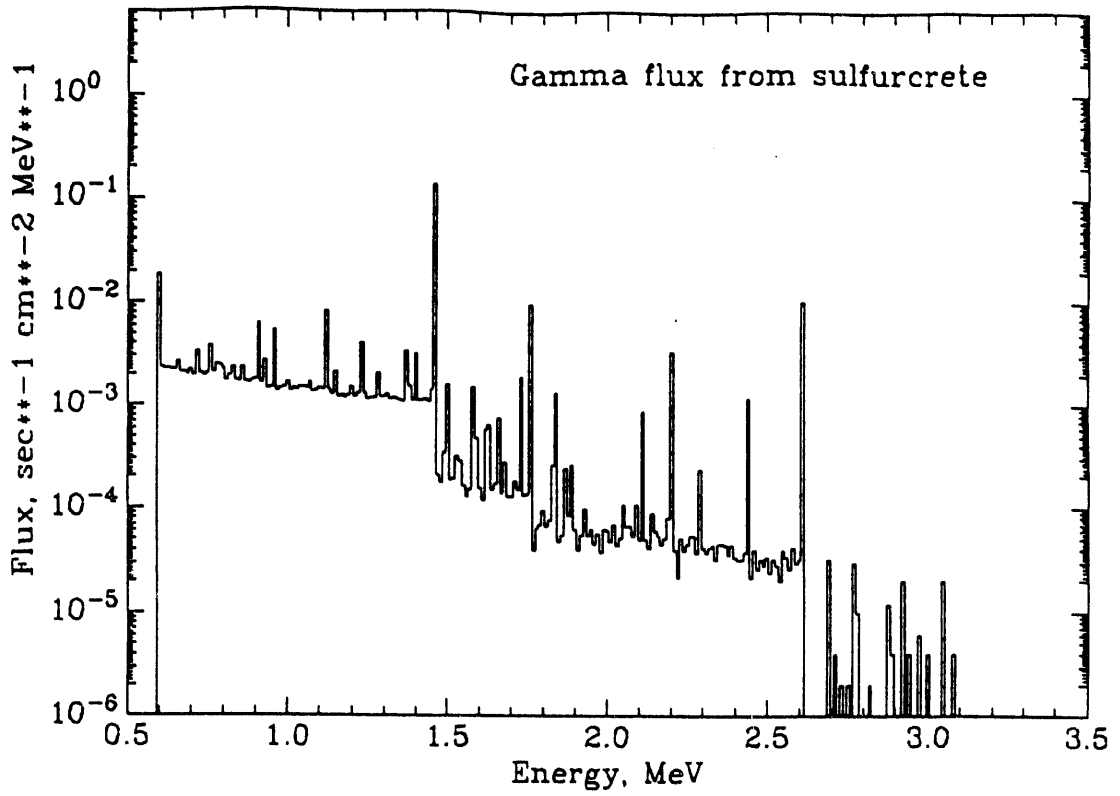
Gamma flux from sulfurcrete
Flux, sec**-1 cm**-2 MeV**-1
10^0
10^-1
10^-2
10^-3
10^-4
10^-5
10^-6
0.5
1.0
1.5
2.0
2.5
3.0
3.5
Energy, MeV

FIG.5

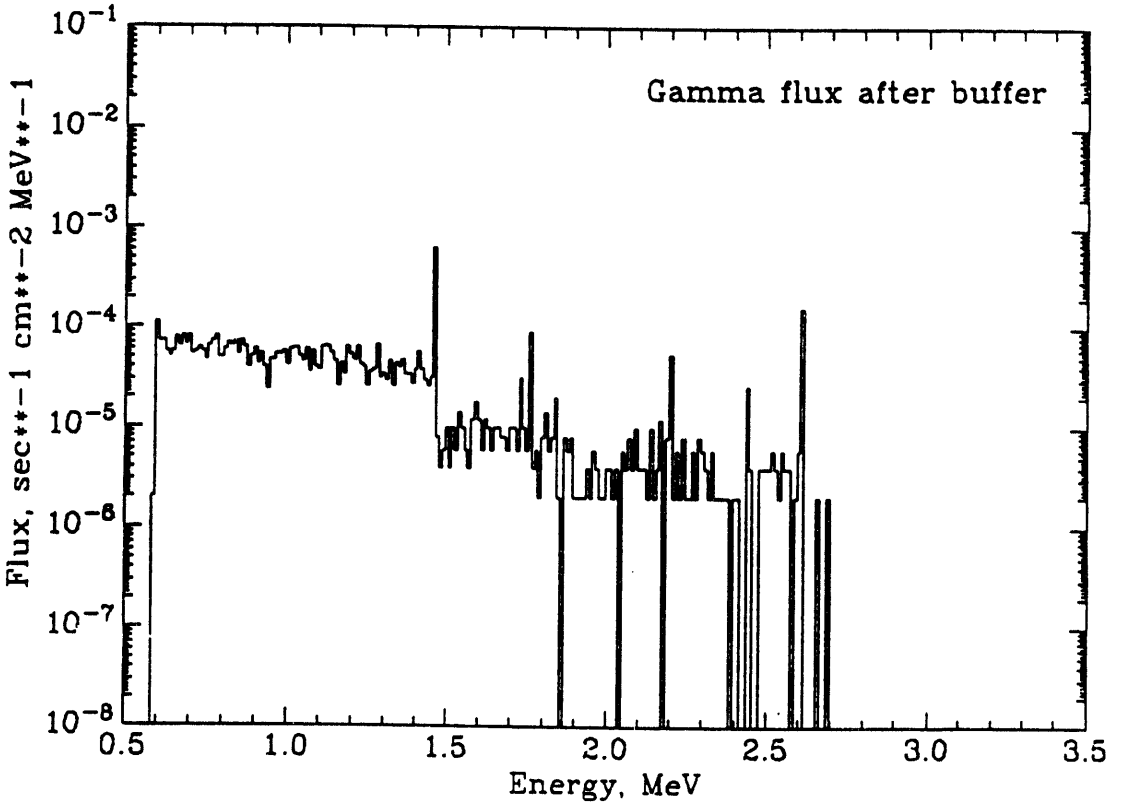
Gamma flux after buffer
Flux, sec**-1 cm**-2 MeV**-1
10^-1
10^-2
10^-3
10^-4
10^-5
10^-6
10^-7
10^-8
0.5
1.0
1.5
2.0
2.5
3.0
3.5
Energy, MeV

FIG.6

APPENDIX 1. Composition of sulfurcrete.

Element	Weight %
H	0.034
C	11.41
O	44.96
Na	0.0434
Mg	11.11
Al	0.0434
Si	0.081
S	12.96
K	0.00868
Ca	19.27
Mn	0.0434
Fe	0.0868
Zn	0.0434
Th	11 ppb
U	9 ppb

Table 4: "Sulfurcrete" Composition. This table does not include the boron which is to be added to improve neutron absorption. For the present design this has been set at the level of 1% by weight, and the above numbers would be modified accordingly. The thorium and uranium content was measured by INAA at the University of Guelph.

APPENDIX 2. Potassium content in photomultipliers.

(184

Philips Photonics Brive

Date: 18/8/92

From: Bob Esmeijer
Tel : 19.33.55.86.37.58
Fax : 19.33.55.86.37.73

To : Wayne Seemungal

Copy: J.Lettieri
P.L'Hermite/J.Nussli/R.Leclercq

Subject:Potassium in XP4512B

Ref. BE/3754

The total weight of the window of the XP4512B is 312.5 grams (type of glass is S80151).
The Weight percentage of Potassium oxyde is 7%

Regards,

Bob Esmeijer

APPENDIX 3. Composition of mineral oil.

Elemental Research Inc.
309-267 West Esplanade
North Vancouver, B.C.
V7M 1A5, Canada

September 15, 1992

ICP-MS Analysis

Sample Identity : Mineral oil + pseudocumene mix
E.R.I. Reference : 3964dup2

Total Element Concentrations [micrograms per litre (ppb)]

ELEMENT	MASS		CONC	ELEMENT	MASS		CONC
Lithium	7		44	Beryllium	9	<	2.4
Boron	10	<	5.5	Sodium	23		not.det
Magnesium	25		1100	Aluminium	27		730
Silicon	28		not.det	Phosphorus	31		not.det
Potassium	39	<	41	Calcium	48	<	26
Scandium	45		mol.int	Titanium	49	<	3.6
Vanadium	51		2.4	Chromium	53		41
Manganese	55	<	1.9	Iron	56	<	25
Cobalt	59	<	2.7	Nickel	62	<	6.6
Copper	63	<	2.2	Zinc	66		64
Gallium	71	<	1.1	Germanium	74		1.5
Arsenic	75	<	0.2	Bromine	79	<	6.4
Selenium	82	<	6.5	Rubidium	85	<	1.0
Strontium	88	<	0.6	Yttrium	89	<	0.7
Zirconium	90	<	0.8	Niobium	93	<	0.9
Molybdenum	98	<	1.1	Ruthenium	101	<	0.9
Rhodium	103	<	0.3	Silver	107	<	0.8
Palladium	108	<	0.8	Cadmium	111	<	1.7
Indium	115		int.std	Tin	120	<	1.7
Antimony	121		1.2	Tellurium	126	<	3.2
Iodine	127	<	2.2	Caesium	133	<	0.6
Barium	138	<	0.8	Lanthanum	139	<	0.6
Cerium	140	<	0.8	Praseodymium	141	<	0.6
Neodymium	146	<	0.9	Samarium	149	<	1.4
Europium	151	<	0.6	Gadolinium	157	<	1.3
Terbium	159	<	0.5	Dysprosium	163	<	0.8
Holmium	165	<	0.6	Erbium	166	<	0.6
Thulium	169	<	0.4	Ytterbium	172	<	1.0
Lutetium	175	<	0.5	Hafnium	178	<	0.8
Tantalum	181	<	0.5	Tungsten	184	<	1.1
Rhenium	185	<	0.6	Osmium	190	<	0.7
Iridium	191	<	0.7	Platinum	194	<	0.8
Gold	197	<	0.8	Mercury	200	<	2.9
Thallium	205	<	0.6	Lead	208	<	1.1
Bismuth	209		0.3	Thorium	232	<	0.6
Uranium	238	<	0.5				

mol.int = molecular interference
int.std = internal standard used
not.det = not determined

Analyst... Jean Cho.....

3964i0r

APPENDIX 4

Part 3

BACKGROUNDS in the SAN-ONOFRE NEUTRINO DETECTOR from MULTIPLE NEUTRON EVENTS

M. Chen and V. M. Novikov

(April 15, 1993)

The problem.

Once two (or more) neutrons are appeared in the fiducial volume of the 12 t detector, the background event can be created in the following way: after both neutrons are captured on protons, two 2.2 MeV gammas are appeared in the detector in time window of $\sim$ 500 μsec. While the first 2.2 MeV γ produces fast triple, the second one complete 4-fold backgroung event.

"Double-neutron soup" intensity.

For the neutron production rate from μ-spallation of 11 $kg^{-1}day^{-1}$ at 25 m w.e. of depth, 130,000 neutrons will be born in the fiducial volume of the detector (12 t of liquid scintillator). The ratio of two-to-one neutron emission was measured to be 0.1 [1]. Therefore, about 12,000 double neutrons will appear in the detector per day.

Since all spallation neutrons are vetoed by 100 μsec muon veto time, only fraction $(1-f)$ of double neutrons will survive, with

$$f = P_n + P_n - P_n^2 = 0.692, \tag{1}$$

where $P_n = 1-e^{-100./170.} = 0.445$ - probability for a single neutron to be captured in 100 μsec. Therefore, 3,700 double neutrons are still alive after 100 μsec.

Probability of 2n to produce background event

The probability of background event from double neutrons can be written approximately as

$$P_{2n} = P_3 P_1 \epsilon_{2n}(E_1, E_2) Disp, \tag{2}$$

where $P_3 = 2.4\text{x}10^{-2}$ is a probability for 2.2 MeV γ to produce fast triple [2], $P_1 = 0.5$ is a probability for 2.2 MeV γ to be attributed as a neutron signal [3], $\epsilon_{2n}(E_1, E_2)$ is a probability for both neutrons with initial energies of E_1, E_2 and with random distribution of the point of their origin over the detector's volume to be captured in the detector (no large error if one uses instead just $\epsilon(E_1)\epsilon(E_2)$, where $\epsilon(E_i)$ is the probability for the neutron of the energy E_i to be captured inside the detector; values of $\epsilon(E_i)$ for a couple of energies are listed in Table 1 as well as the value of $\epsilon_{2n}(10, 10)$), *Disp* - displacement factor; it introduces reduction of efficiency for events other than a real neutrino event. *Disp*=1 for true neutrino event, *Disp*=1/6 for accidental background [3].

Background estimation

Let us estimate background of the San Onofre detector from double neutron events assuming both neutrons have the same energy of 10 MeV.

For this case, $\epsilon_{2n}(10, 10)$=0.6 (see Table 1). Fig.1 shows the distribution of distance between points where two neutrons were captured. Mean distance is $\sim$ 25 cm, i.e. no great difference compare to 10 cm (mean distance between neutrino capture and neutron capture points in a true neutrino event [4]). Due to this, we should accept *Disp* not lower than 1/2. Then, from (1), P_{2n}=3.6x10^{-3}, which leads to background rate of $\sim$13 day^{-1}.

References

1.L.B.Bezrukov et al. Sov. J. Nucl. Phys. 17 (1973) 987.
2.M.Chen, "Monte Carlo Studies ...", internal report, August 27, 1992.
3.V.M.Novikov, "Efficiency of the ...", int. report, August 19, 1992.
4.M.Chen, "Modelling the San Onofre Detector", present. at Albuquerque.

TABLE 1

Energy (MeV)	Probability for capture
5	.797 ± .009 (Monte Carlo statistical error)
10	.753 ± .009
15	.716 ± .008
20	.674 ± .008

for two 10 MeV neutrons - predict probability for random double capture:

$(.753)^2 = .568 \pm .013$

from Monte Carlo - correlated double capture probability:

.601 ± .009

again for two 10 MeV neutrons - predict probability that at least one of the two neutrons will capture:

$1 - (1 - .753)^2 = .939 \pm 0.004$

from Monte Carlo - probability that at least one of the two neutrons was captured:

.864 ± .011

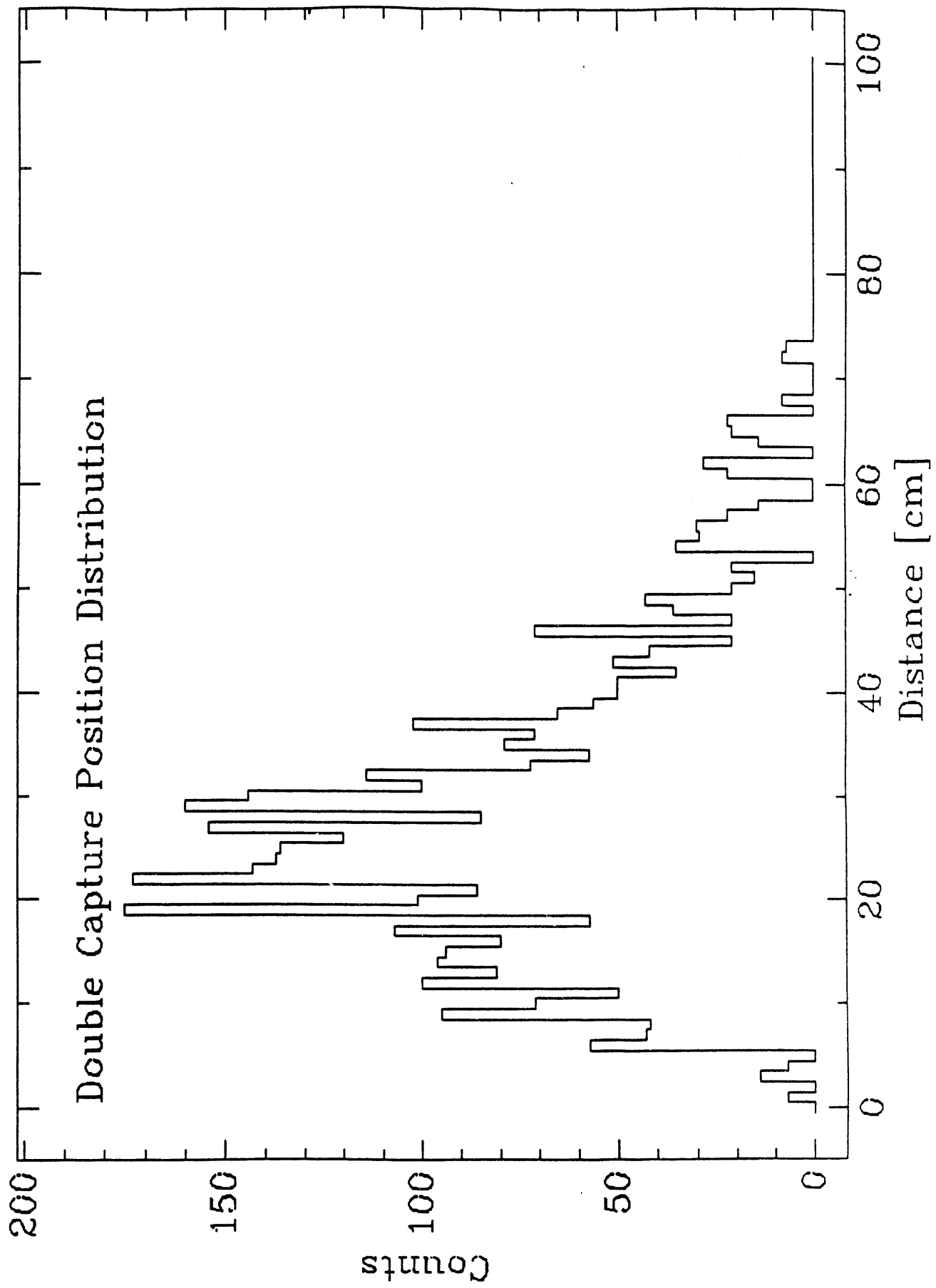
Double Capture Position Distribution
Counts
200
150
100
50
0
0
20
40
60
80
100
Distance [cm]

FIG. 1

APPENDIX 4

Part 4

FAST NEUTRON FLUX MEASUREMENTS at STANFORD

M.Chen, V.M.Novikov
Caltech

and

B.Dougherty
Stanford University

March 10, 1993

1 The purpose of the experiment.

The external fast neutron flux constitutes an important background component of the 12 t San Onofre neutrino detector. After penetrating passive shielding of the detector, a fast neutron can produce a triple coincidence (through triple recoil protons or/and through other reactions such as inelastic scattering off ^{12}C which gives rise to 4.4 MeV gammas) and subsequently capture on ^{1}H. Such a 4–fold correlated background event is not distinguishable from true neutrino events for the current design of the SO detector. To estimate background of the SO detector from fast neutrons, one has to know 1) absolute fast neutron flux at 20 m w.e. of depth, 2) propagation of fast neutrons through buffer, 3)probability to create 4–fold correlated background per neutron. The purpose of this experiment was to measure the absolute neutron flux at 20 m w.e.

2 Experimental setup.

The experiment was performed at the Stanford Underground Facility at a depth of 20 m w.e. Neutron flux was measured in four different configurations: 1) Inside Pb shielding of 10 cm, 2) Inside 2–component shielding: 30 cm wax (inner) and 10 cm Pb (outer), 3) Without shielding (i.e. concrete surroundings), 4) Inside wax shielding of 35 cm. For identification of neutrons, conventional pulse-shape discrimination technique based on CANBERRA 2160A PSD module was used. A 5 L cell filled with NE 235C liquid scintillator was used as a detector of neutrons.

3 The detector. Its calibration and response.

3.1 The detector.

The detector is a cube (17 cm×17 cm×17 cm, external dimensions) made of acrylic sheets with 0.625 cm thick walls. It is filled with ~5 L of NE 235C liquid scintillator which provides the best separation between neutrons and gammas [1]. The scintillator is viewed by four 3" XP2312 PMTs placed on one side of the detector.

3.2 Data taking.

Conventional NIM and CAMAC modules were used for data taking (see Fig.1 for electronics schematic). Both amplitude and width of the incoming pulses were recorded. Data were accumulated on a PC. A hardware lower energy threshold was set at ~0.9 MeV. For short-time runs, data could be taken in "two-dimensional" files in which energy and PSD were recorded directly (with width of energy channel of ~6–7 keV at 2.5 MeV); while for long-time runs, data were binned (with width of energy channel of ~160 keV at 2.5 MeV). The latter was required to save memory.

3.3 Calibration of the detector.

Energy calibration was provided by ^{232}Th source (2.62 MeV γ) and 1 Ci * *PuBe* neutron source (50 mCi*) *AmBe* was used in preliminary measurements at Caltech basement). Typical ^{232}Th spectrum is shown on Fig.2. *PuBe* provides three energy points: 2.2 MeV from neutron capture on ^{1}H as well as 4.4 MeV and 7.6 MeV gammas; the latter two are coming from de-exitation of corresponding levels of ^{12}C [2] which are produced in the reaction $^{9}Be(\alpha,n)^{12}C$. Energy spectrum from *PuBe* is shown on Fig.3.

The *PuBe* source calibrations provided information on the *separation of neutrons* from gammas. The "two-dimensional" spectrum gives the best representation of this separation (Fig.4a). To estimate quantitatively, one can introduce the separation factor S, defined as:

$$S = \frac{D}{(W_\gamma + W_n)}, \tag{1}$$

with notation described in Fig.4b. For a narrow energy interval at 2 MeV, S was found to be ~0.95 (and slightly better at higher energies). Bubbling with nitrogen for 3 hours led to a significantly better value of 1.2. However, this effect was swept out in a few days, presumably, by outgassing from the acrylic walls.

3.4 Response to neutrons.

The response function of the detector to neutrons involves many physics processes. Below we discuss the main ones modelled.

1.*Energy of recoil proton* as a result of neutron elastic scattering off ^{1}H is uniformly distributed from 0 to incident neutron energy. This is due to the fact that the proton and neutron have the same mass.

2.*Electron-equivalent energy* (seen in the detector) is not a linear function of the energy of the recoil proton. Monte-Carlo simulations for this experiment used the following dependence [3]: T_e=f×$T_p^{3/2}$ for $T_p \le T_p^+$ and T_e=g×T_p−h for $T_p \ge T_p^+$, with f=0.18$_3$

* Activity of α-source. Probability for neutron emission is ~6×10^{-5} per α.

$MeV^{-1/2}$, g=0.63, h=1.1 MeV, T_p^+=5.25 MeV. For neutrons in energy interval 8–20 MeV, the above function gives electron–equivalent energy roughly 50 % of the actual energy of the proton (E_e=3.94 MeV for E_p=8 MeV, E_e=11.5 MeV for E_p=20 MeV).

3.The important question is: how is the incident neutron slowing down in the detector? Do we see always only one signal from a neutron or we can resolve the pulses from two recoil protons produced by the same neutron? Fig.6 shows the time distribution between occurrences of the first and last recoil protons, with energies higher than 100 keV, created in the detector by a 10 MeV neutron. As one can see, everything is taking place within $\leq$20 ns, which is much less than the amplifier's (TENNELEC 205A) shaping time of 500 ns. Therefore, independent on how many times a neutron interacted in the detector, we always deal with a single summed pulse from it. (However, the procedure for transformation of recoil proton energy into electron–equivalent energy should be done for each recoil proton separately, with a following summation of the electron–equivalent energies).

4.What is the role of carbon for the energy response function? We suppose that the electron–equivalent energy of a recoil carbon atom is always zero (of course, the effect of slowing down the neutrons as a result of interactions with carbon atoms was taken into account).

5.What happens if a neutron creates, inside the detector, not only recoil protons but also 4.4 MeV gammas from inelastic scattering off carbon? We threw away such signals, presuming that the PSD module would reject them as gamma–like. Actually, it introduces only a small effect if we accept such events as neutron–like counts.

4 Raw data.

For each of the four configurations, data were recorded in short runs of ~10 h of duration. Data were accumulated for 110 h with Pb shield, 250 h with Pb+wax shield, 330 h without shield and 310 h with wax shield. Not all data were accepted but only those runs which satisfied our "visual inspection" (quality of gamma peak in each short run); in all, only 40–70 % of the data were taken into account. Figs.7–10 (as well as tables 1–4) present counting rates of "neutron–like" events for all four configurations in terms $MeV^{-1}hour^{-1}$, with 50 % neutron selection efficiency.

	Time, h	Trigger rate, sec^{-1}	n–like event rate
Pb	44.	3.8	0.394 ± 0.049
Pb+wax	102.	3.3	0.089 ± 0.016
No shield	195.	99.–105.	0.124 ± 0.014
Wax	240.	24.–25.	0.066 ± 0.009

1. Trigger rate for a lower threshold of ~0.9 MeV.

2. Rate of neutron–like events in 4–8 MeV energy interval, with 50 % neutron efficiency, in units $MeV^{-1}h^{-1}$.

Table 5. Measurement time of accepted data, mean trigger rate and neutron–like event rate in all four configurations of the experiment.

Energy, MeV	Rate, $MeV^{-1}h^{-1}$
1.90000	3.34091
2.23333	2.04545
2.49574	2.84849
2.73511	1.42424
3.11808	0.996970
3.59681	0.664646
4.08384	0.734120
4.60548	0.331818
5.15342	0.082955
5.70137	0.539204
6.24932	0.580682
6.79726	0.207386
7.34521	0.124432
7.89315	0.207386
8.44110	0.373296
8.98904	0.165909

Table 1. Pb data.

Energy, MeV	Rate, $MeV^{-1}h^{-1}$
1.74286	0.857843
2.02857	0.446078
2.30336	0.148620
2.56765	0.370370
2.92059	0.133333
3.36176	0.244444
3.80294	0.111111
4.24813	0.196428
4.70000	0.043137
5.15455	0.150981
5.60909	0.064706
6.06364	0.021569
6.51818	0.043137
6.97273	0.043137
7.42727	0.043137
7.88182	0.107843

Table 2. Pb-wax data.

Energy, MeV	Rate, $MeV^{-1}h^{-1}$
1.77500	9.62051
2.02500	3.40513
2.27500	2.42051
2.53500	1.31054
2.89500	0.820513
3.34500	0.284900
3.79500	0.296296
4.23500	0.166965
4.65833	0.209231
5.07500	0.172308
5.49167	0.073846
5.90833	0.098461
6.32500	0.073846
6.74167	0.049231
7.15833	0.073846
7.57500	0.073846

Table 3. No shield data.

Energy, MeV	Rate, $MeV^{-1}h^{-1}$
1.83333	1.73750
2.16667	0.700000
2.43590	0.670313
2.66827	0.369136
3.01442	0.269630
3.44712	0.202222
3.87981	0.144444
4.33344	0.061458
4.81463	0.093958
5.30244	0.059791
5.79024	0.051250
6.27805	0.085416
6.76585	0.059791
7.25366	0.034166
7.74146	0.017083
8.22927	0.076874

Table 4. Wax data.

Tables 1-4. Counting rates of neutron-like events (with 50 % efficiency).

Counting with 50 % efficiency means that only those events were counted which were found on the right side off the expected maximum of the neutron peak (information on relative positions of the gamma and neutron peaks was obtained from measurements with the PuBe neutron source). For each configuration, information from the corresponding calibration was used. Table 5 somehow summarizes the results obtained.

5 Results and conclusion.

5.1 Straightforward solution.

How can we handle the data? One possibility is to fit the experimental data to the expected detector response for a given neutron spectrum. It could be the muon-capture neutron spectrum [4] if we presume the process to be responsible for production of most neutrons. Such a procedure was performed for the Pb-data (Fig.11). The experimental points fit quite well to the Monte-Carlo calculated response.

5.2 Conservative approach.

Careful look at Table 5 forces us to be more conservative. The neutron production rate per cm^3 of Pb is supposed to be much higher than that in wax; at the same time, in wax, neutrons are slowing down much more efficiently than in lead. Both factors should result in a much higher neutron flux in Pb than in wax shielding; for example, in [5] the estimated n-flux in Pb is ~70 times higher than that in Pb+wax. Therefore, the question is: why is the counting rate of neutron-like events in the 4-8 MeV energy interval (Table 5) only ~5 times higher in Pb than in wax? It appears that the answer is clear: inside the wax shielding we have measured the BACKGROUND in the detector caused by muons. Therefore, we should accept the following sequence of data reduction:

1. With detector inside wax we performed a good measurement of background.

2. Data obtained with detector inside Pb+wax shielding are not useful. We should discard them. Compared to measurements inside the wax shielding, the 1.5 σ excess in the counting rate of neutron-like events in the 4-8 MeV region (Table 5) for Pb+wax is explained, presumably, by the somewhat poor quality of the wax shielding in these measurements (there were a few places where the wax shielding was less than 10 cm and even a few small open gaps).

3. The background (wax) counting rate should be subtracted from the "Pb" and "No shielding" rates (all numbers are listed in Table 5, for 4-8 MeV energy interval). This gives (with correction for 50 % neutron counting efficiency), counting rates of neutron-like events, in the 4-8 MeV region, of $2.624 \pm 0.399\ h^{-1}$ and $0.464 \pm 0.133\ h^{-1}$ for the detector inside 10 cm Pb shielding and without shielding, respectively.

4. The last two numbers (2.624 and 0.464) are convolutions of the absolute neutron flux, the neutron spectrum and the detector's response. Therefore, for a known detector response function (discussed here earlier) and neutron spectrum, (we accept the Pb and Si μ-capture neutron spectra [4] for the detector inside Pb and for the unshielded detector, respectively), it is easy to find the absolute neutron flux.

5. Unfortunately, we are not able to define the neutron spectrum from our measured detector spectrum. Instead, we'll use the integral counting rate of "neutron-like" events

in the 4–8 MeV energy region and with some assumption of the spectral shape, we'll give the absolute neutron flux. For an improved design of the experiment (see discussion in 5.3), the shape of the neutron spectrum can be obtained too.

Therefore, everything is based on the integral counting rates in the energy interval of 4–8 MeV. It is important to know the range of neutrons' energies which give rise to this counting rate; Fig.12 presents the probabilities for neutrons of different energies, crossing the detector, to be detected as a neutron–like event with electron–equivalent energy deposition of 4–8 MeV. As it is seen from the Fig.12, for this chosen energy window, the detector is sensitive mostly to neutrons of energy ~10–30 MeV, peaking at ~15 MeV. Fig.13 shows the absolute neutron fluxes obtained in the way discussed here. Fig.14 presents the integral neutron fluxes (corresponding to the mean values of 2.624 and 0.464 h^{-1}).

5.3 How could we do it better?

The technique we used to measure neutrons is quite good for relatively high neutron fluxes. However, its sensitivity is limited by the unfavorable flux ratio of fast neutrons to muons for very low fast neutron fluxes (such as expected inside the wax shielding). Sensitivity can be significantly improved if one places the detector inside an active anti–muon veto.

5.4 Conclusion

Accepting the assumption that neutrons have an energy spectrum like that arising from μ–capture, we have measured the absolute fast neutron flux at 20 m w.e. inside Pb shielding and without shielding (concrete surroundings), see Fig.13. In particular, the integral flux of neutrons with $E_n \geq$ 10 MeV is $(6.0\pm1.7)\times10^{-7}$ $cm^{-2}s^{-1}$ in the concrete surroundings. Besides [5], we do not know if some other data on neutron flux at 20 m w.e. exist; anyway, it would be interesting to compare these numbers with those which exist:

	Flux, $cm^{-2}s^{-1}$	Depth,m w.e.	Energy range	Ref.
1	$(6.5–7.2)\times10^{-3}$	0.	total flux	[6]
2	$(1.1–3.2)\times10^{-3}$	0.	thermal neutrons	[6]
3	$\sim1.5\times10^{-3}$	0.	~ 8–30 MeV	[7,8]
4	$(2.2\pm1.4)\times10^{-6}$	12.	~ 8–30 MeV	[8]
5	$(6–7)\times10^{-4}$	15.	total flux	[6]
6	1.1×10^{-4}	15.	total, μ–capture only	[6]
7	1.2×10^{-5}	20.	"fast flux" (no threshold)	[5]
8	2.3×10^{-8}	550.	20–80 MeV	[9]
9	$(2.3\pm0.7)\times10^{-7}$	3600.	$\geq$2.5 MeV	[10]
10	$(8.9\pm5.8)\times10^{-8}$	3600.	$\geq$2.5 MeV	[11]

Table 6. Experimental data on neutron fluxes at different depthes.

APPENDIX 1: Neutron spectrum after μ–capture [4,12].

Neutrons emitted after μ–capture are usually classified as 1)direct and 2)"evaporation" neutrons.

Direct emission refers to the neutron created in the elementary process

$$\mu^- + p \rightarrow n + \nu_\mu. \tag{1}$$

These neutrons have high energies, from a few MeV to as high as 40–50 MeV.

Most of neutrons emitted after μ–capture seem however to be "evaporation neutrons". In intermediate and heavy nuclei the excitation energy acquired by the neutron formed in thecapture process is shared with other nucleons of the nucleus and a "compound nucleus" is formed. This intermediate excited nuclear state then loses energy by boiling-off mainly low-energy neutrons.

As far as our experiment is concerned, only direct neutrons seem to be of interest for us. For these neutrons, the energy spectrum falls approximately in an exponential manner:

$$N(E) \sim exp(\frac{E}{E_0}). \tag{2}$$

The parameter E_0 was measured to be 8.6±0.5 and 10.3±0.5 for neutrons produced from μ–capture in Pb and Si, respectively. These two numbers were used in Monte Carlo simulations to interpret our experimental results.

The figure below demonstrates a comparison of theory and experiment for ^{214}Bi. In addition to the simple "direct neutrons" approach, the "pre-compound" emission was also included by considering separately the neutrons which have scattered once on other bound nucleons. The calculated integrated intensity of the direct and "pre-compound" emission amounts to 14 % per capture. By adding to it the 86 % of cases of compound nucleus formation, the solid line of the figure is obtained.

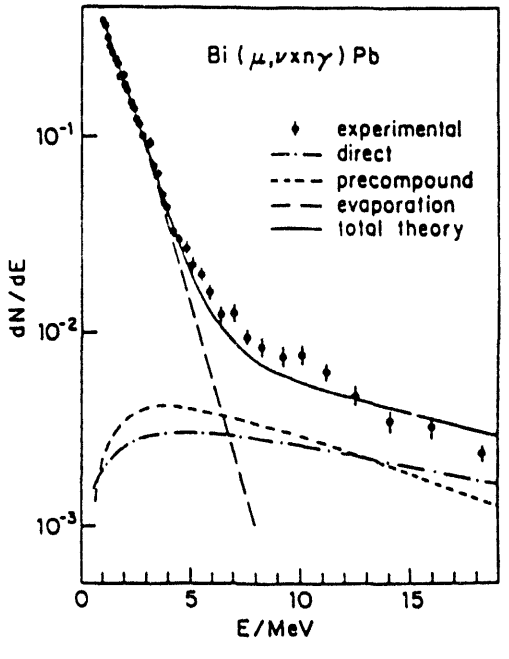

References

1. G.Knoll, Radiation Detection and Measurement, John Wiley & Son, 1979.
2. K.W.Geiger and L.Van der Zwan, Nucl.Instr.Meth.,**131** (1975) 315.
3. K.H.Maier and J.Nitschke, Nucl.Instr.Meth., **59** (1968) 227.
4. T.Kozlowski et al., Nucl.Phys., **A436** (1985) 717.
5. B.L.Dougherty, Report on Thermal Neutron Background Counting in the Stanford Underground Facility Using a Bare ^3He Tube, draft, November 16, 1992.
6. G.Heusser, Nucl.Instr.Meth., **B17 (1986) 418.**
7. S.Hayakawa, Cosmic Ray Physics, Wiley-Interscience, New York, 1969.
8. M.Chen and T.Radcliffe, Measurements of the Fast Neutron Background at 12 m w.e. Underground, Caltech internal report, Sept. 19, 1991.
9. F.F.Khalchukov, A.S.Mal'gin, V.G.Ryassny and O.G.Ryazhskaya, Il Nuovo Cimento, 6 (1983) 320.
10. P.Belli et al., Il Nuovo Cimento, **101A** (1989) 959.
11. G.Heusser, Residual Background in the Gallex Spectrometer, Talk given at 2^{nd} Workshop on Techniques for Low Radioactivity Background Experiments, Berkeley, December 16–18, 1991.
12. P.Singer, Springer Tracts in Modern Physics, **71** (1974) 39.

FIGURE CAPTIONS

Figure 1. Schematic of the apparatus.

Figure 2. Energy spectrum of the detector from γ ^{232}Th source.

Figure 3. Energy spectrum of the detector from neutron PuBe source.

Figure 4. Pulse–width spectra from neutron PuBe source.
a) "Two–dimensional" spectrum.
b) Spectrum for a certain narrow energy window.

Figure 5. Pulse–width spectra from background.
a) "Two–dimensional" spectrum.
b) Spectrum for a certain narrow energy window.

Figure 6. Time distribution between 1st and last recoil protons of at least 100 keV electron–equivalent energy appeared in the detector from a 10 MeV neutron.

Figure 7. Counting rate of neutron–like events of the detector located inside 10 cm lead shielding (50 % efficiency of neutron counting).

Figure 8. Counting rate of neutron–like events of the detector located inside shielding consisting of 30 cm of wax (inner) and 10 cm of lead (outer) (50 % efficiency of neutron counting).

Figure 9. Counting rate of neutron–like events of the not–shielded detector (50 % efficiency of neutron counting).

Figure 10. Counting rate of neutron–like events of the detector located inside 35 wax shielding (50 % efficiency of neutron counting).

Figure 11. Data in Pb with normalized μ–capture neutron spectrum.

Figure 12. Probability for a neutron crossing the detector to deposit 4 to 8 MeV electron–equivalent energy.

Figure 13. Differential neutron flux at 20 m w.e.

Figure 14. Integral neutron flux at 20 m w.e.

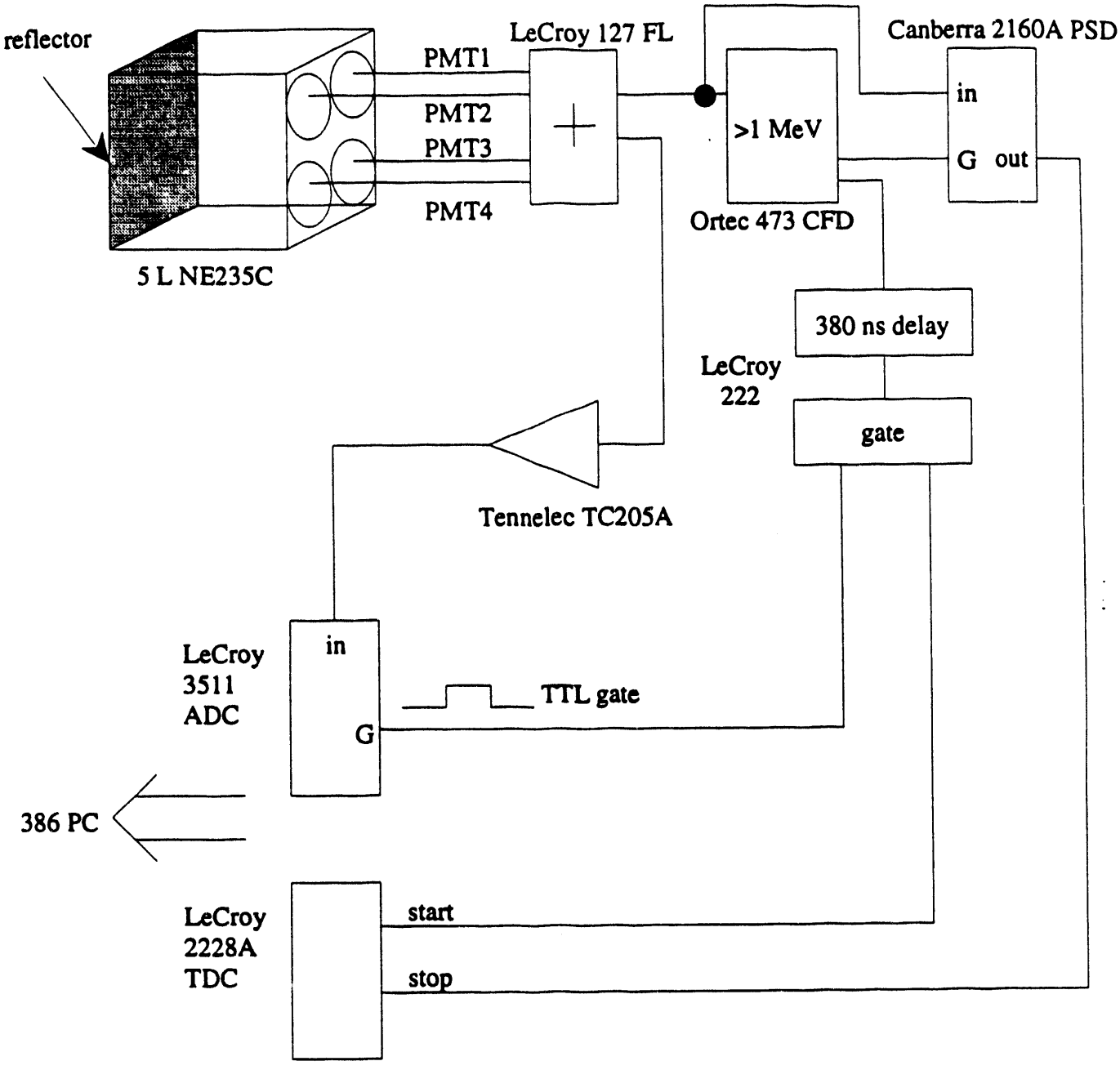
reflector
PMT1
PMT2
PMT3
PMT4
LeCroy 127 FL
Canberra 2160A PSD
in
G out
>1 MeV
Ortec 473 CFD
5 L NE235C
380 ns delay
LeCroy
222
gate
Tennelec TC205A
LeCroy
3511
ADC
in
G
TTL gate
386 PC
LeCroy
2228A
TDC
start
stop

Fig.1

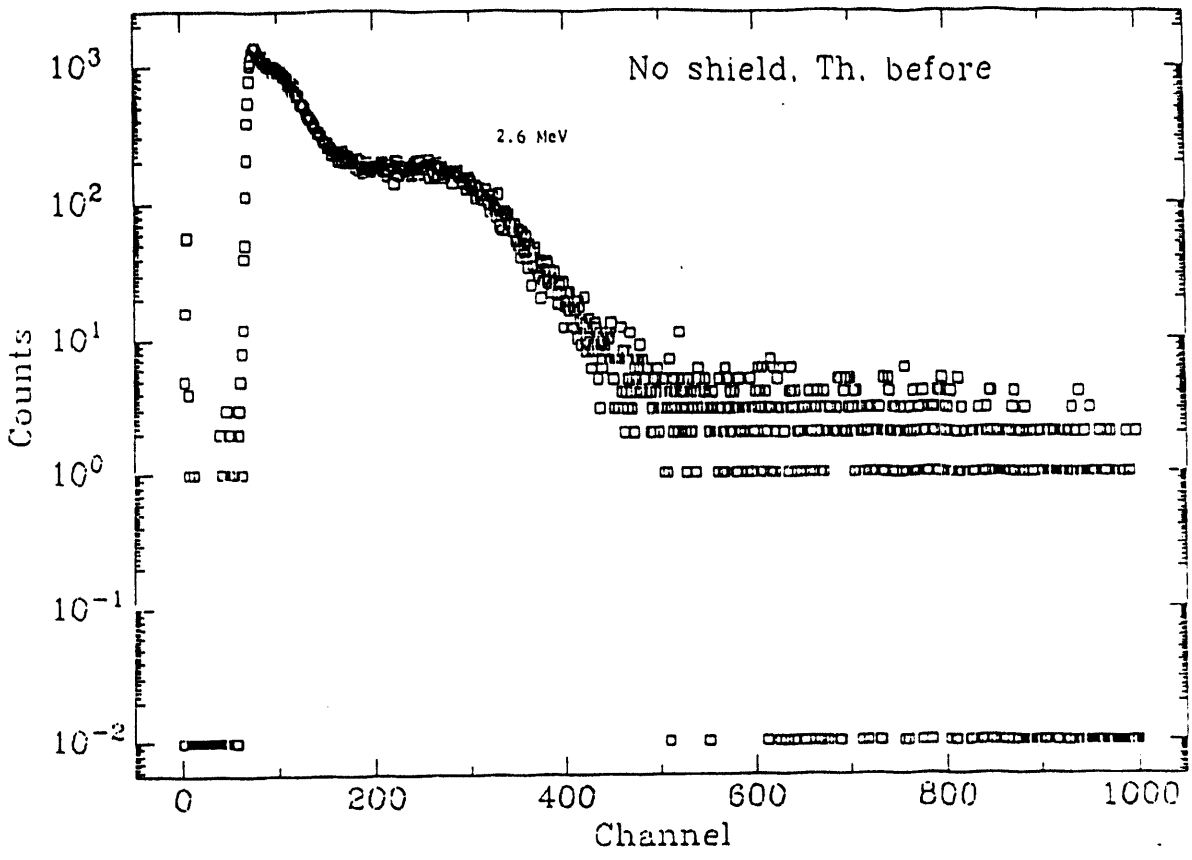
No shield, Th, before
2.6 MeV
Counts
Channel
0
200
400
600
800
1000

Fig.2

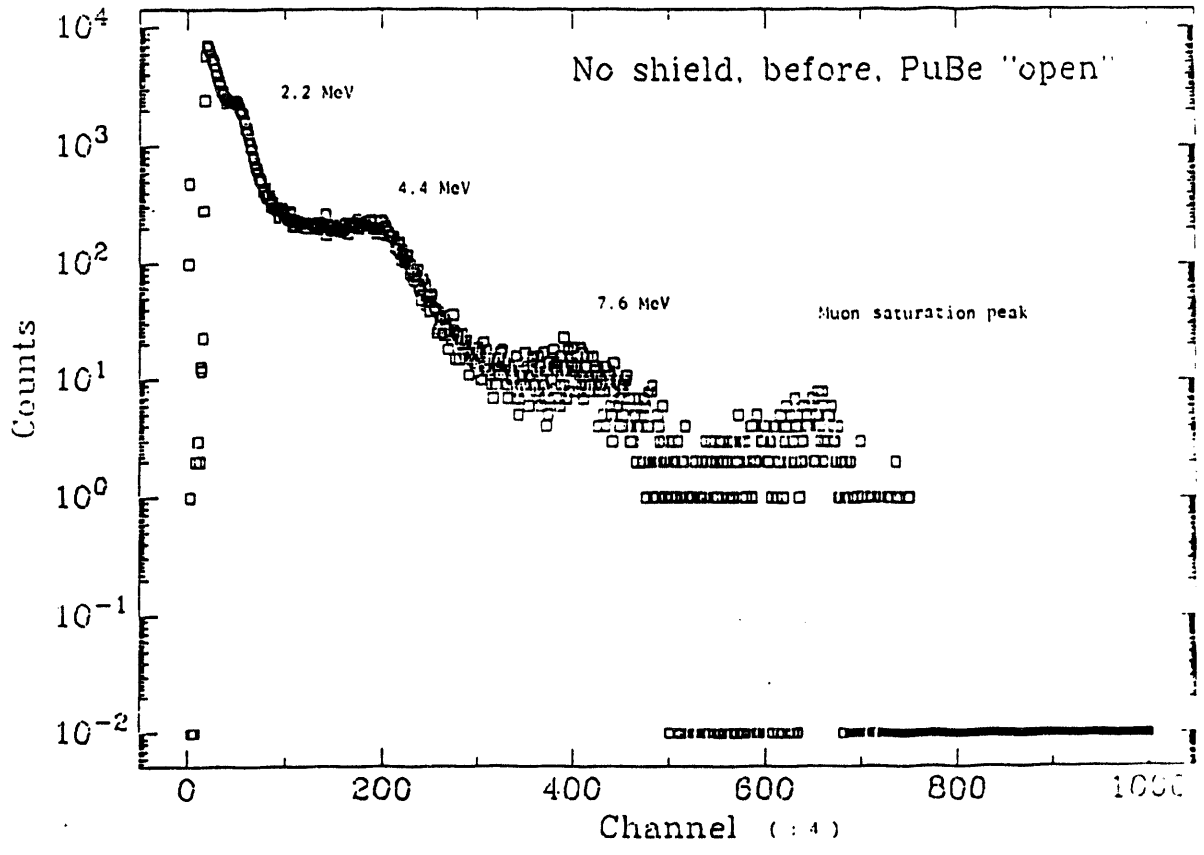
No shield, before, PuBe "open"
2.2 MeV
4.4 MeV
7.6 MeV
Muon saturation peak
Counts
Channel
0
200
400
600
800

Fig.3

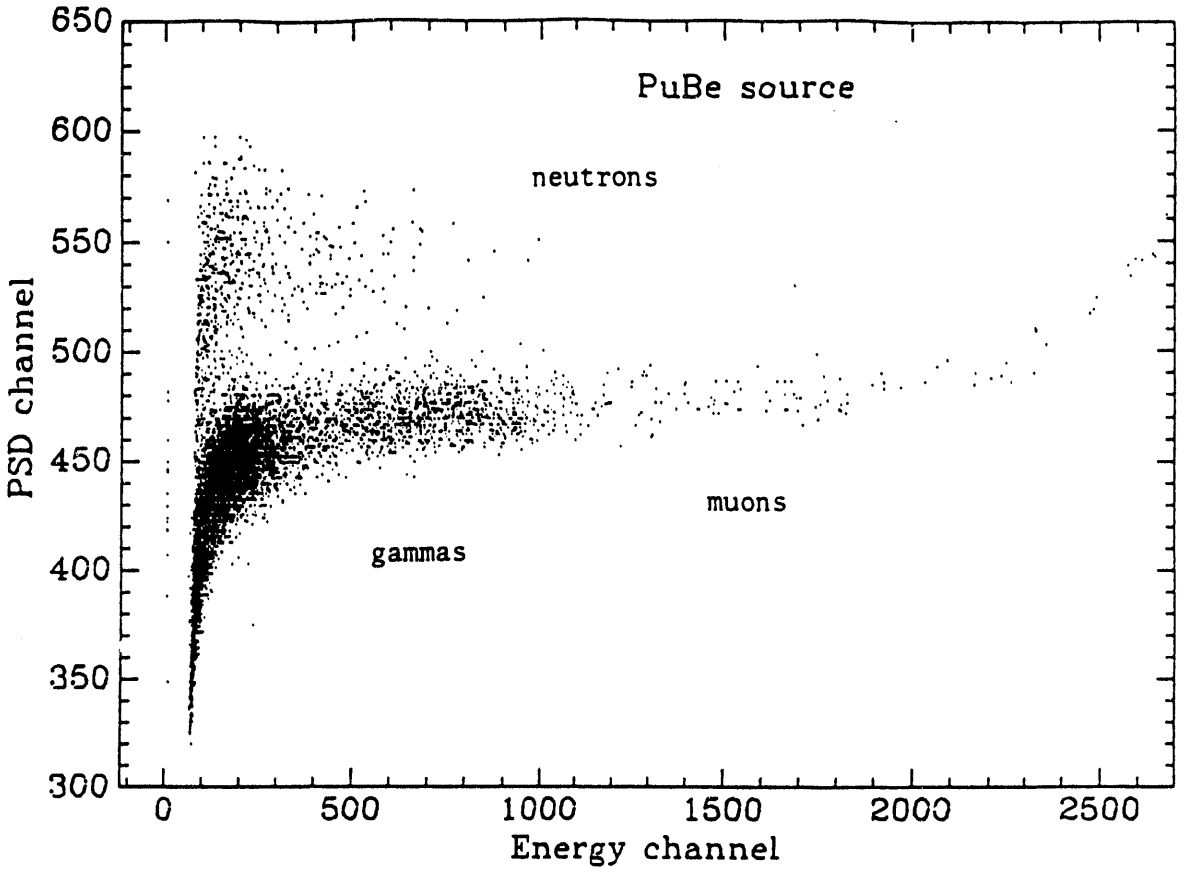
PuBe source
neutrons
muons
gammas
PSD channel
Energy channel
650
600
550
500
450
400
350
300
0
500
1000
1500
2000
2500

Fig.4a

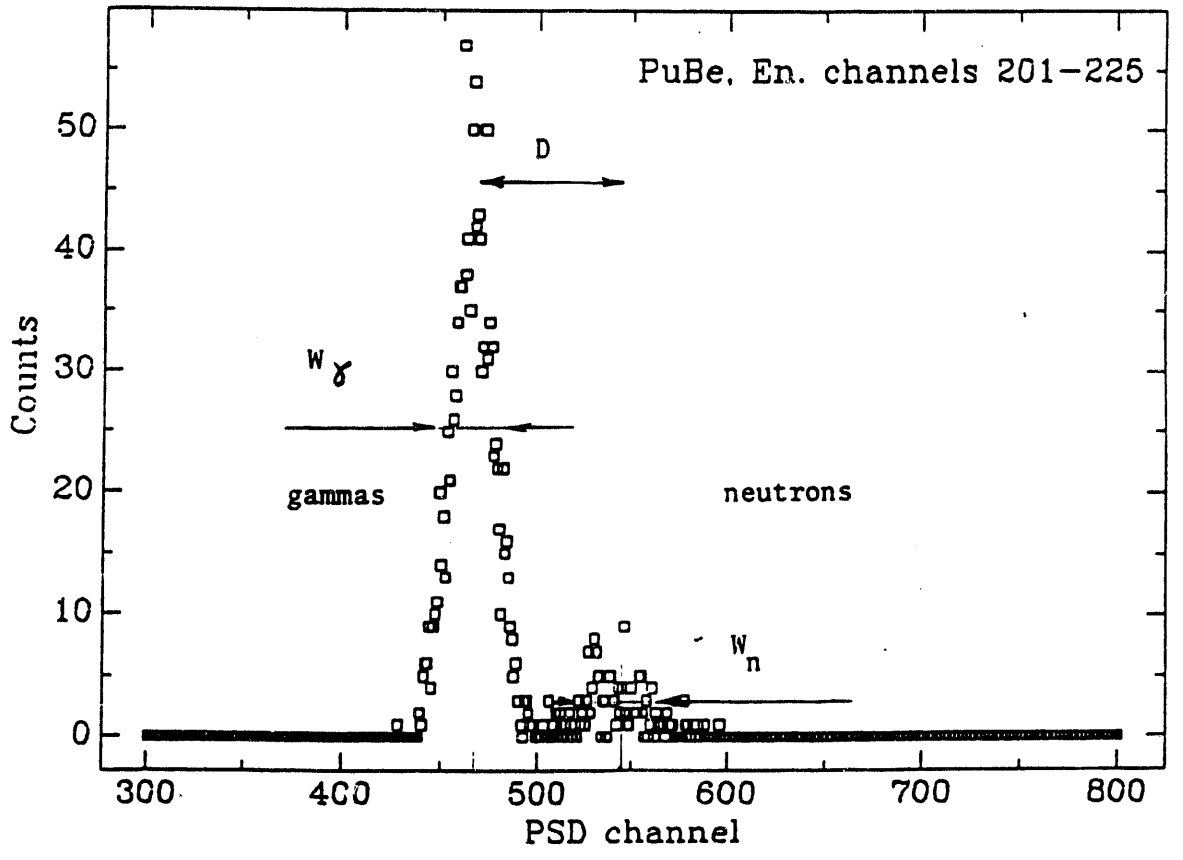
PuBe, En. channels 201-225
D
W γ
gammas
neutrons
W n
Counts
PSD channel
50
40
30
20
10
0
300
400
500
600
700
800

Fig.4b

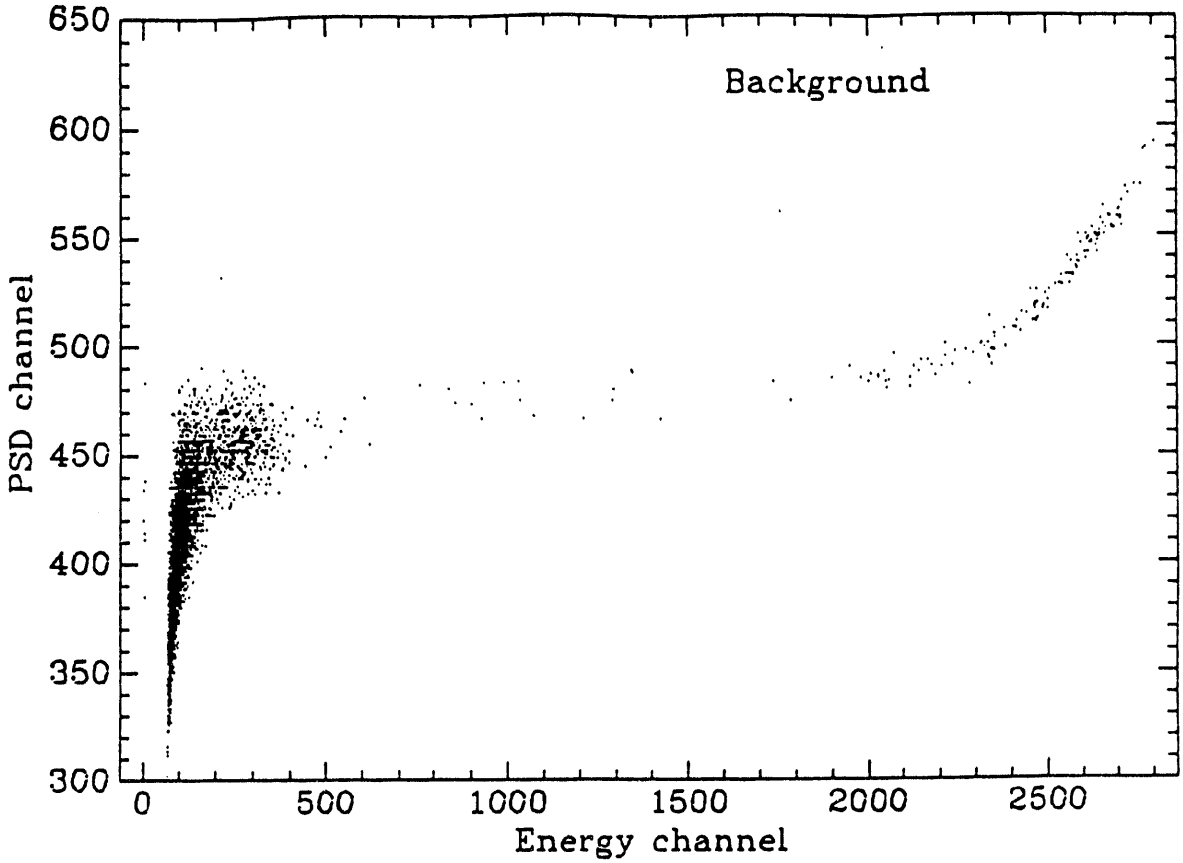
Background
PSD channel
Energy channel
650
600
550
500
450
400
350
300
0
500
1000
1500
2000
2500

Fig.5a

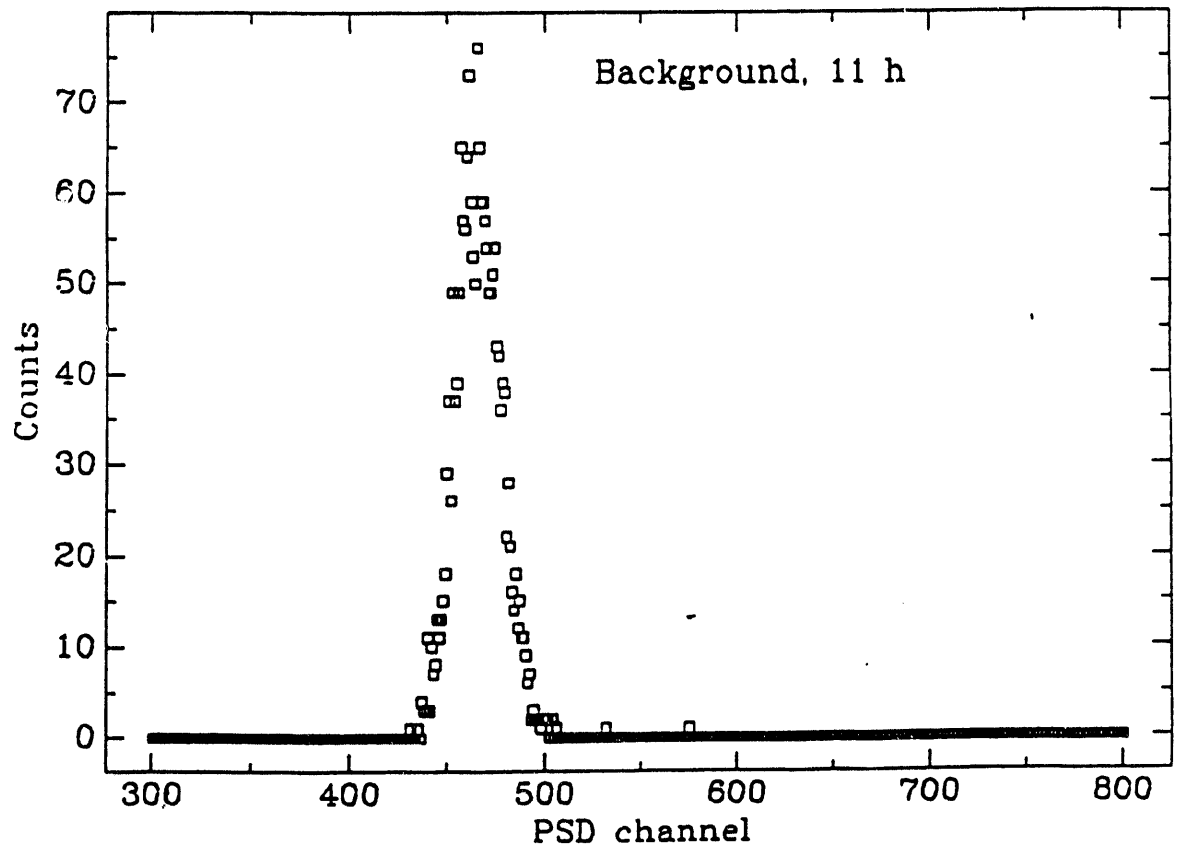
Background, 11 h
Counts
PSD channel
70
60
50
40
30
20
10
0
300
400
500
600
700
800

Fig.5b

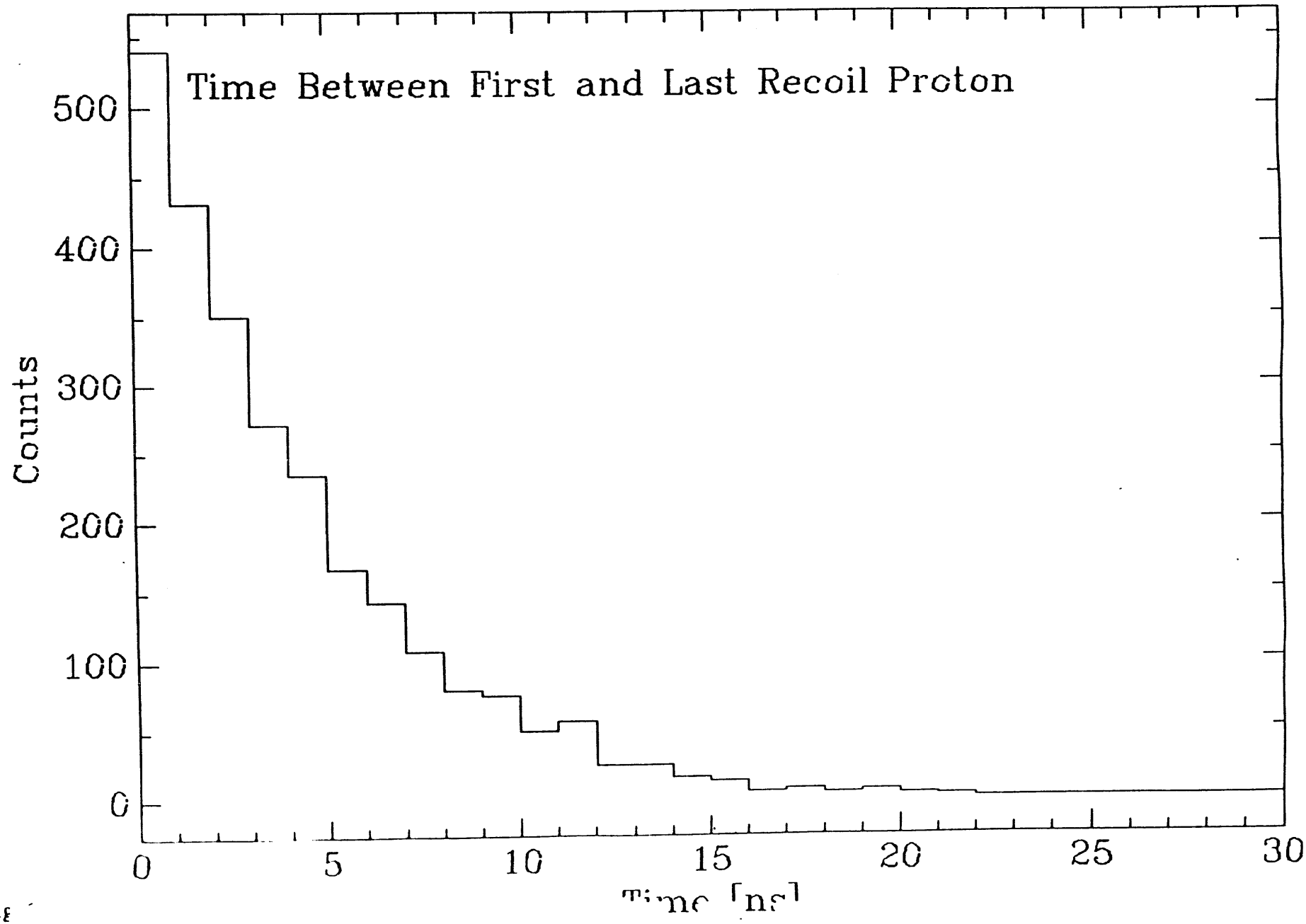
Time Between First and Last Recoil Proton
Counts
500
400
300
200
100
0
0
5
10
15
20
25
30
Time [ns]

Fig

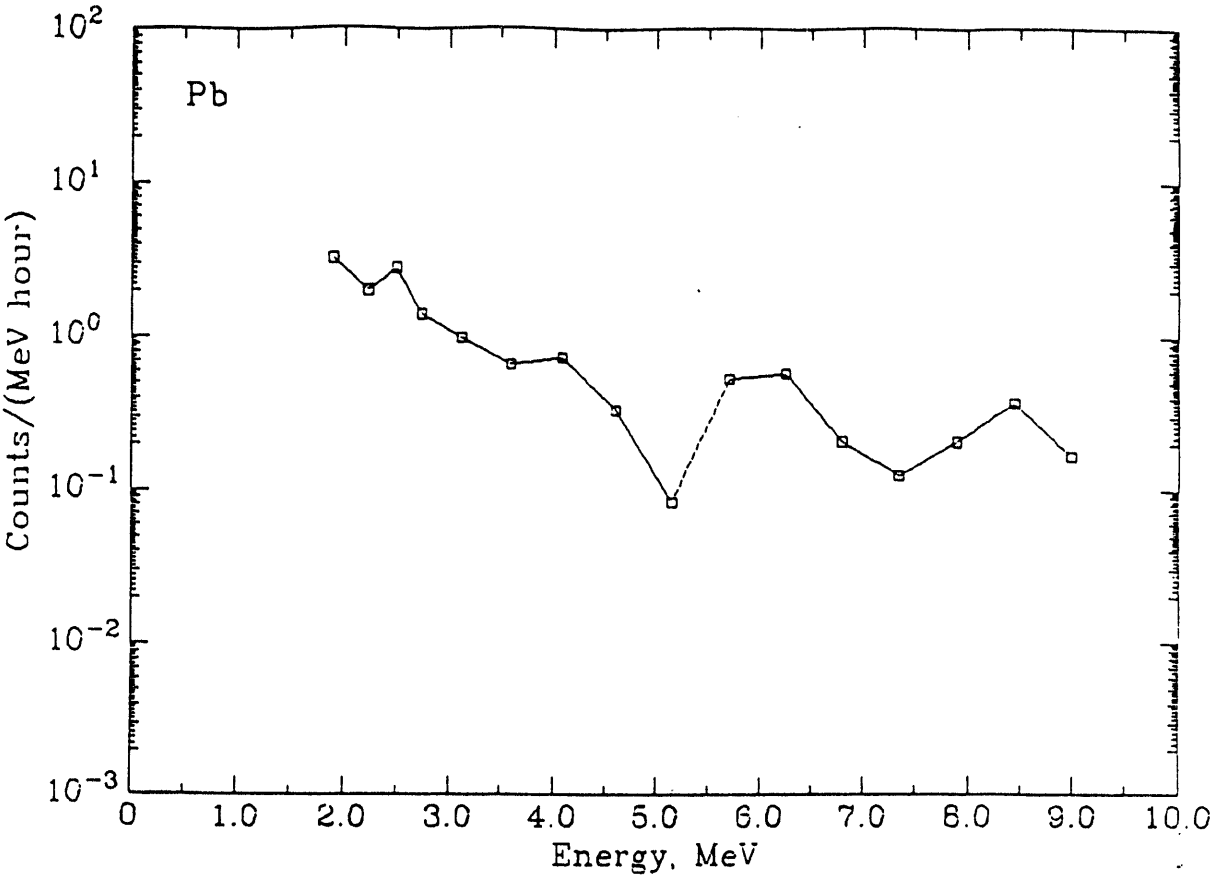
Pb
Counts/(MeV hour)
10^2
10^1
10^0
10^{-1}
10^{-2}
10^{-3}
0
1.0
2.0
3.0
4.0
5.0
6.0
7.0
8.0
9.0
10.0
Energy, MeV

Fig.7

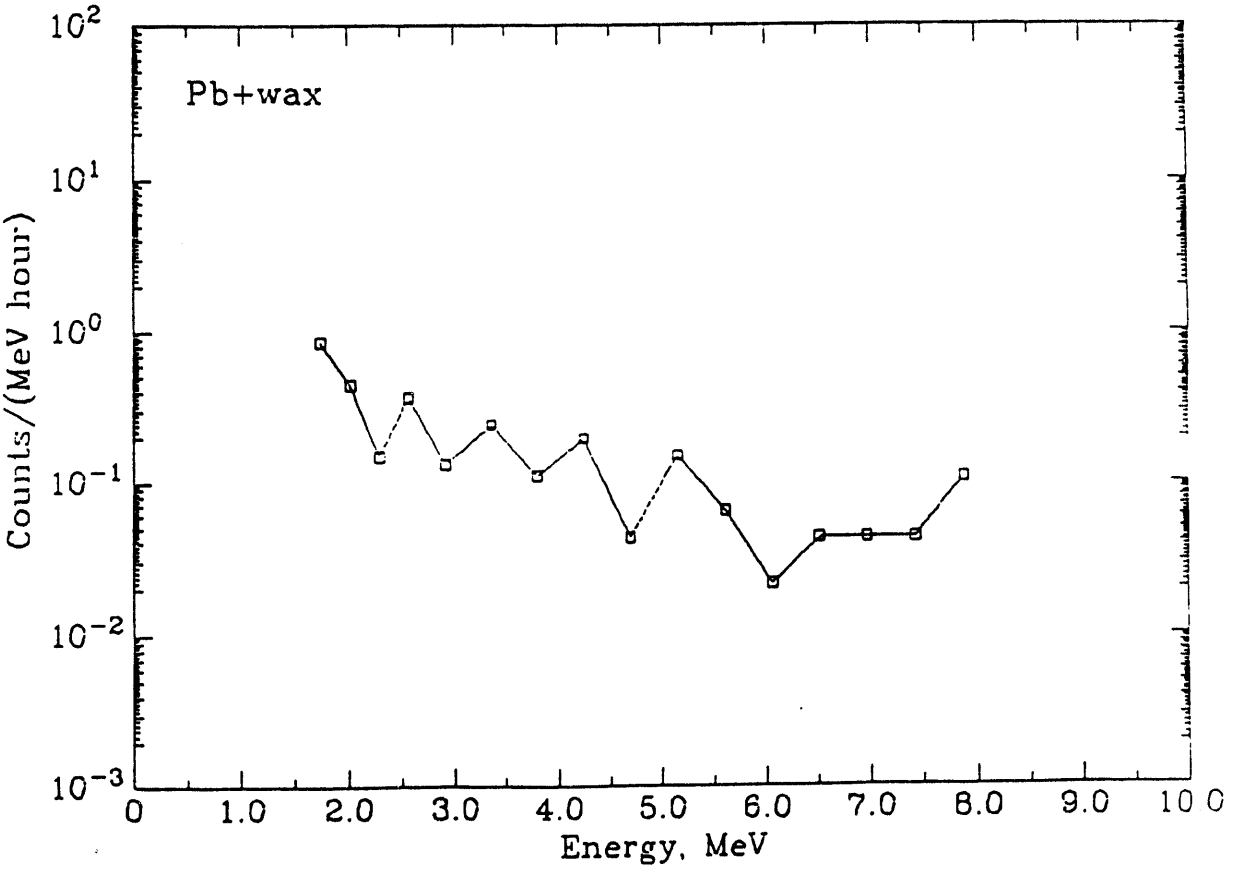
Pb+wax
Counts/(MeV hour)
10^2
10^1
10^0
10^{-1}
10^{-2}
10^{-3}
0
1.0
2.0
3.0
4.0
5.0
6.0
7.0
8.0
9.0
10.0
Energy, MeV

Fig.8

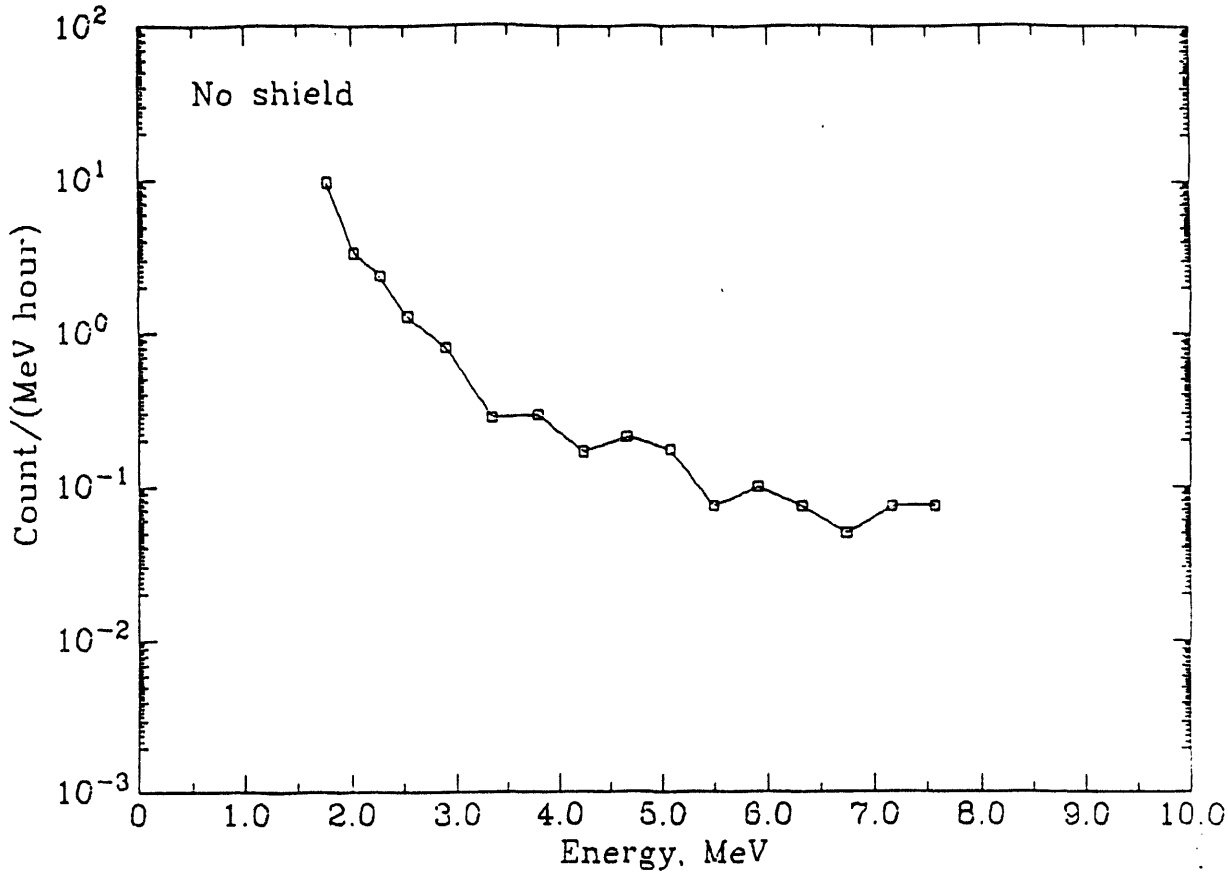
No shield
Count/(MeV hour)
10^2
10^1
10^0
10^{-1}
10^{-2}
10^{-3}
0
1.0
2.0
3.0
4.0
5.0
6.0
7.0
8.0
9.0
10.0
Energy, MeV

Fig.9

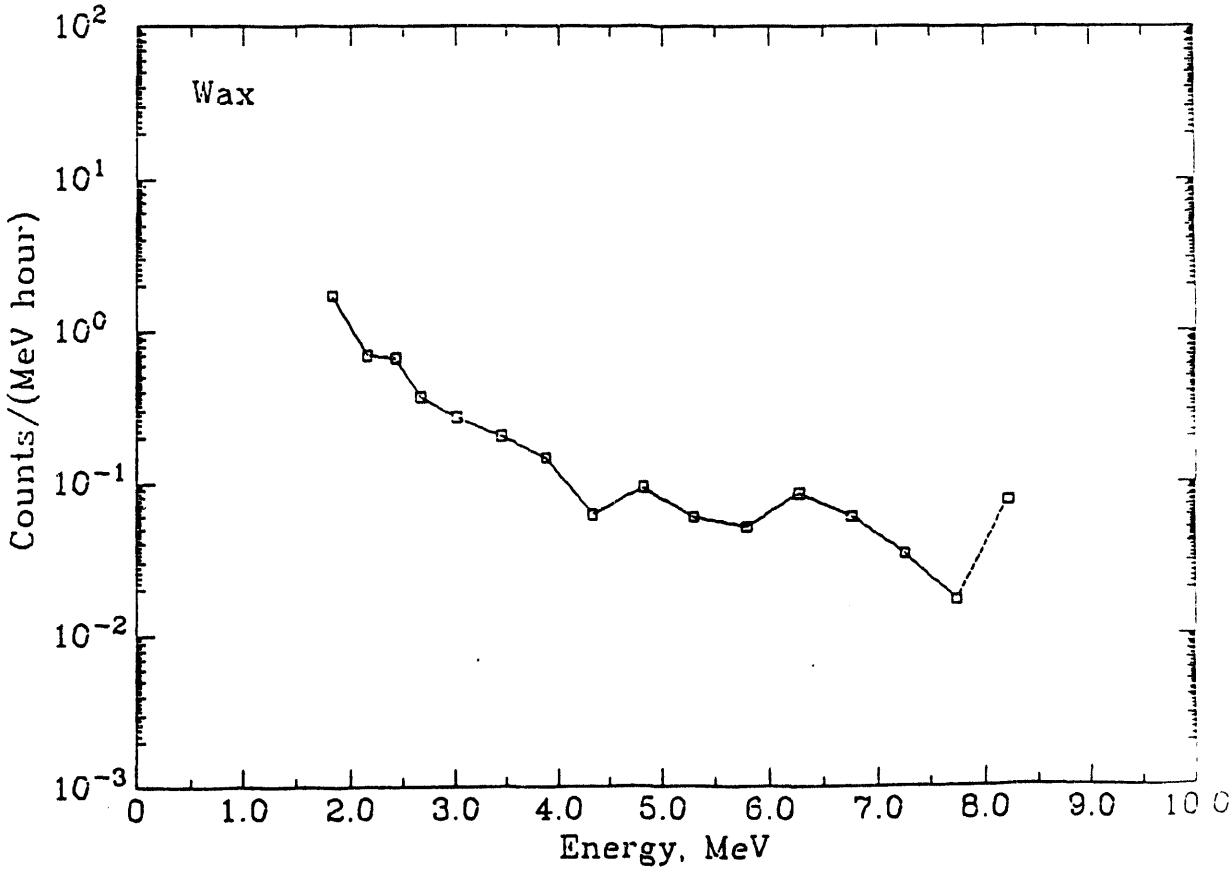
Wax
Counts/(MeV hour)
10^2
10^1
10^0
10^{-1}
10^{-2}
10^{-3}
0
1.0
2.0
3.0
4.0
5.0
6.0
7.0
8.0
9.0
10.0
Energy, MeV

Fig.10

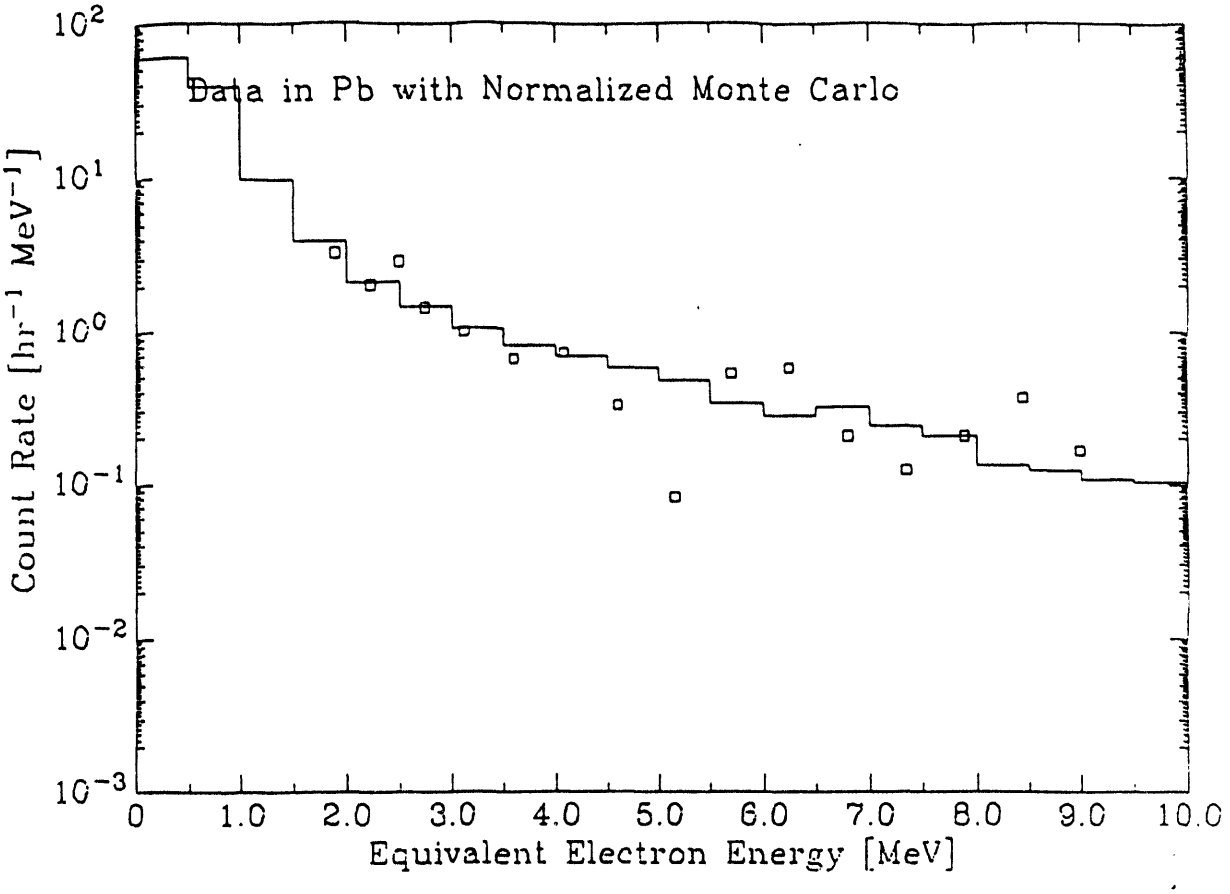
Data in Pb with Normalized Monte Carlo
Count Rate [hr^{-1} MeV^{-1}]
10^{2}
10^{1}
10^{0}
10^{-1}
10^{-2}
10^{-3}
0
1.0
2.0
3.0
4.0
5.0
6.0
7.0
8.0
9.0
10.0
Equivalent Electron Energy [MeV]

Fig.11

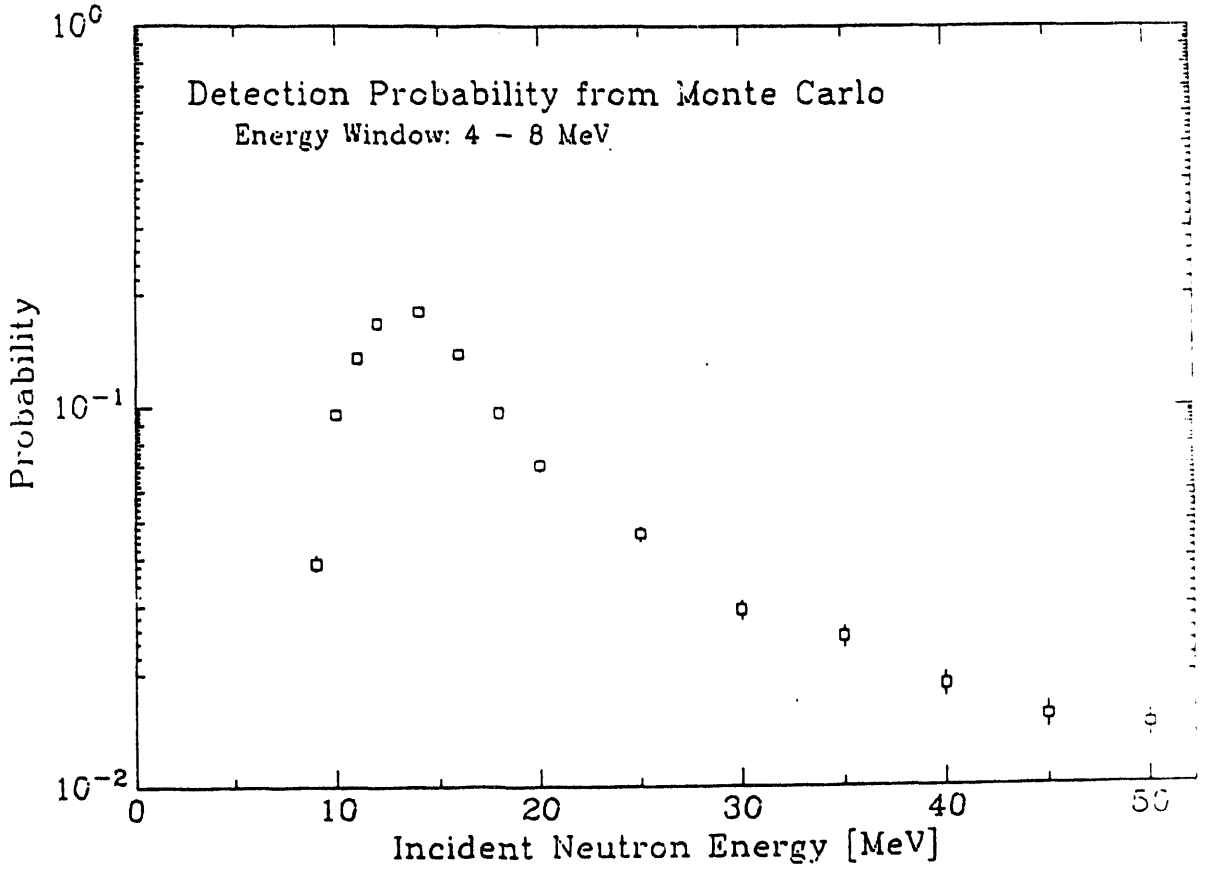
Detection Probability from Monte Carlo
Energy Window: 4 – 8 MeV
Probability
10^{0}
10^{-1}
10^{-2}
0
10
20
30
40
50
Incident Neutron Energy [MeV]

Fig.12

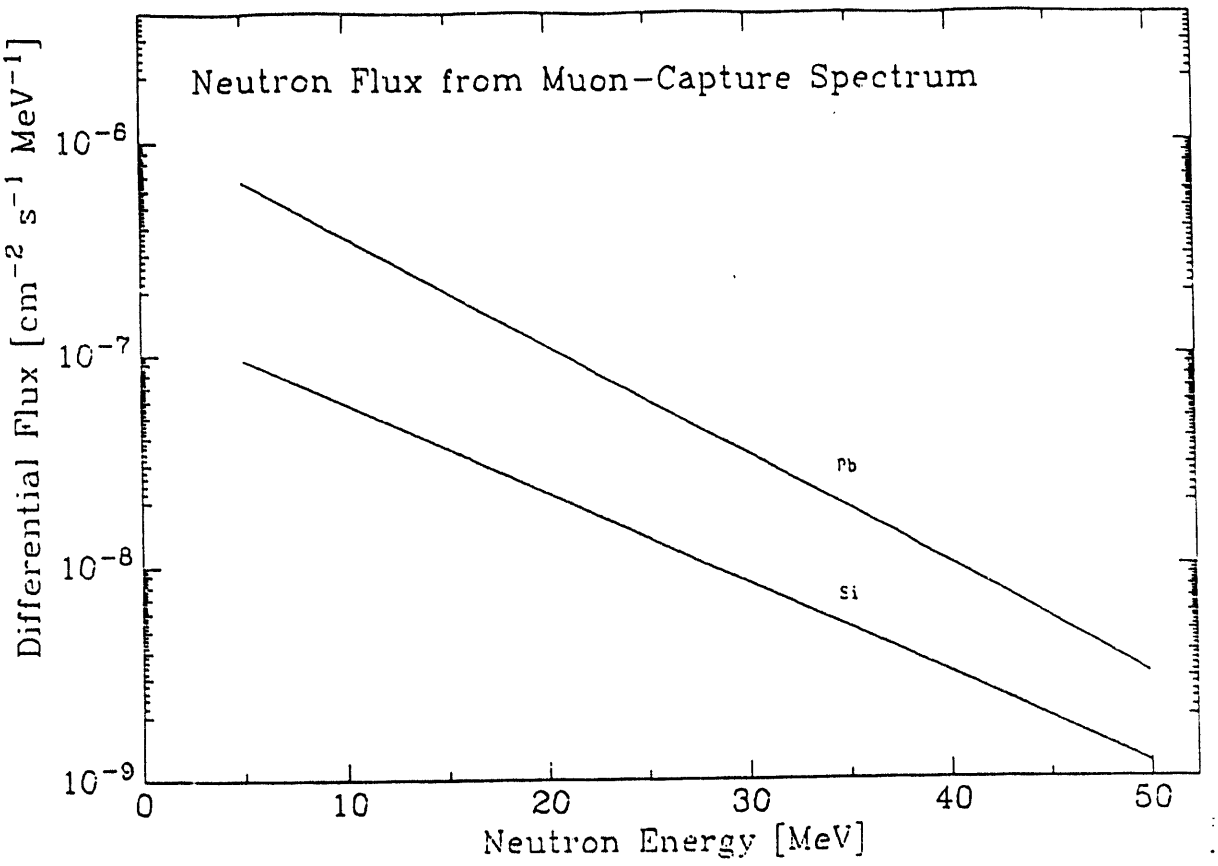
Neutron Flux from Muon-Capture Spectrum
Differential Flux [cm^{-2} s^{-1} MeV^{-1}]
10^{-6}
10^{-7}
10^{-8}
10^{-9}
Pb
Si
0
10
20
30
40
50
Neutron Energy [MeV]

Fig.13

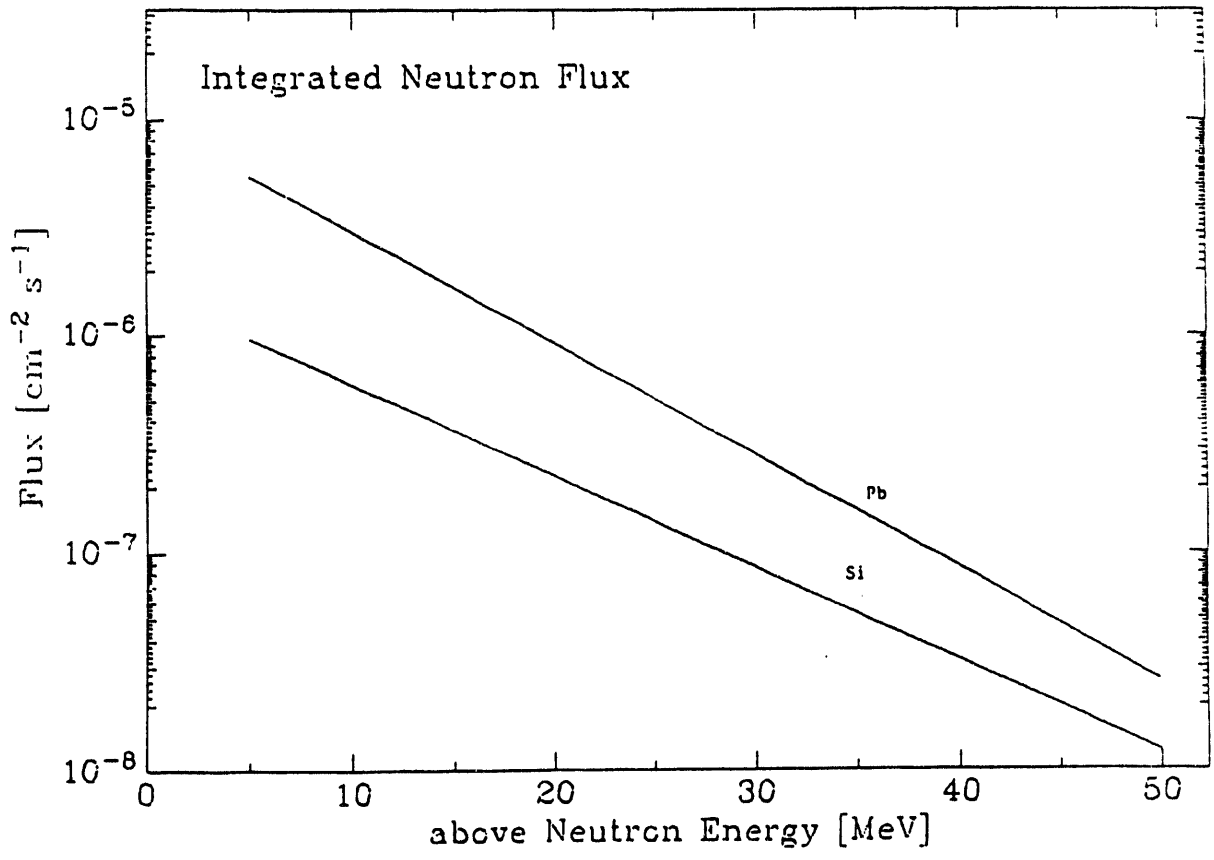
Integrated Neutron Flux
Flux [cm^{-2} s^{-1}]
10^{-5}
10^{-6}
10^{-7}
10^{-8}
Pb
Si
0
10
20
30
40
50
above Neutron Energy [MeV]

Fig.14

APPENDIX 4

Part 5

Estimating the Fast Neutron Background at 25mwe for the San-Onofre Detector

N. Mascarenhas

We estimate the production of neutrons at a depth of 25 m.w.e of soil via two processes: muon capture and muon nuclear disintegration. An estimate is given of neutrons producing a full 4 fold coincidence (background) in the detector. A simple neutron buffer attenuates the neutrons from the surrounding soil and the neutrons in the detector after the buffer is computed. Primary neutrons from cosmic ray showers are strongly attenuated at 25 m.w.e and are negligible.

1)Muon capture neutrons

Neutrons produced via muon capture are computed using the method outlined by S. Charalambus, (Nucl. Phys. A 166) 145.

Let I_{neut} be the rate of neutrons produced via muon capture, then
$I_{neut} = I_m x f_a x f_c x f_n$

Im = 60/kg day,is the m^- stopping rate at 25 m.w.e, (see S. Charalambus).
The atomic capture fractions f_a, in a compound are estimated using the Fermi Teller law. For SiO_2 $f_a(Si)=0.466$, $f_a(O_2) = 0.533$
The nuclear capture probability is $f_c(Si) = 0.6$ (from S. Charalambus) and $f_c(O_2)= 0.2$

The neutron multiplicity f_n from capture is assumed to be 1.

This gives a neutron production rate of 16.8/kg day for Si and 6.5/kg day for O_2 in SiO2 . Soil is assumed here to be mostly SiO_2. Thus the neutron production rate in SiO2 is 23/kg day (from the mass fractions of Si and O2). We assume 1/2 the neutrons have ebergy above 5 MeV. Thus the production rate of neutrons with enough energy to trigger the detector is about 11/kg/day in soil. The same rate for mineral oil is 3/kg/day at 25 m.w.e.

Next the energy spectrum of these neutrons is taken as
$N(E) = e^{-E/10MeV}$. (from T. Kozlowski et al. Nucl. Phys. A 436, (1985) 717)

From this spectrum one can compute the fraction of the total neutrons present in a given energy bin.

The neutron attenuation length for soil is assumed to be the same as for

concrete, which is known for various energies (see Table 1).

Neutrons produced in the soil are also attenuated. So it is incorrect to take a thick (~1m) production layer for all neutron energies. Low energy neutrons are attenuated easily
in the soil and soon removed, higher energy neutrons traverse a longer distance. The full fledged transport of neutrons is a complicated problem. We make a simple assumption: only neutrons produced in one attenuation length of material are relevant.

The density of soil at the site is not known and will depend on the water content. Here we assume soil has a density of 2 g/cm3. (note the density of concrete is 2.3g/cm3 and Nevada test site soil saturated 100% with water is 1.25 g/cm3, however the walls of the Lab can be assumed to be concrete, so this estimate is conservative).

To obtain a neutron rate from the Lab walls we assume 25% of the neutrons produced are incident inward.
Not all the neutrons from the walls will reach the detector, the fraction reaching the detector depends on geometry, we assume about 25% reach the detector. The results are shown in Table 1.

2)Muon induced spallation neutrons

Muon induced spallation neutron production rate is obtained from L.B. Bezrukov et al. (Sov. J. Nucl. Phys. Vol. 17, No. 1, July 1973) and is 11/kg/day for both soil and rock at 25 m.w.e. The energy distribution of neutrons in muon induced spallation is reported to be a power law similar to the spectrum at sea level. We use a spectral distribution $N(E) \sim E^{-1.3}$ (S. Hayakawa Phys. Rev. 84, (1951) 37, and D. Lal.). We assume 100% of the spallation neutrons have energies above 5 MeV. The above function is then integrated to give a normalization and one can compute the fraction of the total in each energy bin. The results are shown in Table 1.

3)Neutrons After a Buffer

Using a 76 cm mineral oil buffer we estimate the number of neutrons after the buffer. The attenuation in a given material varies with neutron energy and this must be included. Neutrons are produced in the buffer from both spallation and

m^- capture. The neutron production rate from muon capture is a strong function of Z (approxiamately proportional to Z^4). Thus mineral oil or polyethylene are suitable choices for buffers.

i. Neutron background from production in the Buffer volume:

The rate of capture neutrons produced in a 76 cm oil buffer (about 70 tons) 210,000/day. The rate of spallation neutrons produced in the buffer with energy above 5 MeV in the detector is about 770,000/ day.
We have optimized the buffer size to reduce the neutrons from outside while keeping the neutrons produced inside the buffer low. In addition it may be necessary to add boron to the buffer to soak up thermal neutrons and reduce the 2.2 MeV gamma rays from capture on hydrogen. ^{10}B which is about 20% of natural B, has a very large thermal capture cross section (3 kb) as compared with a few barns for H. The ^{10}B capture does not produce any gamma above 0.5 MeV, This reduces contributions to singles and triples rates in the 12 ton detector. After correcting for solid angle and self attenuation in the buffer one has the following neutrons in the fiducial volume from production in the buffer a) 15,000/day from capture b) 70,000/day from spallation. Most of these neutrons are rejected by the tight (99.9% efficient) 2 layer muon veto surrounding the buffer. This leaves 85 neutrons/day unvetoed in the detector. Including the $2x10^{-3}$ probability to make a four fold leaves a background of 0.2/day.

ii)Neutron background from production in the surrounding soil.

After accounting for solid angle and attenuation in the buffer we have 214 neutrons/day from capture and 1580 neutrons/day from spallation in the fiducial volume. The correlated background from these neutrons (including the $2x\ 10^{-3}$ probability for a 4 fold) is 3.6/day.

iii) Neutron background from production in the fiducial volume.

The 32 detector cells which form the active detector contain 16 tons of mineral oil. There are 48,000 capture neutrons/day and 176,000 spallation neutrons/day produced in this volume. Most of these are rejected by the muon veto (99.9% efficiency) leaving 224 unvetoed neutrons/day. Including the probability for a 4 fold coincidence gives a background of 0.5 /day.

Table 1

Single neutron background from muon capture and spallation a ter a 76 cm min. oil buffer
11 n/kg day from capture in rock

11 n /kg day from spallation in rock
@ 25mwe

neutrons after buffer

Energy bin (MeV)	E MeV	atten length min oil cm	atten in 76 cm min. oil	μ capture	μ spallation
5-10	5	8.8	0.00018	5.3	0
10-20	15	13	0.0029	121	135
20-30	25	15	0.0063	114	100
30-40	35	17	0.011	78	73
40-50	45	20	0.022	64	121
50-100	75	35	0.114	400	742
100-500	200	52	0.23	71	3483
500-1000	700	58	0.27		273
>1000	2000	65	0.31		366

production of >5MeV neutrons in oil
from spallation 11/kg day
from capture 3/kg day
@25mwe

Total	857 /d	6310 /d
after 25% geometry acceptance	214 /d	1580 /d

monte carlo 2×10^{-3} efficiency to produce a 4 fold coinc. 0.43/d 3.1/d

total external unvetoable single neutron background 3.6/d

neutrons in fid vol from production in buffer 70 tons (after solid angle and self attenuation) 85000/d

neutrons from buffer after veto (0.1% inefficiency) 224/d

background from buffer neutrons after 2×10^{-3} for 4 fold coinc. 0.5/d

neutrons produced in fiducial volume 16 tons 224000/d

background from fid vol neutrons after veto (0.1% ineff) and 2x10^{-3} for 4 fid coinc 0.5/d

Total 4.3/d

APPENDIX 5

APPENDIX 5

Notes on Rates and Target Parameters for the San Onofre Detector

Nicholas Mascarenhas

We present an estimation of the rates and some target parameters for the San Onofre neutrino detector. The Goesgen reactor oscillation experiment (Ref 1) is used to scale the rates to our experiment.

1. San Onofre (32 cell volume):

The 12 ton San Onofre detector contains 32 cells of mineral oil based liquid scintillator in the central detector volume. Each cell is 9 m x 0.5 m x 0.13 m. The scintillator contains 85% mineral oil , 15 % pseudocumene and 3 g/l PMP. The volume of each cell is 585 liters.

a) Volume

total volume in 32 cells	18720 liters
mineral oil (85% vv)	15912 liters
pseudocumene (15% vv)	2808 liters
3 gm/L PMP	56 kg

The density of mineral oil is 0.838 gm/cc and the density of pseudocumene is 0.889 gm/cc, thus

b) Weight

mineral oil in 32 cells	13.32 tons
pseudocumene	2.49 tons
Total	15.8 tons

c) Protons (H/C = 1.894)

mineral oil	$1.147\ 10^{30}$
pseudocumene	$0.15\ \ 10^{30}$
PMP	$0.00255\ 10^{30}$
Total	$1.299\ 10^{30}$

d)H/C ratio in San Onofre scintillator

H/C 1.894

e)Fiducial target (28 cells, 7.4 m long)

protons in fiducial volume (9m - 2x0.8m)xo.5m /0.13m x 28 cells 0.934×10^{30}

weight 11.37 tons of target.

2) Goesgen detector

In Goesgen there were 30 active cells filled with NE 325 C mineral oil based scintillator.

a) Volume

in 30 cells 377 liters

b) Protons (H/C = 1.7)

in 30 cells $2.5\ 10^{28}$

3)Scaling the Rates

The rates expected at San Onofre are scaled using the following formula

nevents = k x effic x power x Nprotons / (distance ^{2})

These rates are summarized in Table 1 for the 12 ton San Onofre detector and the Tendon gallery detector. The positron annihilation detection efficiency for the 12 ton detector is 20 % at a 50 keV threshold (for the 511 keV gamma rays). The neutron detection efficiency is about 50%. This gives a combined efficiency of 10%.

PARAMETER	GOESGEN	SAN ONOFRE(tendon)	SAN ONOFRE(12t)
reactor power	2814 MW	3300 MW	3300 MW x2
distance	37.9m	24.5m	650m
active cells	30	6	28
total cells	30	12	32
cell volume	12.54liter	12.56liter	585liter
target mass	0.324tons	0.065 tons	11.4 tons(fid)
protons	2.5 10^{28}	0.5 10^{28}	0.934 10^{30}
H/C	1.7	1.7	1.894
detection effic	16.7%	3%	10%
e+ threshold	0.8MeV	0.8MeV	0.8MeV
overburden	4mwe	20mwe	25mwe
buffer	20cm water 5mmB4C 14cm Fe	none	76cm oil,B loaded
veto	muon	muon	muon
signal/day	91.1	9	16.3
background/day	90	20	13

References
1)Zacek *etal.* Physical Rev. D 34 (2621) 1986.
2)Nicholas Mascarenhas, *Constituents of scintillator and acrylic* Caltech internal report. 22 April 1992
3)S. Banerjee, C. Delany and N Mascarenhas. *Some more on the efficiency to detect positron annihilation.* Caltech internal report.

DATE
FILMED
10/28/94
END